République Algérienne Démocratique et Populaire
Ministère de l'Enseignement Supérieur et de la Recherche Scientifique

Université de Batna 2
Faculté de Technologie
Département d'Électrotechnique

THÈSE

Présentée pour l'obtention du diplôme de
DOCTORAT 3ème cycle LMD en Électrotechnique

OPTION

Conception, Contrôle et Diagnostic des Systèmes Electriques

Par

ALNEJAILI Tareq

Thème

Commande dynamique de l'énergie dans un bâtiment multi-sources

Dynamic control of energy in a multi-source building

Soutenue le **06/05/2017** devant le jury composé de :

Dr. **AZOUI Boubekeur**	Prof.	Université de Batna 2.	Président
Dr. **DRID Saïd**	Prof.	Université de Batna 2.	Encadreur
Dr. **MEHDI Driss**	Prof.	Université de Poitiers, France	Co- Encadreur
Dr. **CHRIFI-ALAOUI Larbi**	M.C.A	Université de Picardie Jules Verne, France	Examinateur
Dr. **BETKA Achour**	Prof.	Université de Biskra	Examinateur
Dr. **NAIT-SAID Nasreddine**	Prof.	Université de Batna 2.	Examinateur

Résumé

L'objectif principal de ce travail est de développer un système de gestion de l'énergie (EMS) qui contrôle l'utilisation des technologies d'énergie renouvelable au niveau de la production locale d'électricité de l'énergie demandée par un bâtiment hors réseau, de développer des techniques de gestion des charges, gérer la consommation d'énergie dans le bâtiment et réduire les émissions nocives pour l'environnement.

Le système de gestion de l'énergie EMS effectue le contrôle global du système pendant deux intervalles de temps différents, le premier étant un contrôle dynamique en temps réel. Dans cet intervalle de temps, les références de puissance pour chaque source sont calculées en fonction du flux de puissance dynamique dans le système, tandis que la seconde est un intervalle de temps long qui concerne le contrôle du côté de la demande. Dans cet intervalle de temps, le EMS gère le profil de charge du bâtiment étudié afin d'augmenter la durée de vie du composant du système, de réduire la consommation d'énergie et de minimiser les coûts d'exploitation du système.

Le système EMS développé est principalement utilisé pour un système d'énergie hybride zéro émission comprenant un panneau photovoltaïque, une pile à combustible, un électrolyseur, une batterie au plomb et un super-condensateur. Le système d'alimentation hybride a été testé par simulation à l'aide de logiciels Matlab/Simulink. La simulation est effectuée sur une courte et une longue période de temps afin d'évaluer la performance des contrôleurs dynamiques et l'efficacité de la stratégie de gestion. Pour une longue période de simulation, une maison située dans la province de Batna (35 ° 33'N 6 ° 10'E) a été prise comme étude de cas avec une étude approfondie du profil de charge réel pour une maison moyenne avec toutes les données météorologiques requises par rapport à l'emplacement. De plus, une seconde étude de cas est ajoutée pour un système d'alimentation hybride constitué d'une source d'énergie conventionnelle et d'une source d'énergie renouvelable. La deuxième étude de cas porte sur l'application du DSM proposé sur un système hybride (photovoltaïque-vent-diesel) pour un bâtiment de santé rural moyen situé dans la région du Sahara. L'objectif principal de la deuxième étude de cas présentée est de tester l'efficacité du DSM pour un tel système d'alimentation hybride. Les résultats de la simulation confirment l'efficacité du SME proposé, car il augmente la fiabilité énergétique du système électrique, réduit l'émission de gaz à effet de serre dans le cas d'une deuxième étude de cas et minimise fortement le coût d'exploitation des systèmes.

Mots-clés - Système de gestion de l'énergie, contrôle dynamique, système d'alimentation hybride, profil de charge, efficacité énergétique.

Abstract

The main goal of this work is to develop an energy management system (EMS) that control the use of renewable energy technologies at the point of local electricity production of the energy needed by an OFF grid building, furthermore its develop an advance load management techniques to adjust the energy consumption within the building and reduce the harmful emissions to the environment.

The energy management system effected the overall system control throughout two different time interval, the first one is a real-time dynamic control. In this time interval, the power references for each source is calculated according to dynamic power flow within the system, while the second one is a long time interval that concerns the demand side control. In this time interval the EMS manages the load profile of the building under study in order to increase the service life of the system component, reduce the energy consumption and minimize the operation cost of the system.

The developed EMS is applied mainly for zero emissions hybrid energy system that includes a photovoltaic panel, a fuel cell, an electrolyzer, a lead acid battery bank and a supercapacitor. The hybrid power system has been tested by simulation using models implemented in Matlab/Simulink software. The simulation is performed over a short and a long period of time in order to evaluate the performance of the dynamic controllers and the effectiveness of the management strategy. For a long simulation period, a house located in the province of Batna (35°33′N 6°10′E) has been taken as a case study with a deep study on real load profile for an average house with all required weather data with respect to the location. Moreover second case study is added for hybrid power system that consist of a conventional and a renewable energy sources. The second case study focuses on the applying the proposed DSM on a (photovoltaic–wind–diesel) hybrid system for medium rural health building located in the Sahara region. The main aim of the presented second case study is to test the efficacy of the proposed DSM for such hybrid power system. The simulation results confirm the efficiency of the proposed EMS, as it increases the energy reliability of the power system, reduce the greenhouse gas emission in the case of second case study and minimize highly the operation cost of the systems.

Keywords— Energy management system, dynamic control, hybrid power system, load profile, energy efficiency, OFF grid building.

ملخص

إن الهدف الرئيسي من هذا العمل هو تطوير نظام إدارة للطاقة يستهدف التحكم في سريان الطاقة في مبنى معتمد على الطاقة المتجددة بالإضافة إلي ذلك هذا العمل يطور نظام إدارة ذكي للأحمال الكهربائية داخل المبنى ممايؤدي الي إستقرار إستهلاك الطاقة والإنقاص بشكل فعال من الإنبعاثات الضارة للبيئة.
بشكل أساسي التحكم يتم من خلال سلمين مختلفين للوقت. الأول يهتم بالتحكم على مدى زمني قصير في هذا المدى الزمني يهدف التحكم أساسا الي تحديد كميه الطاقة المرجعية لكل جزء من النظام. بينما سلم الوقت الثاني يهتم بإدراة الأحمال الكهربائية على مدى زمني طويل.
نظام التحكم المطور في هذه الدراسه يطبق على نظام طاقة هجين مشكل أساسا من وحدات الطاقة المتجددة. والذي يحتوي على خلايا شمسيه خلايا وقود بطاريات ومكثفات فائقة. تم أختبار النظام بواسطه المحاكاه في برنامج ماتلاب . المحاكاه تمت على فترتين من الوقت قصيرة وطويله . بالنسبه للمحاكاة على المدى الزمني الطويل تم أخذ منزل يقع في ولاية باتنة كحالة دراسه مع الأخذ بعين الإعتبار كافة المعطيات المناخيه لذلك الموقع الجغرافي. بالإضافة الي ذلك تم أخد حاله دراسة ثانيه لنظام يتكون من خليط من مصارد طاقه متجدده وتقليديه معا. نتائج المحاكاه أكدت فعاليه النظام المقترح حيث أنه زاد بشكل ملحوظ من الفعاليه الطاقويه للنظام وقلل من كمية الغازات الضارة المنبعثة.

Acknowledgments

Firstly, I would like to express my sincere gratitude to my advisor Prof. **Said DRID** for the continuous support of my Ph.D. study and related research, for his patience, motivation, and immense knowledge. His guidance helped me in all the time of research and writing of this thesis. I could not have imagined having a better advisor and mentor for my Ph.D study.

Besides my advisor, I would like to thank my co-advisor Prof. **Driss Mehdi** for his insightful comments and encouragement, but also for the hard question which incented me to widen my research from various perspectives.

ABBREVIATIONS

EMS	Energy management system
GHG	Greenhouse gas
RE	Renewable energy
FC	Fuel cell
EL	Electrolyzer
PV	Photovoltaic
HPS	Hybrid power system
MPPT	Maximum Power Point Tracking
SC	Super-capacitor
PEM	Proton exchange membrane
VSI	Voltage-source inverter
DLC	Direct Load Control
LDC	Load duration curve
O&M	Operating and maintenance
SOC	State of charge
SMC	Sliding mode control
DSM	Demand side management
LSM	Load side management
LM	Load management
DR	Direct response
NPC	Net present cost
COE	Cost of energy
Ga	Natural irradiance
Ta	Ambient temperature
O_c	Occupancy
P_{H_2}	Hydrogen tank pressure
FLC	Fuzzy logic controller
LMD	Load management device
A/C	Air conditioner
DG	Diesel generator
Td	Temperature difference between the indoor temperature and the setting temperature

TABLE OF CONTENTS

Chapter 3

Demand Side Management Techniques

Chapter 6

The second case study on the proposed demand side management and control algorithm

LIST OF FIGURES

LIST OF TABLES

General Introduction

1. Context and problems

For more than a century, Fossil fuels have been man's primary sources of energy, it is estimated that 86% of the world's energy comes from these fuels. The risk of shortages of fossil fuels and their effects on climate change, have powered an increasing interest around the importance of renewable energy (RE) sources such as solar, wind, hydro power, biomass and hydrogen. RE can be integrated into all types of electricity supply systems, from large, interconnected, continental-scale grids to on-site generation and utilization in small, autonomous buildings.

Residential and commercial buildings account for almost 38 percent of the world Greenhouse gas emissions. Nearly all of the (GHG) emissions from the residential and commercial sectors can be attributed to energy use in building. Residential and commercial activities contribute to emissions in a variety of ways:

- Combustion of natural gas and petroleum products for heating and cooking needs.
- Organic waste and wastewater treatment consume considerable amount of energy and emit different GHG such as methane (CH_4), and nitrous oxide (N_2O).
- Fluorinated gases (mainly hydro fluorocarbons, or HFCs) used in air conditioning and refrigeration systems can be released during servicing or from leaking equipment.

Many researches have been done to reduce the energy consumption of the building. These researches can be classified in two main categories. The first interested on the improvement of the architecture, the structure, the insulation or the materials in the building. The second deal with the local production of a part of the energy needed by the building without greenhouse gases emissions.

Building sites are surrounded by natural energy in the forms of wind, solar radiation, and geothermal heat. Renewable energy systems can be used to supplement or eliminate traditional heating, cooling, and electrical systems through the utilization of this natural energy. Components that encourage daylighting, passive and active solar heating, and on-site power generation are included in this category. Solar power can be utilized in many forms, both for heating and production of electricity. Wind power is a feasible way to generate electricity and pump water. Active solar or geothermal heat requires outside electricity for pumps but still saves energy in comparison to the operation costs of traditional mechanical systems.

The opportunities of the integration of different RE technologies throughout the building depend on many factors such as: the building designs, the availability of renewable energy resources and the costs of the renewable energy technology

A successful RE integration require an advanced energy management system (EMS) that responsible for multiple objectives including the effective integration of different RE technologies, dynamic system control, data management, grantee maximum comfort level for those living or working in the building with minimum use of energy, managing energy use throughout load side management techniques and reducing environmental impacts, all for minimal cost.

RE integration efficiency can be highly improved by the use of load side management techniques Usually the DSM techniques shared three common objectives, which can be presented as:

a) Reducing of energy consumption
b) Reducing demand through more efficient processes, buildings or equipment
c) Changing the load pattern and move the energy consumption from ON to OFF peak period

2. Thesis structure and objectives

The main aim of this work is to develop an energy management system (EMS) that control the use of renewable energy technologies at the point of local electricity production of the energy needed by an OFF grid building, The main objectives of the EMS are:

- Increase the reliability of the system and improves its energy balance.
- Reduce energy consumption and reducing the harmful emissions to the environment
- Achieve a significant economic benefits.

In addition to that the EMS employs an advance load management techniques to adjust the energy consumption within the building and to reduce the harmful emissions to the environment. This work comprise six chapter and is organized as follows:

The first chapter presents the background, problem statement, and value of the study. Firstly it introduces a general information about the study problem. This is followed by a discussion on the specific objectives and the scope of this study.

The second chapter briefly presents the system components description and modeling. Chosen appropriate model is extremely important to effectively manage and control the energy flow within the system. The chosen models must allow us to specify the structure or the

behavior of the system and represents a template that guides in the system constructing and in the decisions making.

The different techniques of demand side management (DSM) are presented in chapter three. Firstly it describes the background information of different DSM technique, including objectives, methods, and current research status. The review of the appliance level of DSM for various types of demands from statistical, simulated, and monitored sources is also reported. Moreover an economical analyze of the different economical terms that used in the economic optimization is presented.

The chapter four briefly presents the power flow management system. Moreover it describes the dynamic controller's design of the different subsystem components. Firstly the appropriate control of the different DC-DC converters is designed. This is followed by adscription of the proposed energy management system. Finally the validation of the system by simulation is presented, using models implemented in Matlab/Simulink software.

The chapter five describes the DSM methodology developed for this study in detail. Two main DSM techniques load shifting (LS) and demand side controls (DSC) are illustrated in detail within this chapter. Different levels of control algorithm suitable for historical demand, simulated demand and monitored real-time demand are also addressed respectively. In addition to that a case study is presented to assume the effectiveness of the developed DSM. The proposed DSM strategy is applied for zero emissions hybrid system for off grid house.

The chapter six test the efficacy of the proposed DSM for hybrid power system that consist of a conventional and a renewable energy sources. Moreover a second case study focuses on applying a modified DSM for medium rural health building located in the Sahara region is presented. Designing a suitable DSM for such facility is a critical issue because of the activity nature of such important facility. The modified version of the proposed DSM employ a combination of ON/OFF direct load control and fuzzy logic control strategy. Using these combinations of control minimize highly the impact on users and at the same time maximize the match between demand and supply through identifying the best control depending on many standers such as energy availability and occupancy.

Finally the last part of this thesis presents a general conclusion of the accomplished work and illustrates the different obtained results. More over a future work is suggested.

3. Contributions

The research carried out within the framework of this thesis lead to the following scientific publications

- **Tareq ALNEJAILI**, Said Drid, Driss Mehdi, Larbi Chrifi-Alaoui, Rafik Belarbi, and Aziz Hamdouni. Dynamic control and advanced load management of a stand-alone hybrid renewable power system for remote housing. Energy Conversion and Management **2015**; 105: 377–392.

- **Tareq ALNEJAILI**, Drid S, Mehdi D, Chrifi-Alaoui L. A Developed energy management strategy for a stand-alone hybrid power system for medium rural health building. International transactions on electrical energy systems **2015**; 25(7).

- **Tareq ALNEJAILI**, Said DRID, Driss MEHDI, Larbi CHRIFI-ALAOUI. Sliding Mode Control of a Multi-Source Renewable Power System. 3RD International conference on control, engineering & information technology, Tlemcen, Algeria; **2015**.

- **Tareq ALNEJAILI,** Driss Mehdi, Said Drid, *Senior Member, IEEE***,** and Larbi Chrifi-Alaoui**.** Advanced Supervisor Control for A Stand- Alone Photovoltaic Super Capacitor Battery Hybrid Energy system for Remote Building. The 4th International Conference on Systems and Control, Sousse, Tunisia; **2015.**

- **Tareq ALNEJAILI,** Said DRID, Driss MEHDI, Larbi CHRIFI-ALAOUI. Advanced strategy of Demand-side management for photovoltaic-wind energy system. 15th International Conference on Sciences and Techniques of Automatic Control and Computer Engineering (STA), Hammamet, Tunisia; 2014: 797 – 802.

- **Tareq ALNEJAILI,** Drid Said. Design and implementation of a modified DC-DC converter suitable for charging solar batteries. International Conference on Industrial Engineering & Manufacturing ICIEM, Batna, Algeria; 2014.

Chapter 1

Background and research problem

1.1 Introduction

In this chapter the background, the problem statement, the purpose and the value of the study are discussed. At the beginning the general information about the study problem is introduced to give a brief overview of the treated subject. This is followed by a discussion on the specific objectives and the scope of this study. In addition, the procedures for the empirical study are listed and the outline of the study is revealed

1.2 Building, energy and environment

Global energy consumption has increased steadily for much of the twentieth century. According to the International Energy Agency, during the last two decades primary energy has grown by 49% and CO2 emissions by 43%, with an average annual increase of 2% and 1.8% respectively. Current predictions show that this growing trend will continue supported by the growing in the emerging economies (Middle East, Southeast Asia, South America and Africa). In the last decade coal was the source of energy with the largest growth. The use of oil and natural gas also had considerable growth, followed by hydro power and renewable energy. Renewable energy grew at a rate faster than any other time in history during this period, which can possibly be explained by an increase in international investment in renewable energy (Fig. 1.1) [1, 2].

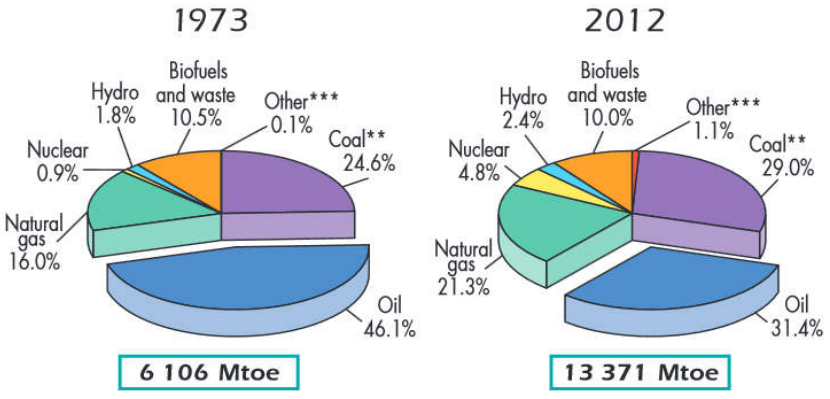

Fig. 1.1. World total primary energy supply from 1973 to 2012 by fuel (Mtoe)

Energy consumption grew most quickly in the transport, industry and building sectors (Fig. 1.2). In the last two decade the global energy use in the building sector increased by 19% to reach 92 EJ. Around 4 EJ (±15%) of this total consumer energy was from combustion of around 31 EJ of traditional biomass for cooking and heating, assuming efficiency of combustion was around 15% [3]. These increases were driven by strong growth in population, enhancement of building services and comfort levels, together with the rise in time spent inside buildings, have raised building energy consumption to the levels of transport and industry. The residential sector consumed over half of the total building energy demand followed by the commercial and public service buildings that slightly increased their share of the total since 1990.

Residential and commercial buildings account for almost 38 percent of the world Greenhouse gas emissions. Nearly all of the (GHG) emissions from the residential and commercial sectors can be attributed to energy use in building. Residential and commercial activities contribute to emissions in a variety of ways:

- Combustion of natural gas and petroleum products for heating and cooking needs emits carbon dioxide (CO_2), methane (CH_4), and nitrous oxide (N_2O). Emissions from natural gas consumption represent about 81% of the direct fossil fuel CO_2 emissions from the residential and commercial sectors. Coal consumption is a minor component of energy use in both of these sectors.
- Organic waste sent to landfills emits CH_4.
- Wastewater treatment plants emit CH_4 and N_2O.
- Fluorinated gases (mainly hydro fluorocarbons, or HFCs) used in air conditioning and refrigeration systems can be released during servicing or from leaking equipment.

Historically the majority of emissions emanated from developed countries, it is expected that in the near future the level of emissions from buildings in rapidly industrializing countries will surpass emission levels from buildings in developed countries. Emission reductions from buildings can be achieved by reducing emissions from the energy supply or by reducing energy consumption through improved building design, increased energy efficiency and conservation, and other mechanisms that reduce energy demand in buildings.

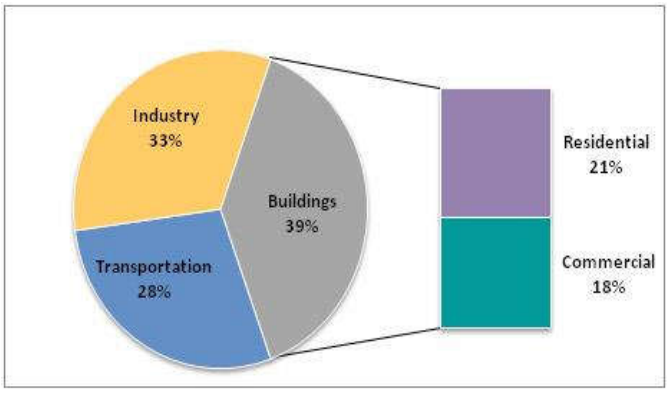

Fig. 1.2. World energy consumption in the transport, industry and building sectors

1.2.1 Energy consumption of the building in Algeria

During the last two decades the electrical energy consumption in Algeria has increased significantly, recent studies expected that electrical energy consumption will rise to 83 TWh by 2020 and up to 150 TWh by 2030 [4]. Algeria depend strongly on hydrocarbons, the natural gas is the principal source of energy with 94% of the electrical energy coming from it. Some research expect that the hydropower plants contribute around 5% of the country's electricity and less than 1% comes from other renewable energy source (mainly wind and solar energy). On the other hand, current research forecast that the natural gas will only be available over the next 70 years while the country's oil reserves will only cover the next 50 years. Consequently Algeria faces a big challenge to change it dependence on fossil fuels toward the renewable energy.

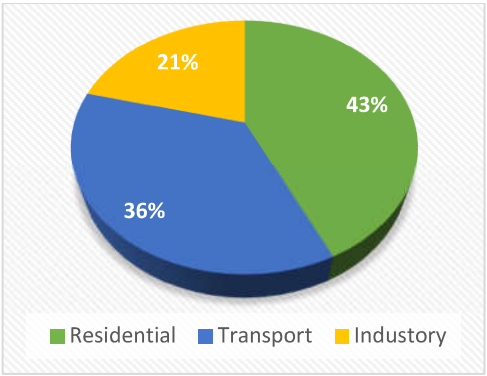

Fig 1.3. Energy usage in Algeria

The residential sector is the largest sector of energy usage namely 43%, followed by the transport sector (36%) and the industry 21% (Fig. 1.3) [5]. There are a lot of factors that drive the increasing in energy demand in this sector such as:

- The important increase of population and housing.
- Increase number of electricals equipment's in each house.
- Use of non-economic electricals equipment's such as incandescent lamps and cheap air conditioners.
- Absence of awareness and lack of culture on the energy control.
- Growing desire of people to comfort and the low prices of conventional energy.

Thus, the increase in energy demand has put ever-increasing pressure on identifying and implementing ways to save energy. Within this context, the development of energy efficiency standards for home appliances is part of the National Energy Efficiency Program of the Algerian Ministry of Energy and Mines. The energy efficiency law outlines the general rules concerning the energy efficiency of home appliances operating on electricity, gas and petroleum products. Moreover the integration of the different renewable energy technology (solar, wind, geothermal and biomass) in buildings as well as effective engineering applications can potentially contribute towards energy provision for this sector and help move the country towards a more sustainable position in terms of energy provision and consumption [6].

1.3 Renewable Energy Integration in Buildings

Concerning the building sector, the RE technologies can be integrated in electric power systems, heating and cooling networks and gas grids or by installing directly and integrated into the building structure.

The opportunities of the integration of different RE technologies throughout the building depend mainly on the life span of the building. Many buildings in developed countries have average life spans of 120 years and above, hence energy efficiency measures and the integration and deployment of RE technologies will need to result mainly from the retrofitting of existing buildings. Developing countries currently have stock turnover rates of 25 to 35 years on average with relatively high new building construction growth, which offering a good opportunities to integrate RE technologies through new building designs. Moreover, greater integration of RE into the built environment is depend else on how urban planning, architectural design, engineering and a combination of technologies can be integrated [3]. Therefore, the renewable energy technologies assessment process must subject to many criteria such as:

- The availability of renewable energy resources: Renewable energy technologies depend strongly on resources like sunlight, wind, biomass, or heat from the earth.
- The space availability: additional space may be required by many type of technologies either on a roof or on land,
- The costs of the technology: this include the cost of energy generated by the technology and any financial incentives like grants, favorable tariffs, etc.
- Building architect characteristics.
- The Ability to connect to the grid, which answer the equation of what size and type of technologies can be interconnected economically.
- The existing of technical support: This important criteria include the existing of the technical support in the emergency case and the availability of the technology in the local market which include if the technology is classified as locally Manufactured or Imported
- The goals: It's so important to set different goals and objectives and comparing the various technologies according to these goals.
- Additional criteria: the additional factors which can effect on the decisions making include energy security.

Various RE technologies can be install to fulfill the energy requirement of the building such as: solar thermal, solar cooling systems and hybrid technologies such as combining solar thermal with biogas boilers, heat pumps, Fuel cell, small wind turbine and PV systems. These various technologies are intended to provide a variety of basic energy services including for:

- Space heating, water heating, cooking
- Cooling, refrigeration
- Lighting, electronic and electrical appliances
- Water pumping and waste treatment

Reducing energy demand for heating and cooling represents one of the most important issue of integrating RE within the building. For both heating and cooling, the design of a building can contribute to lowering the energy demand, optimization of window surfaces, and insulation levels can contribute to reduce the demand for heating as well as facilitating natural lighting. In warm climates where cooling loads dominate adapting bio-climatic principles of traditional designs to new building stock, such as extensive shading and natural ventilation, can contribute to

decreasing energy demand [3]. Moreover the additional costs of integration RE must be minimize to meet the regulation and exemplifies the links between RE and efficiency.

In order to achieve an efficient integrating of RE technologies, the efficiency of the electrical appliances must be improved. For example using light-emitting diodes and energy smart electronic appliances can contribute to reduce energy demand. In dwellings currently without access to electricity even for basic lighting, installing RE technologies such as small PV systems or micro-hydropower can be relatively expensive. So electricity demand should be minimized by use of energy efficient appliances such as LEDs. In addition to that the smart energy management systems can play very important role in the improving of the energy usage and efficiency.

1.4 Energy and load side management techniques in the building

An energy management system for a commercial, a service or a multi-unit apartment building is mainly responsible for multiple objectives including the effective integration of different RE technologies, dynamic system control, data management, grantee maximum comfort level for those living or working in the building with minimum use of energy, managing energy use throughout load side management techniques and reducing environmental impacts, all for minimal cost (Fig. 1.4). Measuring and monitoring both energy use and the building environment are usually required. Monitoring techniques can also be deployed in apartment buildings with home energy management standard technologies installed to control and actuate appliances as part of a distributed energy network.

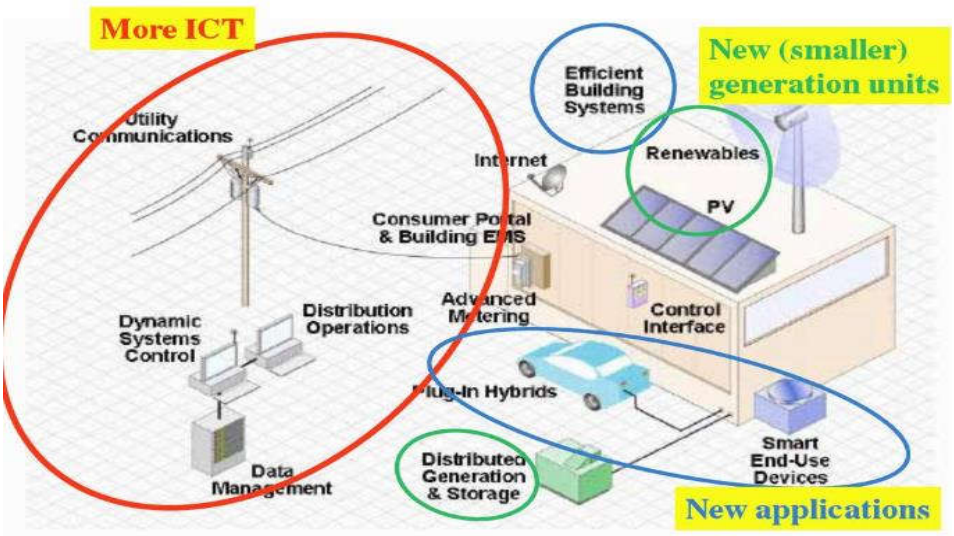

Fig. 1.4. Energy management system

Energy demand management, also known as demand side management (DSM), entails actions that reduce or shift the energy consumption through efficiency improvements or load shifting on the customer side of the electrical meter, during periods when energy - supply systems are constrained. In fact by reducing the overall load on an electricity network, DSM has various beneficial effect including:

- Increasing system reliability.
- Mitigating electrical system emergencies.
- Reducing the number of blackouts.
- Reducing depends on expensive import of fuel.
- Reducing energy price and reducing the harmful emissions to the environment.
- Achieve a significant economic benefits.

Usually the DSM techniques shared three common objectives, which can be presented as (Fig. 1.5):

a) Reducing of energy consumption
b) Reducing demand through more efficient processes, buildings or equipment (amplitude modulation load mode)
c) Changing the load pattern and move the energy consumption from ON to OFF peak period (time shifting load mode)

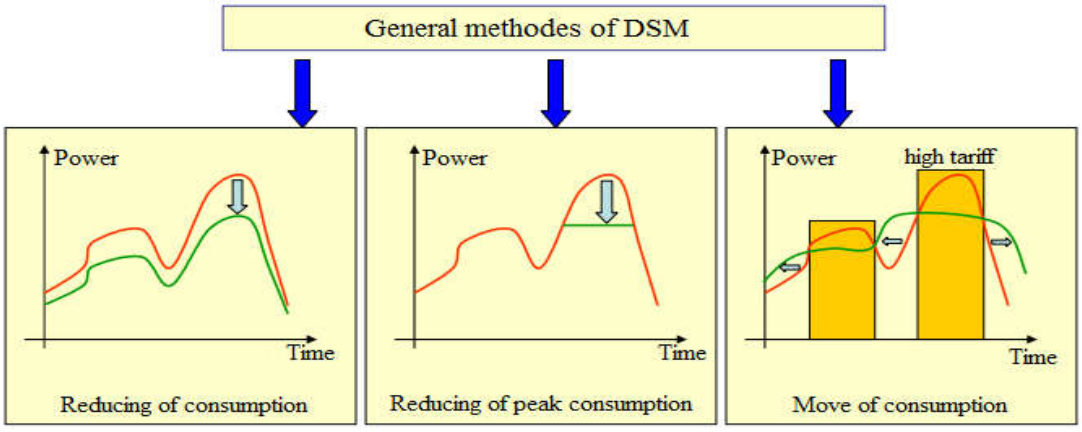

Fig. 1.5. General method of DSM

The DSM achieve the last mention goals throughout various techniques, the main types of DSM techniques maybe classified in main three categories [7]:

Load shedding (shifting): This technique can reduce the peak power demand by an intelligent control of the residential appliance. The reduction in the energy cost and in the co2 emission can be varied in the range of 10-50% depending in the load shifting percentage.

Load time shifting load: This technique move the energy consumption from more expensive energy tariff periods to less expensive one or from ON to OFF peak period.

Time programming: This technique allows to control the opening and closing of the appliances based on the occupancy and use of place.

1.5 Problem statement and research objectives

Today, buildings are responsible for more than 40 % of global energy used, and as much as one third of global greenhouse gas emissions, both in developed and developing countries. Furthermore, the Buildings and Construction Sector is also responsible for significant GHG emissions such as halocarbons, CFCs, and hydro fluorocarbons (HFCs). In order to achieve the maximum level of emission reductions the renewable energies will have to play a much bigger role in meeting energy needs in buildings. This can be achieved through two avenues: first, by substituting fossil fuels with renewable energy sources at the point of electricity generation; and second, through the use of different DSM techniques at the point of consumption.

A transition from a fossil fuel-based, centralized energy supply system to a more distributed energy system with increased RE integration would need a comprehensive revision of how urban space has been traditionally planned and occupied and the RE resources availability. Changes in land and resource use, as well as modifying planning regulations to better accommodate RE technologies with the existing energy supply, are major strategic amendments that could be made to shape their integration. Moreover the technical challenges of integrating variable and distributed RE power and heat generation can be partly resolved by the smart use of appliances in buildings. Technological advances can assist the integration of RE into the built environment, including energy storage technologies, real-time smart meters, demand side management and more efficient systems. Properly managed, appliances could contribute to maintaining the supply/demand balance of the energy system especially at higher penetration levels of variable RE sources.

The integration of multi-source energy system in building must pass through several important stages. The optimal sizing of the system including feasibility and reliability analysis is considered to be one of the most important stage in the RE technologies integration. The economic and the technical's feasibility of the different technology options that are used in the system must be evaluated according to different criteria such as, technology options, component costs, and resource availability. Moreover the successful RE integration require an advanced energy manager that provides overall control of the power system and sets the power reference for the different converters that control the power system components. Furthermore the RE integration efficiency can be highly improved by the use of load side management techniques which can reduce highly the stress on the energy system and increase the energy balance.

The main aim of this work is to develop an energy management system (EMS) that control the use of renewable energy technologies at the point of local electricity production of the energy needed by an OFF grid building, The main objectives of the EMS are:

- Achieve an efficient integration of RE technologies in the building.
- Increases the reliability of the system and improves its energy balance.
- reducing energy consumption and reducing the harmful emissions to the environment
- Achieve a significant economic benefits.

In addition to that the EMS employs an advance load management techniques to adjust the energy consumption within the building and to reduce the harmful emissions to the environment.

The energy management system effected the overall system control throughout two different time interval, the first one is a real-time dynamic control. In this time interval, the power references for each source is calculated according to dynamic power flow within the system, while the second one is a long time interval that concerns the demand side control. In this time interval the EMS manages the load profile of the building under study in order to increase the service life of the system component, reduce the energy consumption and the operation cost.

The developed EMS is applied mainly for zero emissions hybrid energy system includes a photovoltaic panel, a fuel cell, an electrolyzer, a lead acid battery bank and a supercapacitor. The hybrid power system has been tested by simulation using models implemented in Matlab/Simulink software. The simulation is performed over a short and a long period of time in order to evaluate the performance of the dynamic controllers and the effectiveness of the management strategy. For a long simulation period, a house located in the province of Batna

(35°33′N 6°10′E) has been taken as a case study with a deep study on real load profile for an average house with all required weather data with respect to the location. Moreover a second case study is added for a hybrid power system that consist of a conventional and a renewable energy sources. The second case study focuses on the applying the proposed DSM on a (photovoltaic–wind–diesel) hybrid system for medium rural health building located in the Sahara region. The main aim of the presented second case study is to test the efficacy of the proposed DSM for such hybrid power system .The simulation results confirm the efficiency of the proposed EMS, as it increases the energy reliability of the power system, reduce the GHG emission in the case of second case study and minimize highly the operation cost of the systems.

1.6 References

[1] Perez-Lombard L, Ortiz J, Pout C. A review on buildings energy consumption information. Energy and Buildings 2008; 40:394–398.

[2] International energy agency (IEA). Key world energy statistics 2014.

[3] Sims, R., P. Mercado, W. Krewitt, G. Bhuyan, D. Flynn, H. Holttinen, G. Jannuzzi, S. Khennas, Y. Liu, M. O'Malley, L. J. Nilsson, J. Ogden, K. Ogimoto, H. Outhred, Ø. Ulleberg, F. van Hulle. Integration of Renewable Energy into Present and Future Energy Systems. In IPCC Special Report on Renewable Energy Sources and Climate Change Mitigation, Cambridge University Press, Cambridge, United Kingdom and New York, NY, 2011,USA.

[4] Menani S. Algeria Renewable Energy Program Outlook and applications. Energy week 2012, Finland.

[5] Ghedamsi R, Settou N, Gouareh A, Khamouli A, Saifi N, Recioui B. Estimating the energy consumption in building sector in Algeria using bottom-up mode. 6th International Renewable Energy Congress (IREC) 2014.

[6] Algerian Renewable Energy and Energy Efficiency Program, 2012.

[7] Ky LE. Gestion optimale des consommations d'énergie dans les bâtiments.A Dissertation Submitted in Partial Fulfillment of the Requirements for the Degree of Doctor of Philosophy in Electrical Engineering, Polytechnic Institute of Grenoble, France 2008.

Chapter 02

System Modeling

2.1 Introduction

This chapter briefly presents the system components description and modeling. Chosen appropriate model is extremely important to effectively manage and control the energy flow within the system. The chosen models must allow us to specify the structure or the behavior of the system and represents a template that guides in the system constructing and in the decisions making.

2.2 Fundamental on the hybrid system

Fig. 2.1 shows the proposed structure of the hybrid power system (HPS). The different system are linked to a common DC bus through appropriate DC-DC power converters and assumed to be controlled by independent control system. The PV array is the primary source of the HPS, it is connected to the DC bus through DC-DC boost power converter, which achieves the PV Maximum Power Point Tracking (MPPT) control. The FC is sized to be the main backup source when the power generated by the PV or stored in the battery is insufficient to support the loads. It is connected to the DC bus through DC-DC boost converter. Generally a FC is characterized by its high efficiency and reliability, but its dynamic is limited by the hydrogen/oxygen delivery system. Therefore, a fast response auxiliary power source is needed to compensate its slow dynamic, which can be achieved by the utilization of supercapacitor bank. The electrolyzer is connected to the DC bus via DC-DC buck converter, when the battery is fully charged the excess power is transferred to the electrolyzer unless the H_2 storage tank is full. The battery bank is mainly sized to support the low power demand, it is connected to the DC bus via bidirectional converter, which is controlled to follow the reference of charge or discharge current and to regulate the DC bus voltage (or super-capacitor SOC). The super-capacitor (SC) is directly connected to the DC bus in order to compensate the slow dynamic of the FC and support the sharp load. The SC has a greater power density, which allows it to supply the power over a short period [21]. Utilizing the super capacitor has many advantages, such as reducing the size of the battery, improving the performance of the FC and stabilizing the DC bus voltage under fast load changes.

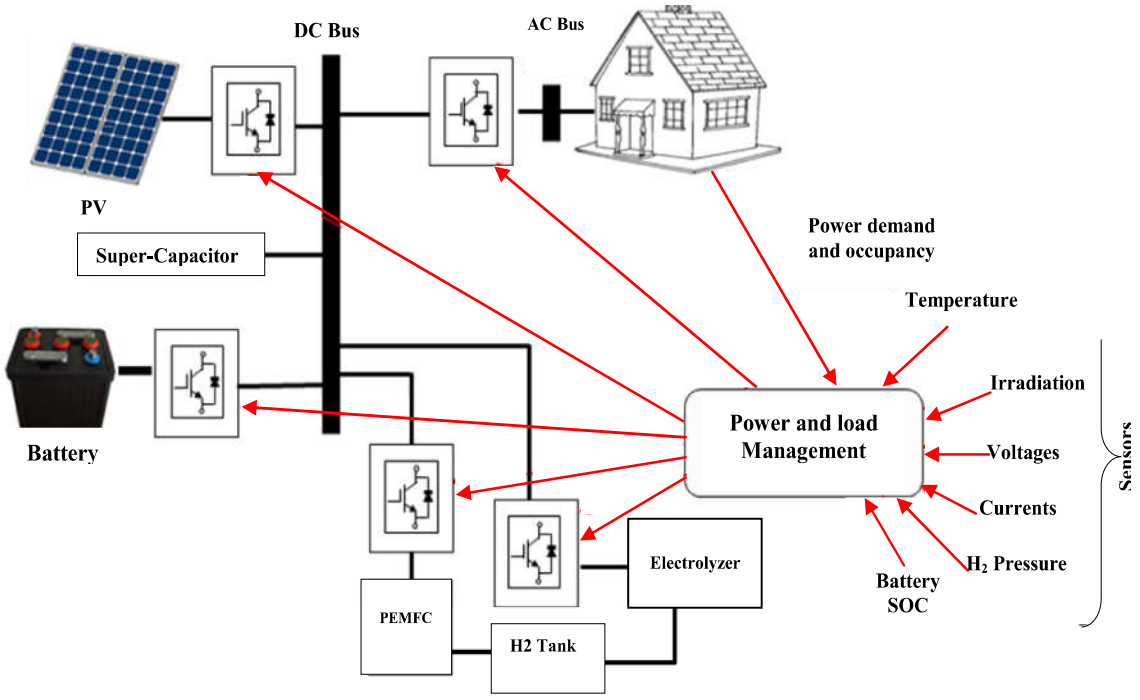

Fig. 2.1 Hybrid system structure

2.3 PV principle of operation and modeling:

The photovoltaic (PV) power technology uses semiconductor cells (wafers), generally several square centimeters in size. From the solid-state physics point of view, the cell is basically a large area PN diode with the junction positioned close to the top surface. The cell converts the sunlight into direct current electricity. Numerous cells are assembled in a module to generate required power. Unlike the dynamic wind turbine, the PV installation is static, does not need strong tall towers, produces no vibration or noise, and needs no cooling.

All PV cells work in essentially the same way. Like diode (Fig 2.2) they contain a junction between two different materials which there is an electric field. When the cell absorbs light mobile electrons and holes are created. This flow of opposite directions across the junction, in this way the flow of absorbed photons is converted into a flow of DC power from the illuminated cell.

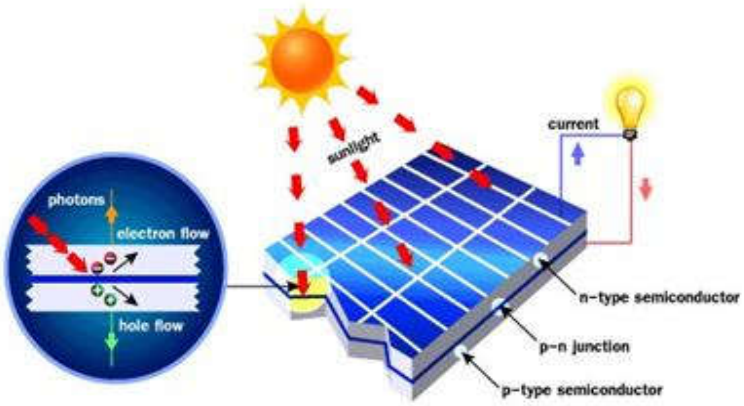

Fig. 2.2. Construction of the solar cell

2.3.1 PV model

Several PV models have been reported in literature. Such models normally consist in non-linear equations due to the physical variables involved in the PVM operation.

The non-linear models are useful for electrical simulation purposes and energy harvesting evaluation, but they introduce a high complexity in terms of control systems analysis and design. The photovoltaic system can be modeled by a current source, a diode and a combination of a series and a parallel resistance. The output current of the cell can be given by [1, 2]:

$$I_{PV} = I_{ph}(t) - I_{rs}(t)\left[\exp\left(\frac{q(V_{pv}(t)+I_{pv}(t)R_S)}{A_c K T(t)}\right)-1\right] \tag{2.1}$$

where I_{ph} is the photocurrent, I_{rs} is the cell reverse saturation current, V_{PV} is the voltage level on the PV cell terminals, q is the electron charge, R_s is the intrinsic cell resistance, A_c is the cell deviation from the ideal pen junction characteristic, K is the Boltzman constant and T is the cell temperature. The photocurrent of the PV cell can be expressed as [1]:

$$I_{ph}(t) = \frac{(I_{sc} + K_l[T(t) - T_r])\lambda(t)}{100} \tag{2.2}$$

Where I_{sc} is the short-circuit cell current, K_l is the short-circuit current temperature coefficient and λ is the insolation in (mW.cm^{-2}). The reverse saturation current is mainly depends on the temperature and it can be expressed as:

$$I_{rs}(t) = I_{or}\left(\frac{T(t)}{T_{ref}}\right)^3 \exp\left(\frac{qE_{go}(\frac{1}{T_r} - \frac{1}{T(t)})}{KA_c}\right) \tag{2.3}$$

Where I_{or} is the reverse saturation current at the reference temperature T_{ref} and E_{go} is the band-gap energy of the semiconductor used in the cell. The simulation parameters of the solar system are summarized in Table 2.1.

Table 2.1 Parameters of the solar system

Parameters	Value
Q	1.6×10^{-19}C
A_c	1.6
K	1.3805×10^{-23} NmK^{-1}
K_l	0.0017A°C^{-1}
I_{or}	2.0793×10^{-6}A
T_{ref}	301.18K
E_{go}	1.10

2.4 Fuel cell principal of operation

Fuel cells (FC) are electrochemical devices that convert the chemical energy of a gaseous fuel directly into electricity. FC are widely regarded as a potential alternative stationary and mobile power source [3]. Proton exchange membrane (PEM), also known as polymer electrolyte membrane fuel cell that use hydrogen is considered to be one of the most common type of the FCs, it can be used for commercial stationary power generation, residential applications, and transportation technologies, because it has high power density, solid electrolyte, long cell and stack life, as well as low corrosion. PEM fuel cells operate in the temperature range of 50 to 100°C which allow safer operation and eliminates the need for thermal insulation. Using pure hydrogen as fuel can eliminate local emissions problems in densely populated urban environments, where the hydrogen can be generated based on renewable energy from wind, water, and solar energy. A PEM fuel cell consists of a polymer electrolyte sandwiched between two electrodes. The electrolyte has a special property that allows positive ions (protons) to pass through while blocking electrons. Hydrogen gas passes over one electrode, called an anode, and with the help of a catalyst, separates into electrons and hydrogen protons (Fig 2.3) [3].

$$2H_2 \Rightarrow 4H^+ + 4e^-$$

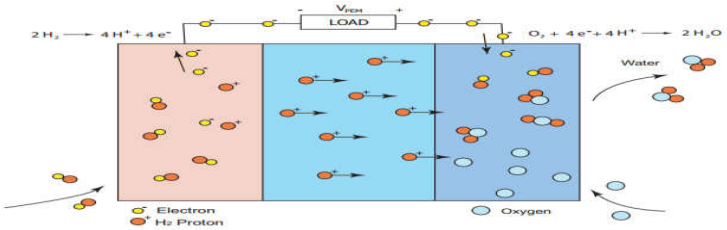

Fig 2.3 Fuel cell reaction

The electrolyte polymer membrane permits transfer of protons, enabling the electrons to flow through an external circuit before recombining with protons and oxygen at the cathode to form water [3].

$$O_2 + 4H^+ + 4e^- \Rightarrow 2H_2O \tag{2.4}$$

The overall reaction of the fuel cell is therefore.

$$2H_2 + O_2 \Rightarrow 2H_2O \tag{2.5}$$

The electrical characteristics of fuel cells are normally given in the form of a polarization curve which is a relation of cell voltage versus cell current density (current per unit cell active area). The voltage produced from one cell is between 0 and 1 volts [3] depending on fuel cell operating conditions and the size of the load connected to the fuel cell. The voltage decreases as more current is drawn from the fuel cell, due to fuel cell electrical resistance, inefficient reactant gas transport, and low reaction rate. Lower voltage indicates lower efficiency of the fuel cell. The loss in the cell turns into heat which can damage the polymer membrane. Many cells are typically combined in a stack to satisfy the power requirements of the targeted application.

2.4.1 FC modeling

The PEMFC is modeled, according to the relationship between the output voltage and the partial pressure of hydrogen, oxygen, and water. The detailed model is shown in Fig. 2.4. The relationship between the partial pressure of hydrogen with it molar flow can be given as [4]:

$$\frac{q_{H_2}}{p_{H_2}} = \frac{K_{an}}{\sqrt{M_{H_2}}} = K_{H_2} \tag{2.6}$$

Where q_{H_2} is the input molar flow of hydrogen [kmol/s], p_{H_2} is the hydrogen partial pressure [atm], K_{an} is the anode valve constant $\left[\sqrt{Kmol\ kg(atm\ s)^{-1}}\right]$, M_{H_2} is the molar mass of hydrogen [kg kmol^{-1}] and K_{H_2} is the hydrogen valve molar constant [kmol/(atm s)]. Using the perfect gas equation, the derivative of the partial pressure can be calculated as [4]:

$$\frac{d}{dt} p_{H_2} = \frac{RT}{V_{an}} \left(q_{H_2}^{in} - q_{H_2}^{out} - q_{H_2}^{r}\right) \tag{2.7}$$

Where R is the universal gas constant [J/(kmol K)], T is the absolute temperature [K], V_{an} is the volume of the anode [m3] , $q_{H_2}^{in}$ is the hydrogen input flow [kmol/s], $q_{H_2}^{out}$ is the hydrogen

output flow [kmol/s] and $q_{H_2}^r$ is the hydrogen reacted flow [kmol/s], which can be expressed as [4]:

$$q_{H_2}^r = \frac{N_0 N_s I_{FC}}{2F} = 2K_r I_{FC} \tag{2.8}$$

Where N_0 is the number of series fuel cells in the stack, N_s is the number of stacks used in the FC power plant, I_{FC} is the FC system current [A], F is the Faraday's constant [C/kmol] and K_r is the modeling constant [kmol/(s A)]. Using Eqs. (5) and (6), the hydrogen partial pressure can be expressed in the (*s*) domain as [5]:

$$p_{H_2} = \frac{\frac{1}{K_{H_2}}}{1 + \tau_{H_2} S}(q_{H_2}^{in} - 2K_r I_{FC}) \tag{2.9}$$

Where τ_{H_2} is the hydrogen time constant [s], and it can be expressed as:

$$\tau_{H_2} = \frac{V_{an}}{K_{H_2} RT} \tag{2.10}$$

The PEMFC polarization curve is obtained from the sum of the Nernst's voltage (E), the activation over voltage (η_{act}), and the ohmic over voltage (η_{ohmic}). Assuming constant temperature and oxygen concentration, the FC output voltage can be expressed as [6]:

$$V_{cell} = E + \eta_{act} + \eta_{ohmic} \tag{2.11}$$

Where

$$\eta_{act} = -Bln(CI_{FC}) \tag{2.12}$$

and

$$\eta_{ohmic} = -R^{int} I_{FC} \tag{2.13}$$

where B and C are constants, and R^{int} is the FC internal resistance [U]. In term of gas molarities, the Nernst voltage is given as [4]:

$$E = N_0 \left[E_0 + \frac{RT}{2F} log \left[\frac{P_{H_2} \sqrt{P_{O_2}}}{P_{H2O}} \right] \right] \tag{2.14}$$

Where P_{H2O} is the water partial pressure [atm]. The amount of the hydrogen consumed by the FC is mainly determined by the power demand. The hydrogen flow rate is controlled, according to the output power of the FC system, where FC output current is taken back to the input while

converting the hydrogen into molar form. The amount of hydrogen flow required to meet the load is given as [5]:

$$q_{H_2}^{req} = \frac{N_0 N_S I_{FC}}{2FU} \tag{2.15}$$

Where U is the utilization rate. The FC model parameters are summarized in Table 2.2.

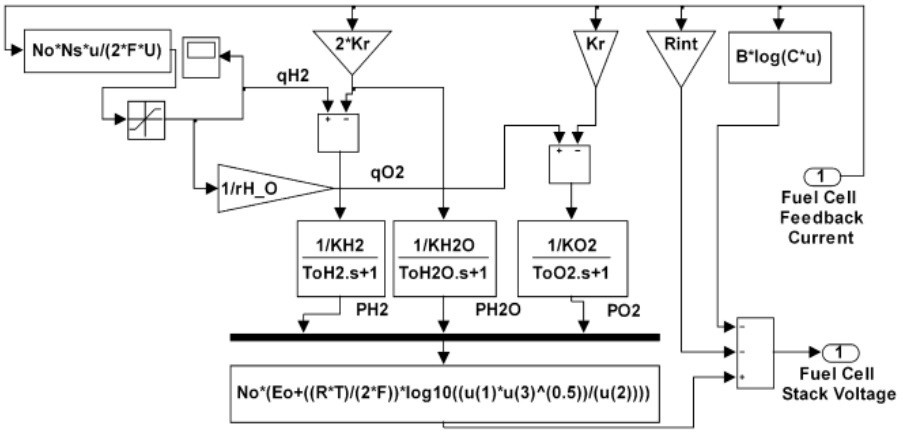

Fig. 2.4 PEMFC model

Table 2.2 FC model parameters

Parameters	value
Activation voltage constant (B)	0.04777 [A^{-1}]
Activation voltage constant (C)	0.0136 [V]
Conversion factor (CV)	2
Faraday's constant (F)	96484600 [kmol/(atm s)]
Hydrogen time constant τ_{H_2}	3.37 [s]
Hydrogen valve constant K_{H_2}	4.22×10^{-5} [kmol/(atm s)]
Hydrogen–oxygen flow ratio (rH–O)	1.168
Kr constant =No/4F	2.2802×10^{-7} [kmol/(s A)]
No load voltage (Eo)	0.5 [V]
Number of cells (No)	88
Number of stacks (NS)	1
Oxygen time constant τ_{o_2}	6.74 [s]
Oxygen valve constant k_{o_2}	2.11×10^{-5} [kmol/(atm s)]
FC system internal resistance (Rint)	No×0.00303[Ω]
FC absolute temperature (T)	343[K]
Universal gas constant (R)	8314.47
Utilization factor (U)	0.8
Water time constant τ_{H2O}	18.418 [s]
Water valve constant k_{H2O}	7.716×10^{-6} [kmol/(atm s)]

2.5 Electrolyzer principal of operation and modeling

An electrolyzer is an electrochemical device that convert electricity and water into hydrogen and oxygen by passing a current through a water in the presence of suitable substances, called electrolytes. Electric current causes positively charged hydrogen ions to migrate to the negatively charged cathode, where a reduction takes place in order to form hydrogen atoms. The atoms formed then combine to form gaseous hydrogen molecules (H2). On the other hand, oxygen is formed at the other electrode (the positively charged anode (Fig 2.5)).

$$H_2O_{(liquid)} + electrical\ \ energy \Rightarrow H_{2(gas)} + \frac{1}{2}O_{2(gas)} \tag{2.16}$$

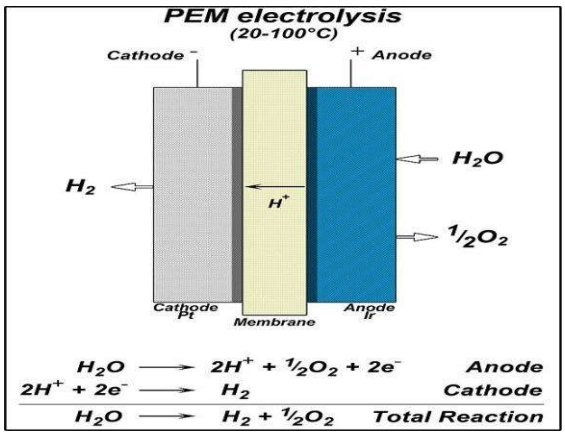

Fig. 2.5 PEM electrolysis reactions.

Usually the PEM electrolyzer utilizes a solid polymer as electrolyte (SPE) to conduct protons from the anode to the cathode while insulating the electrodes electrically.

2.5.1 Electrolyzer model

According to Faraday's law, the rate of hydrogen production is directly proportional to the electrical current in the equivalent electrolyzer circuit and it can be given by [7, 8]:

$$n_{H2} = \frac{\eta_F . \eta_G . i_e}{2F} \tag{2.17}$$

Where η_F is the Faraday efficiency, n_G is the number of electrolyzer cells in series and i_e is the electrolyzer current [A]. Generally, there is a difference between the real flow rate of hydrogen and the theoretical one defined as the Faraday's efficiency, which can be expressed as [7]:

$$\eta_F = 96.5e^{(0.09/i_e - 75.5/i_e^2)} \tag{2.18}$$

Fig. 2.6 illustrates a simple electrolyzer model that developed based on Eqs. (2.17) and (2.18).

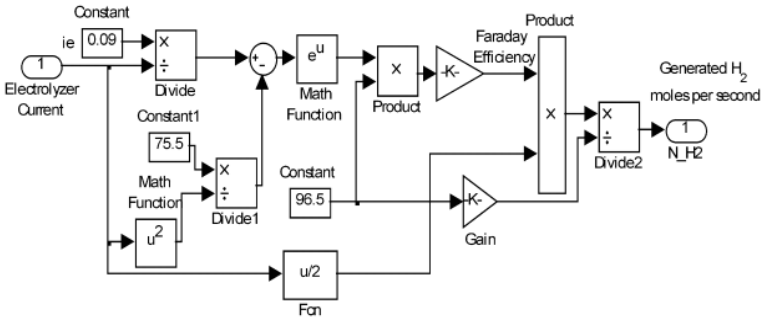

Fig. 2.6. Electrolyzer model

2.5.2 Hydrogen storage model

The Hydrogen storage system is necessary to make the balance between the hydrogen produced by the electrolyzer and consumed by the PEMFC. Eq(2.19) describes the hydrogen storage model, this model calculates the tank pressure based on the hydrogen flow. The dynamics of the storage system can be expressed as [9]:

$$P_b - P_{bi} = z\frac{N_{H2}RT_b}{M_{H2}V_b} \tag{2.19}$$

where P_b is the hydrogen tank pressure [Pascal], P_{bi} is the initial pressure of the hydrogen tank [Pascal], z is the compressibility factor as a function of pressure, N_{H2} is the hydrogen moles per second delivered to the storage tank [kmol/s], T_b is the operating temperature [K] and V_b is the volume of the tank [m^3].

In this model all supplementary power requirements such as pumps, valves were ignored. The Simulink version of the hydrogen storage model is shown in Fig. 2.7.

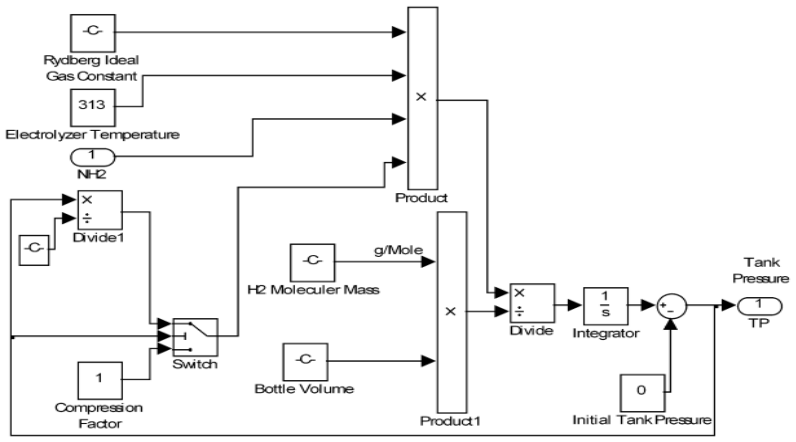

Fig. 2.7. Hydrogen storage model

2.6 Lead-acid battery and it Principle

Lead-acid batteries consist of multiple individual cells, each with a nominal voltage of 2V. Connecting the cells in series or parallel, different system voltages and capacities can be created. The Anode is lead (Pb), the cathode oxide lead (PbO_2) and electrolyte used is dilute sulfuric acid (H_2SO_4).In the discharged state both the positive and negative plates become lead sulfate ($PbSO_4$) and the electrolyte loses much of its dissolved sulfuric acid and becomes primarily water (Fig 2.8). The discharge process is driven by the conduction of electrons from the negative plate back into the cell at the positive plate in the external circuit. The total reaction can be written:

$$Pb + PbO_2 + 2H_2SO_4 \rightarrow 2PbSO_4 + 2H_2O \quad (2.20)$$

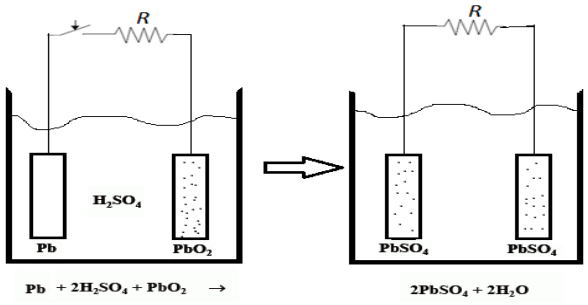

Fig. 2.8. Discharge process

2.6.1 Battery modeling

Mainly there are three types of battery models presented in the literature, specifically: experimental, electrochemical and electric circuit-based. Experimental and electrochemical models are not well suited to represent cell dynamics for the purpose of state-of charge estimations of battery packs. However, electric circuit-based models can be useful to represent

electrical characteristics of batteries. The simplest electric model consists of an ideal voltage source and a resistor r in series connection as the internal resistance. However, this model, does not take into account the battery SOC. There is another model based on an open circuit voltage in series with a resistance and parallel RC circuits with the so-called Warburg impedance [10]. The identification of all the parameters of this model is based on a rather complicated technique called impedance spectroscopy. Shepherd developed an equation to describe the electrochemical behavior of a battery directly in terms of terminal voltage, open circuit voltage, internal resistance, discharge current and state-of charge [11], and this model is applied for discharge as well as for charge. The battery was modeling based on a modified Shepherd curve fitting model, where an additional term (voltage polarization) is added to the battery discharge voltage expression to better represent the effect of the battery SOC on the battery performance. Also, to ensure the simulation stability, a filtered battery current instead of the actual battery current, is used to account for the polarization resistance. Similar to the fuel cell model, the model parameters are easily derived from datasheets or simple dynamic tests. The battery discharge voltage equation is expressed as [12]

$$V_{batt} = E_0 - R.i - K\frac{Q}{Q - it}(it + i^*) + Exp(t) \tag{2.21}$$

Where $E_0$is the battery constant voltage (V), R is the internal resistance (Ω), i is the battery current (A), k is the polarization constant (Ah^{-1}) or polarization resistance (Ohms), Q is the battery capacity (Ah), it is the actual battery charge (Ah), i^* is the filtered current (A) and $Exp(t)$ is the exponential zone voltage (V).

The term $K\frac{Q}{Q-it}it$ from Eq. 5 is referred as polarization voltage while the term $K\frac{Q}{Q-it}i^*$ is the polarization resistance (Pol_{res}). During charging, the battery voltage increases abruptly after being fully charged, this behavior is represented by modifying the polarization resistance (only during charging) as follows:

$$Pol_{res} = K\frac{Q}{it - 0.1Q} \tag{2.22}$$

As a results the charge voltage equation can be expressed as:

$$V_{batt} = E_0 - R.i - K\frac{Q}{Q - it}it - K\frac{Q}{it - 0.1Q}i^* + Exp(t) \tag{2.23}$$

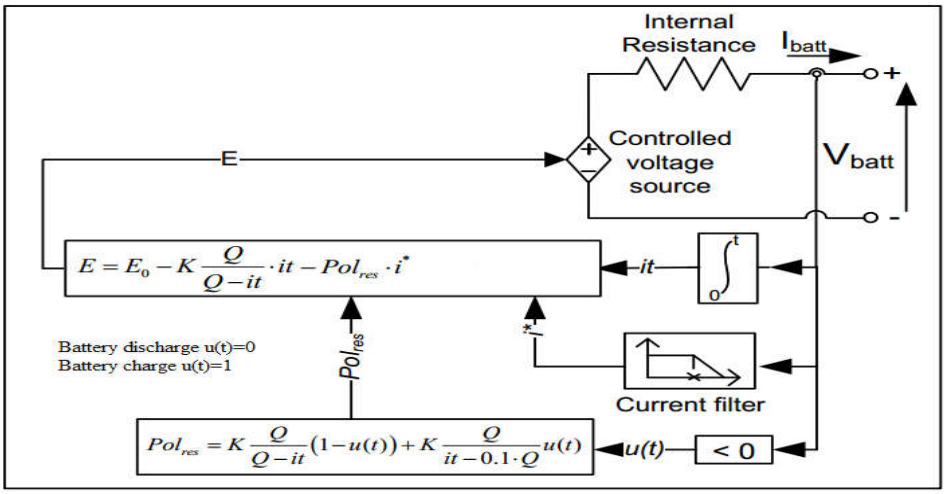

Fig 2.9. Battery model

2.7 Supercapacitor

A supercapacitor (SC) (sometimes ultra-capacitor, formerly electric double-layer capacitor (EDLC)) is a high electrochemical capacitor. It can typically store 10 to 100 times more energy per unit volume or mass than electrolytic capacitors, can accept and deliver charge much faster than batteries, and tolerate many more charge and discharge cycles than rechargeable batteries. Supercapacitor are used in applications requiring many rapid charge/discharge cycles rather than long term compact energy storage [13].

The SC is mainly designed depending on the phenomenon called electric double layer whereby electricity is stored where a solid and a liquid come into contact. Concretely, the structure of an electric double-layer capacitor involves two electrodes made by forming active carbon into thin sheets that are separated by a semi-permeable membrane called a separator and placed in an electrolyte solution such as diluted sulfuric acid (Fig 2.10). The electrodes are subjected to a low voltage (about 0.8 volts) that does not cause electrolysis of electrolyte, this therefore results in ions rapidly being stored on the surface of the active carbon [13, 14].

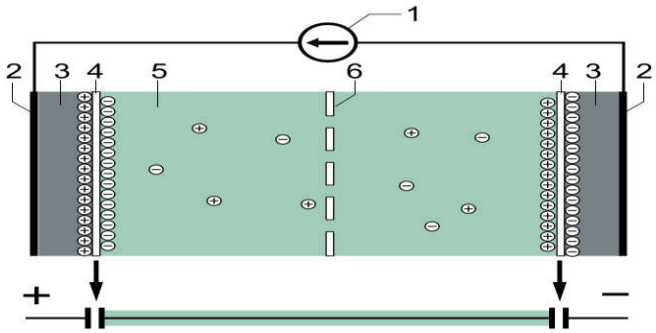

Fig 2.10 Typical construction of a supercapacitor: 1) Power source, 2) Collector, 3) Polarized electrode, 4) Helmholtz double layer, 5) Electrolyte having positive and negative ions, 6) Separator.

2.7.1 Supercapacitor model

The EL is modeled based on the Stern model, which combines the Helmholtz and Gouy Chapman models [15]. The capacitance of a SC cell can be given by [15]:

$$C = [\frac{1}{C_{GC}} + \frac{1}{C_H}]^{-1} \tag{2.24}$$

where

$$G_{GC} = \frac{FQ_c}{2N_e RT} \sinh(\frac{Q_C}{N_e^2 A_i \sqrt{8RT\varepsilon_o C}}) \tag{2.25}$$

and

$$C_H = \frac{N_e A \varepsilon_o}{d} C \tag{2.26}$$

where C_{GC} and C_H are the Helmholtz and Gouy-Chapman capacitance [F] respectively, F is the Faraday constant, Q_c is the cell electric charge [C], Ne is the number of electrode layers, R is the ideal gas constant, A_i is the interfacial area between electrodes and electrolyte [m^2] , ε and ε_o are the permittivity's (F/m) of the electrolyte material and free space respectively, C is the molar concentration [$mol.m^{-3}$] and d is the Helmholtz layer length (or molecular radius) [m]. The total capacitance of SC module consist of Np cells in parallel and Ns cells in series can be expressed as:

$$C_T = \frac{N_p}{N_s} \cdot C \tag{2.27}$$

The supercapacitor output voltage is expressed considering resistive losses as:

$$V_{SC} = \frac{Q_P}{C_T} - R_{SC} i_{sc} \tag{2.28}$$

with

$$Q_T = N_P Q_c \int i_{sc} dt \tag{2.29}$$

where Q_T is the total electric charge [C], R_{SC} is the super capacitor module resistance (Ω) and i_{SC} is the super-capacitor module current [A].

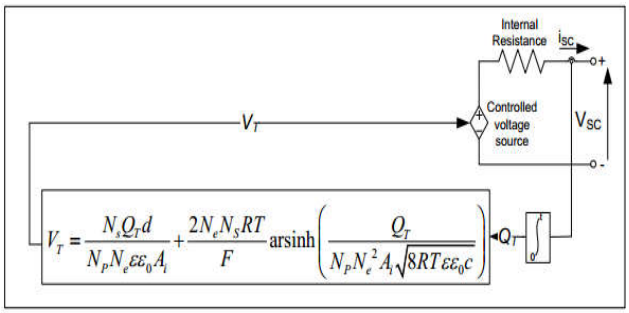

Fig. 2.11. Supercapacitor model

The MATLAB simulation parameters of the SC are summarized in Table 2.3.

Table 2.3. SC MATLAB simulation parameters

Parameters	Value
Rated capacitance (F)	80
Equivalent DC series resistance (Ohms)	2.1e-3
Rated voltage (V)	120
Number of series capacitors	4
Number of parallel capacitors	1
Initial voltage (V)	120
Leakage current (A)	5.2e-3
Operating temperature (Celsius)	25
Number of layers	6
Molecular radius (m)	1.23e-9
Over potential (V)	0.3
Charge transfer coefficient alpha	0.3

2.8 Modeling of the power converters

2.8.1 Modeling of the DC-DC bidirectional converter

The bi-directional DC-DC buck-boost converter is used to interlink the battery with the DC bus. Fig 2.12 shows the power circuit and the voltage-current direction for boost-buck operation mode of the converter. Each mode of operation is characterized with two intervals coincide with the conducting of appropriate IGBT or diode [16, 17].

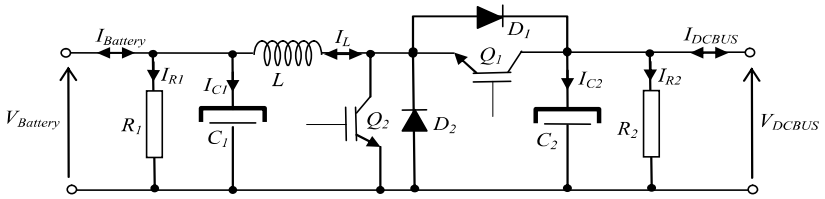

Fig. 2.12. Voltages and currents for the bi-directional buck-boost DC-DC converter.

In boost mode of operation the IGBT Q1 is in OFF condition. The IGBT Q2 is conducting through the first interval and the diode D1 is conducting during the second interval, choosing the voltage over the capacitor V1, V2 and the current through the inductor as state variable the average model can be given as follows:

$$\begin{cases} \dfrac{dV_1}{dt} = \dfrac{I_1}{C_1} - \dfrac{V_1}{C_1 R_1} - \dfrac{I_2}{C_1} \\ \dfrac{dI_2}{dt} = \dfrac{V_1}{L} - \dfrac{V_2}{L}(1-\alpha_2) \\ \dfrac{dV_2}{dt} = \dfrac{I_2}{C_2}(1-\alpha_2) - \dfrac{V_2}{C_2 R_2} - \dfrac{I_3}{C_2} \end{cases} \tag{2.30}$$

In buck mode of operation the IGBT Q2 is in oFF condition. The IGBT Q1 is conducting through the first interval and the diode D2 is conducting during the second interval, the state average model can be given as follows:

$$\begin{cases} \dfrac{dV_1}{dt} = -\dfrac{I_1}{C_1} - \dfrac{V_1}{C_1 R_1} + \dfrac{I_2}{C_1} \\ \dfrac{dI_2}{dt} = \dfrac{V_1}{L}\alpha_1 - \dfrac{V_2}{L} \\ \dfrac{dV_2}{dt} = -\dfrac{I_2}{C_2}\alpha_1 - \dfrac{V_2}{C_2 R_2} + \dfrac{I_3}{C_2} \end{cases} \tag{2.31}$$

With: $I_1 = I_{Battery}$; $I_2 = I_L$; $I_3 = I_{DCBUS}$; $V_1 = V_{Battery}$; $V_2 = V_{DCBUS}$

2.8.2 Boost Converter Modeling

The PV panel and the FC are connected to the DC bus through a DC-DC boost power converter, which achieves the PV and the FC control. The boost converter electric scheme is illustrated in Fig. 2.13.

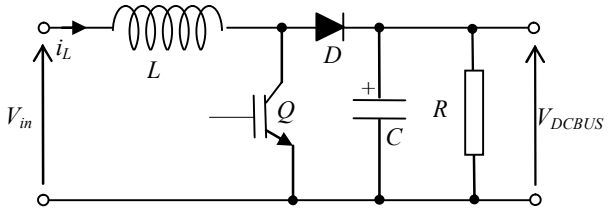

Fig. 2.13. DC-DC Boost Converter

The state space average equations are used to model the converter as expressed in (30). By assuming continuous conduction mode, the state space average equations can be written on the time interval ($0 < t < T$) as follows:

$$\begin{cases} \dot{x}_1 = \lambda_1 V_{in} - \lambda_1 x_2 u \\ \dot{x}_2 = \lambda_2 x_1 u - \lambda_3 x_2 \end{cases} \quad (2.32)$$

Where $\lambda_1 = \frac{1}{L}; \lambda_2 = \frac{1}{C}; \lambda_3 = \frac{1}{RC}; u = (1-\alpha)$ and $[x_1 \quad x_2] = [i_L \quad V_{DCBUS}]$.T is the switching period and α is the duty cycle.

2.8.3 Buck Converter Modeling

The electrolyzer is connected to the DC bus through a DC-DC buck power converter (Fig. 2.14), which achieves its control. The state space average equations are used to model the converter as expressed in (2.33).

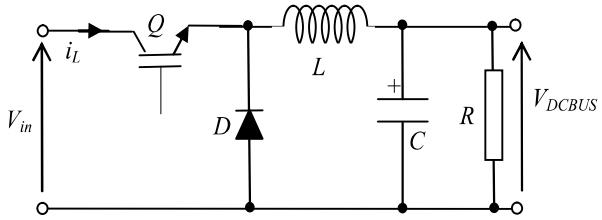

Fig. 2.14. Buck converter

$$\begin{cases} \dot{x}_1 = \lambda_1 V_{in} u - \lambda_1 x_2 \\ \dot{x}_2 = \lambda_2 x_1 - \lambda_3 x_2 \end{cases} \quad (2.33)$$

where $\lambda_1 = \frac{1}{L}; \lambda_2 = \frac{1}{C}, \lambda_3 = \frac{1}{RC}$; u= α and $[x_1 \quad x_2] = [i_L \quad V_{DCBUS}]$

2.8.4 DC/AC converter model

A mathematical model of a three-phase voltage-source inverter (VSI) is presented based on a functional representation (Fig. 2.15). The inverter can be controlled using a switching function C_i {*i= A, B, C*}, according to the following conditions [18, 19]:

- if $C_i = 1$, then K_i is OFF et $K_i^{'}$ is ON
- if $C_i = 0$, then K_i is ON et $K_i^{'}$ is OFF.

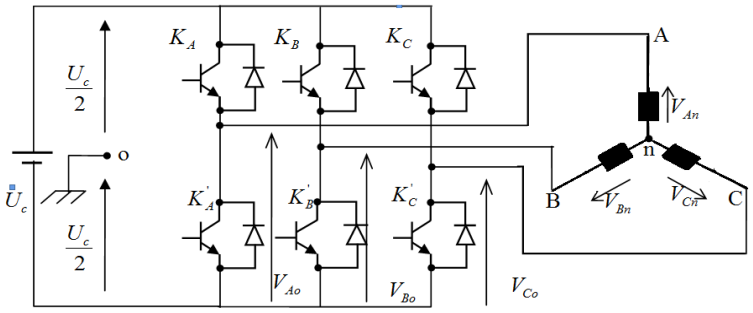

Fig. 2.15. Power circuit of a three-phase VSI.

At the outputs of the inverter the line-to-line voltages U_{AB} , U_{BC} , U_{CA} can be derived as [18]:

$$\begin{cases} U_{AB} = V_{Ao} - V_{Bo} \\ U_{BC} = V_{Bo} - V_{Co} \\ U_{CA} = V_{Co} - V_{Ao} \end{cases} \tag{2.34}$$

Since the phase voltages in a star connected load sum to zero, we can obtain the following relationship:

$$\begin{cases} V_{An} = 1/3[U_{AB} - U_{CA}] \\ V_{Bn} = 1/3[U_{BC} - U_{AB}] \\ V_{Cn} = 1/3[U_{CA} - U_{BC}] \end{cases} \tag{2.35}$$

Phase-to-neutral voltages of a star-connected load are most easily found by defining a voltage difference between the star point *n* of the load and the negative rail of the dc bus *o*. Then the following correlation holds true:

$$\begin{cases} V_{An} + V_{no} = V_{Ao} \\ V_{Bn} + V_{no} = V_{Bo} \\ V_{Cn} + V_{no} = V_{Co} \end{cases} \tag{2.36}$$

And we can deduce that:

$$V_{no} = \frac{1}{3}\left(V_{Ao} + V_{Bo} + V_{Co}\right) \tag{2.37}$$

For ideal switching, the following relation can be obtained:

$$V_{io} = C_i U_c - \frac{U_c}{2} \tag{2.38}$$

With

$$\begin{cases} V_{Ao} = \left(C_A - 0.5\right)U_c \\ V_{Bo} = \left(C_B - 0.5\right)U_c \\ V_{Co} = \left(C_C - 0.5\right)U_c \end{cases} \tag{2.39}$$

Substitution of (2.37) into (2.36) yields phase-to-neutral voltages of the load in the following form [30]:

$$\begin{cases} V_{An} = \frac{2}{3}V_{Ao} - \frac{1}{3}V_{Bo} - \frac{1}{3}V_{Co} \\ V_{Bn} = -\frac{1}{3}V_{Ao} + \frac{2}{3}V_{Bo} - \frac{1}{3}V_{Co} \\ V_{Cn} = \frac{-1}{3}V_{Ao} - \frac{1}{3}V_{Bo} + \frac{2}{3}V_{Co} \end{cases} \quad (2.40)$$

Replacing (2.39) with (2.40), we obtain the following relation:

$$\begin{bmatrix} V_{An} \\ V_{Bn} \\ V_{Cn} \end{bmatrix} = \frac{1}{3}.U_c \begin{bmatrix} 2 & -1 & -1 \\ -1 & 2 & -1 \\ -1 & -1 & 2 \end{bmatrix} \begin{bmatrix} C_A \\ C_B \\ C_C \end{bmatrix} \quad (2.41)$$

The inverter specifications are summarized in Table 2.4. The inverter control is implemented using Proportional-Integral controller using PWM techniques [20].

Table 2.4. Inverter specifications

Parameters	Value
$P_{nominal}$	2.5kW
P_{max}	2.7kW
Peak inverter efficiency	94-95.3%
Output frequency	49.8-50.2Hz

2.9 Conclusion

This chapter presented the system components description and modeling. The appropriate model for each component in the hybrid system was chosen. It started with the description and modulation of the PV cell, then the hydrogen system was fully described and modeled. Finally the different power converter that used in the power flow control within the system was modeled.

2.10 References

[1] Feroldi D, Rullo P, Zumoffen D. Energy management strategy based on receding horizon for a power hybrid system. Renewable Energy 2015; 75: 550-559.

[2] Alnejaili T, Drid S, Mehdi D, Chrifi-Alaoui L. Advanced Strategy of Demand-Side Management for Photovoltaic-Wind Energy System. The 15th International conference on Sciences and Techniques of Automatic control & computer engineering 2014, Hammamet-Tunisia,797-802.

[3] Jay T, Anna G, Peng H. Control of Fuel Cell Power Systems Principles, Modeling, Analysis and Feedback Design. Spring, London 2004.

[4] Padulles J, Ault G.W, McDonald J.R. An integrated SOFC plant dynamic model for power systems simulation. Journal of Power Sources 2000; 86(2):495–500.

[5] Lajnef T, Abid S, Ammous A. Modeling, Control, and Simulation of a Solar Hydrogen/Fuel Cell Hybrid Energy System for Grid-Connected Applications. Advances in Power Electronics 2013; 13:1-7.

[6] El-Shark MY, Rahman A, Alam MS, Byrne PC, Sakla AA, Thomas T. A dynamicmodel for a stand-alone PEM fuel cell power plant for residential applications. Journal of Power Sources 2004; 138(2):199–204.

[7] Ganguly A, Misra D, Ghosh S. Modeling and analysis of solar photovoltaic-electrolyzer-fuel cell hybrid power system integrated with a floriculture greenhouse. Energy and Buildings 2010; 42:2036–2043.

[8] Ulleberg O. Stand-alone power systems for the future: optimal design, operation and control of solar-hydrogen energy systems. A *Dissertation Submitted* in *Partial Fulfillment* of the *Requirements* for the *Degree* of Doctor of Philosophy in Electrical *Engineering*, Norwegian University of Science and Technology, USA 1998.

[9] Gorg H. Dynamic modeling of a proton exchange membrane (PEM) electrolyzer. International Journal of Hydrogen Energy 2006; 31:29–38.

[10] Mukund R. Wind and Solar Power Systems. Merchant Marine Academy Kings Point. NewYork 1999

[11] Tremblay O, Dessaint L, Dekkiche A. A Generic Battery Model for the Dynamic Simulation of Hybrid Electric Vehicles. *IEEE Vehicle Power Propulsion Conf* 2007. 284-289.

[12] Njoya S, Dessaint L, Al-Haddad K. A Comparative Study of Energy Management Schemes for a Fuel Cell Hybrid Emergency Power System of More Electric Aircraft. IEEE Transactions on Industrial Electronics 2014; **61**(3): 1320 - 1334.

[13] Namisnyk A. A survey of electrochemical supercapacitor technology. submitted in partial fulfillment of the requirement for the Degree of Bachelor of Engineering. University of Technology, Sydney,2003.

[14] BELHACHEMI F. Modelisation et caracterisation des supercondensateurs a couche double electrique utilises en electronique de puissance. A Dissertation Submitted *in* Partial Fulfillment *of the* Requirements *for the* Degree of Doctor of Philosophy in Electrical *Engineering* ,Sidi Bel Abbes, Algérie 2001.

[15] Oldham K.B. A Gouy-Chapman-Stern model of the double layer at a (metal)/(ionic liquid) interface," *J. Electro analytical Chem 2008*, 613(2):131-138.

[16] Cultura A, Salameh Z. Design and Analysis of a 24 VDC to 48 VDC Bidirectional DC-DC Converter Specifically for a Distributed Energy Application. Energy and Power Engineering 2012; 4(5):315-323.

[17] Patel J, Chandwani H, Patel V, Lakhani H. Bi-directional DC-DC Converter for battery charging- discharging Applications using Buck-Boost switch. IEEE Students' Conference on Electrical, Electronics and Computer Science (SCEECS) 2012, Bhopal, 1-4.

[18] Iqbal A, Lamine A, Ashraf I, bulla M. Matlab/simulink model of space vector pwm for three-phase voltage source inverter. Proceedings of the 41st International Universities Power Engineering Conference 2006, Newcastle-upon-Tyne, 1096-1100.

[19] BK L, Ehsani M. A simplified functional model for 3-phase voltagesource inverter using switching function concept. The 25th IEEE Annual Conference of the Industrial Electronics Society IECON 1999, San Jose, 462-467.

[20] Nachiappan A, Pondicherry E.C, Puducherry I, Sundararajan K, Malarselvam V. Current controlled voltage source inverter using Hysteresis controller and PI controller. International Conference on Power, Signals, Controls and Computation (EPSCICON) 2012, Kerala, 1-6.

[21] Gao L, Dougal R.A, Liu S. Power enhancement of an actively controlled battery/ ultracapacitor hybrid. IEEE Transactions on Power Electronics 2005; 20:236–43.

Chapter 3

Demand Side Management Techniques

3.1 Introduction

This chapter presents briefly the different techniques of demand side management (DSM). The background information of different DSM technique is firstly described. Including objectives, methods, and current research status. The review of the appliance level of DSM for various types of demands from statistical, simulated, and monitored sources is also reported. Moreover an economical analyze of the different economical terms that used in the economic optimization is presented.

3.2 demand side management strategies

Mainly there are three demand side strategies that able to influence load demand which are peak load management, demand response and energy efficiency [1]. These different strategies achieve load reduction throughout different methods such as, energy savings, energy carrier switching or self-generation (distributed generation), and load management. The next section will explain in detail the different demand side strategies.

3.2.1 Load Management

Load management programs aims to manage the power on the demand side by using various economic and technical measures to reshape the load curve into the target curve [2, 3]. The purpose of load management techniques is to reduce peak demand to level daily, seasonal or annual electricity demand. The techniques help to economize system operation by making best use of its available generation and transmission (network) capacity. It could be implemented on a daily basis, by limiting the demand or shifting the usage from peak to off-peak periods, or even on weekly by shifting the usage from weekday to weekend. Load management could reshape the load curve to achieve the purpose of cost-effective operations within electricity networks. At the same time it reduces the users' electricity bills. Six load shape objectives for load management programs are stated in the literature, which are categorized under basic level [4, 5].

***a)* Peak clipping**

Peak clipping is considered to be one of the most traditional forms of load management, mainly it used to reduce the system peak loads during short usage peaks. Generally the peak clipping is achieved by using Direct Load Control (DLC) method. In a grid connected system the utility have a direct control over customers' appliance. Which allow it to control directly the loads when there is not enough generating capacity to satisfy maximum demand during peak times. Therefore in grid off power system the control can be achieved manually or by automatic system. As a results the shape of the load profile will be modified as shown in the Fig. 3.1(a).

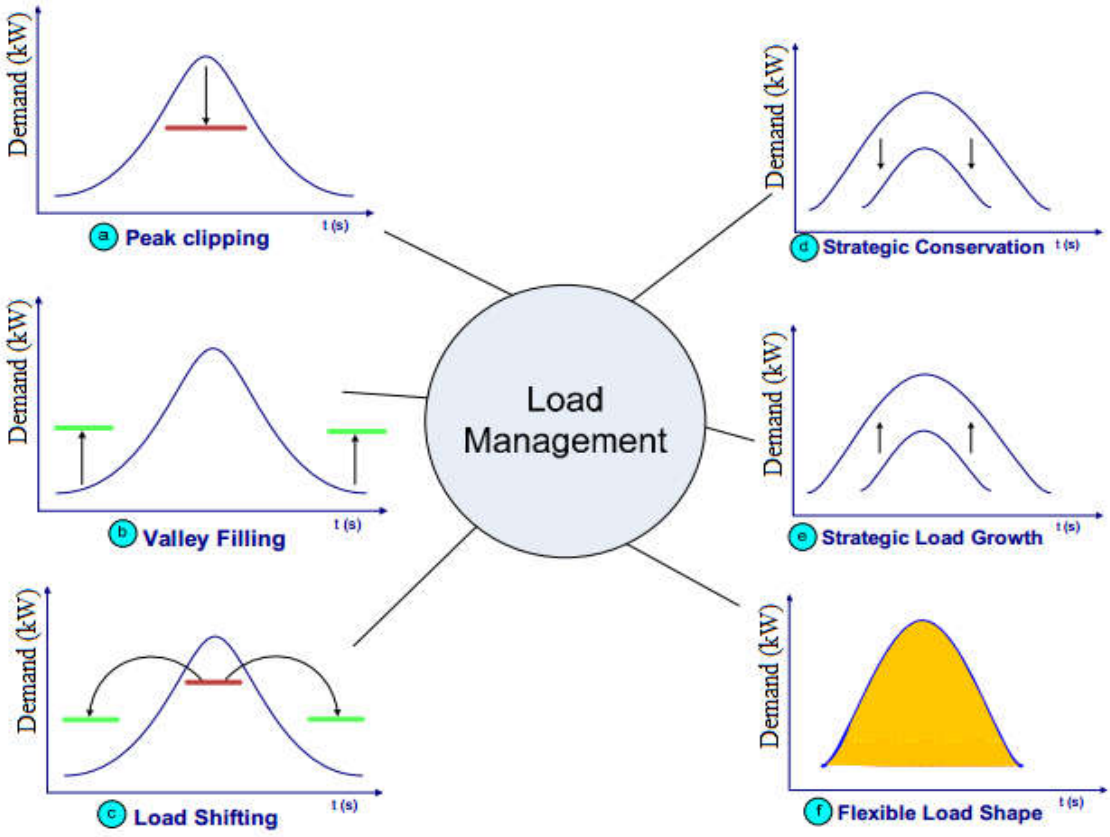

Fig. 3.1. Load control strategies

b) Valley filling

Valley filling is another classic techniques of load management, is mainly builds the loads during the off-peak period. Valley filling can be achieved in many ways, the most popular one is by the utilization of electric-based thermal energy storage (water and / or space heating or cooling). The shape of a load profile through the valley filling technique is given in **Fig. 3.1(b).**

c) Load shifting

Load shifting technique combines the benefits of peak clipping and valley filling by moving existing loads from on-peak hours to off-peak hours without necessarily changing the overall energy consumption, through which peak clipping and valley filling can be achieved at the same time. Popular applications include the use of storage water heating, storage space heating, and cold storage. The shape of a load profile using load shifting techniques is shown in **Fig. 3.1(c).**

d) Strategic conservation

Strategic conservation is classified as an advanced load management options. It decreases the overall load demand by increasing the efficiency of energy use, for example replacing regular light bulbs with compact fluorescent light bulbs. This technique reduces the demand not only during peak hours but also at other hours of the day. The shape of a load profile through the strategic conservation technique is shown in **Fig. 3.1(d)**.

e) Strategic load growth

Strategic load growth increased electric energy use either to replace inefficient fossil-fuel equipment at point of use or to improve consumer productivity and quality of life the shape of a load profile through the strategic load growth technique is shown in **Fig. 3.1(e)**.

f) Flexible load shape

Flexible load shape is a concept related to the reliability of energy supply with the possibility of variably controlling customers' equipment. The shape of a load profile through the flexible load shape technique is illustrated in **Fig. 3.1(f)**.

3.2.2 Demand Response

Demand response is a dynamic real time loads control. It is normally not set up as a daily action, but takes place when there is a specific situation at the production or transmission side. The main objective of DR is to handling emergency situations and preventing blackouts. DR requires dynamic control capability, to shed the loads or shift them to other periods. The Demand Response automation can be classified in three types [6, 7, 8]:

Manual Demand Response - involves manually turning off lights or equipment; this can be a labor-intensive approach.

Semi-Automated Response - involves the use of building energy management control systems for load shedding, where a preprogrammed load shedding strategy is initiated by facilities staff.

Fully-Automated Demand Response - initiated at a building or facility through receipt of an external communications signal; specialists set up a pre-programmed load shedding strategy which is automatically initiated by the system without the need for human intervention.

3.2.3 Energy efficiency

Energy efficiency is mainly objectives to decrease the demand throughout an efficient use of energy. For example, use of more efficient lighting bulbs and develops an energy-efficient building envelopes and systems (appliances), as well as energy conscious behavior by users. These actions reduces average fuel cost and can postpone the need for future additional power capacity. Energy efficiency and savings strategies are usually assessed on a daily and/or weekly basis for systems benefit.

3.2.4 Link between DR and energy efficiency

The direct response, the load management and the Energy efficiency techniques are very similar in their strategies and methods. The main difference is that the LM strategy that operates on a “regular” basis (daily or weekly according to preset strategy), while DR normally responds

to “emergency” situations in the system ,or in the another word it's a dynamic real time loads control that takes place when there is a specific situation at the production or transmission side. Furthermore the Energy efficiency is lower energy use to provide the same level of service throughout an efficient use of energy [9].

3.3 Analyzing load demand

The load demand is the total electrical power used by a building at a given moment. The load changes with time in response to changes in lighting levels; heating, ventilating, and air conditioning (HVAC) requirements; and uses such as computers, copy machines, and so on. The curve that represents load as a function of time, called the “load shape,” that can refer to a number of different forms of data. It can refer to demand and consumption data or it can be a reference to derived data types, such as regression and profile coefficients. However, all these data types have one thing in common; that they represent the pattern of electricity usage of a segment of supply market customers. Load demand and its variation (called the ‘profile’) depend on several factors:

- Consumer type (household, commercial, industry, etc.)
- Consumer installations (building envelope, existing HVAC systems, appliances and equipment)
- Climate (outdoor temperature, daylight, wind)
- Behavioral factors (consumption patterns, habits, etc.)

In a standalone power system, accurate models for electric power load forecasting are essential to an efficient operation of the power system. Use this information to plan how much power they will need to generate at any given time. The load demand conditions are usually described and analyzed by using several established terms, such as load curve, typical load curve, load duration curve, load factor, superposition factor [10].

3.3.1 Load curve

Load curve shows the pattern of demand (average value) during a specific period. The load curve can be constructed based on a different time period. Fig. 3.2 illustrates an example load curve based on half hourly mean values of energy usage across a day, while Fig. 3.3 illustrates an example load curve based on a day mean values of energy usage across a year.

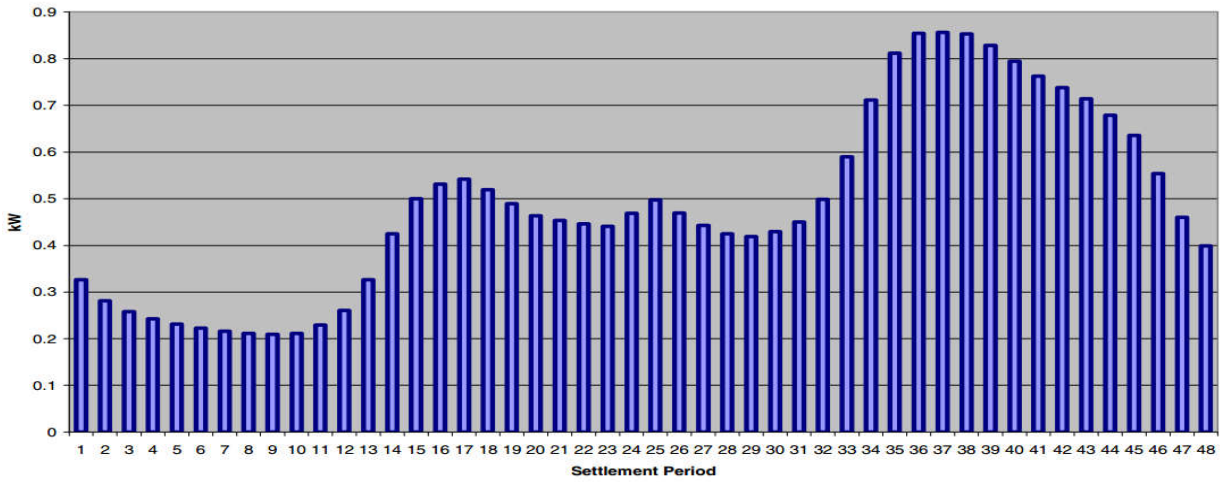

Fig. 3.2. Daily pattern of demand in kW based on Half Hourly mean values

Moreover the shape of the load curve depend on many factor including, weather factors, seasonal load change, annual load growth and the latest daily load change.

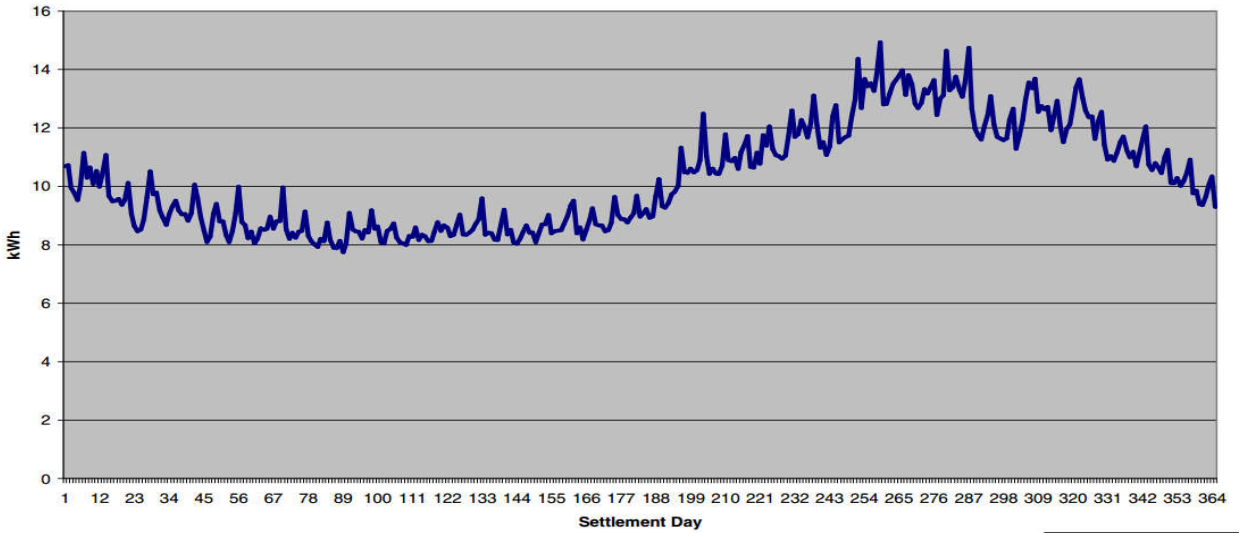

Fig. 3.3. Shows the yearly pattern in kWh per Day.

3.3.2 Load duration curve

The load duration curve (LDC, Fig. 3.4) reflects the activity of a population quite accurately with respect to electrical power consumption over a given period of time. A load duration curve illustrates the variation of a certain load in a downward form such that the greatest load is plotted

in the left and the smallest one in the right. On the time axis, the time duration for which each certain load continues during the day is given. The LDC has principle characteristic including:

- It generally used in electric power generation to illustrate the relationship between generating capacity requirements and capacity utilization.
- It can be used in reliability and feasibility assessment.
- The energy consumption is represented by the area under LDC.
- A LDC is similar to a load curve but the demand data is ordered in descending order of magnitude, rather than chronologically.

Similarly to LDC a price duration curve shows the proportion of time for which the price exceeded a certain value.

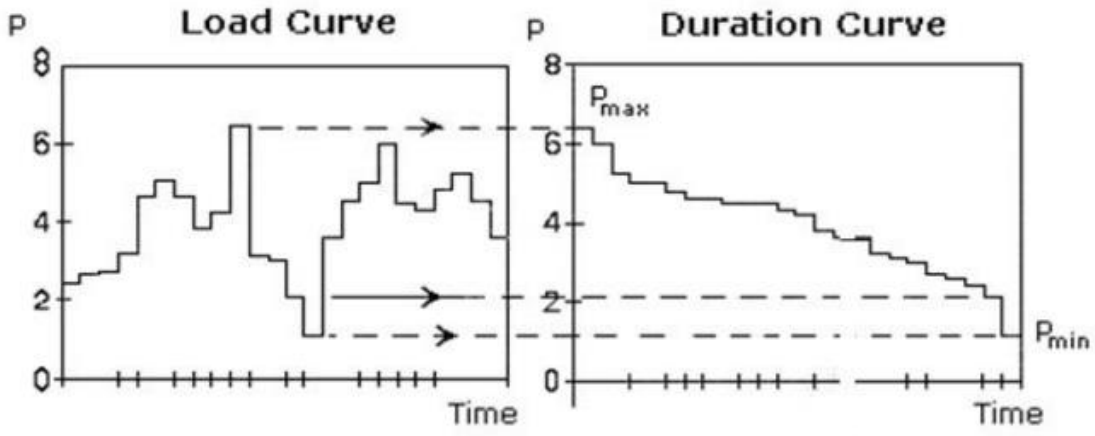

Fig. 3.4. Load curve and load duration curve

3.3.3 Peak demand

Peak demand, peak load or on-peak are terms that describing a period in which electrical power is expected to be provided for a sustained period at a significantly higher than average supply level. Peak demand fluctuations may occur on daily, monthly, seasonal and yearly cycles. For an electric utility company, the actual point of peak demand is a single half hour or hourly period which represents the highest point of customer consumption of electricity.

3.3.4 Load factor

The load factor is measured as the degree of variation of load [L (t)] over a period of time, and can be defined as the ratio of average demand to maximum demand during a given period

$$LF = \frac{Load_{average}}{Load_{max}} \tag{3.1}$$

Where

$$L_{av} = \frac{Energy(consumed)}{total\ time\ (h)} = \frac{E}{h} \tag{3.2}$$

The load factor may be used to demonstrate variations of the household's load demand. This factor can range between 0 and 1, where a value of 1 would indicate that the household load curve was completely flat during the period considered and no peaks were present.

3.3.5 Superposition factor

Superposition describes the contribution of a partial load to the total load. Superposition factor SF is the ratio of the consumer's partial load demand, ΔP_{max} during the total network peak and the maximum partial load P_{max} during the same time period, as it is expressed in Fig. 3.5 and equation (3.3).

$$SF = \Delta P_{max}/P_{max} \tag{3.3}$$

Where:
ΔP_{max} = increase of total load peak value due to partial load p (kW),
P_{max} = partial load maximum value (kW).

The range of values that this factor can take is between 0 and 1, where a value of 1 would indicate, that the peak of the partial load coincided with the peak of total load.

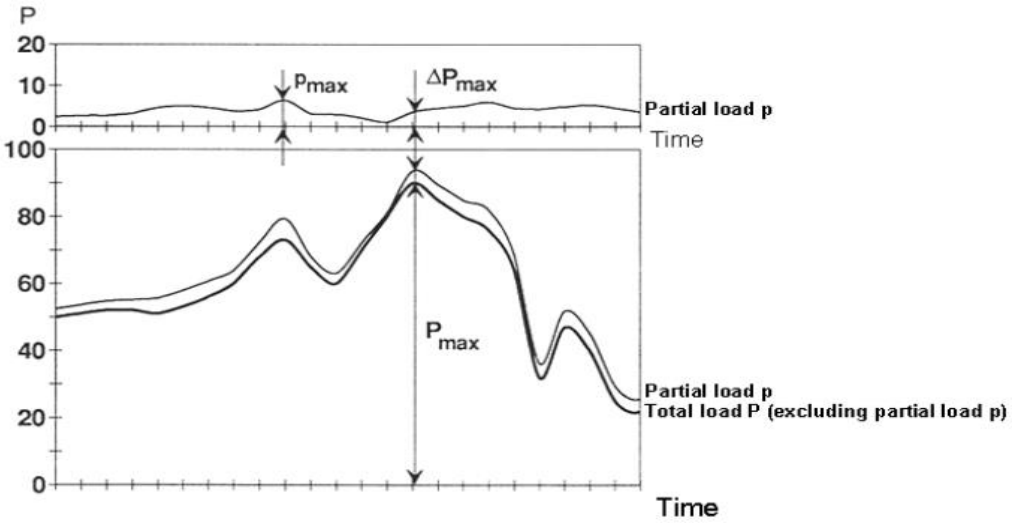

Fig. 3.5. Superposition and superposition factor

3.3.6 Loads operation parameters

There are several parameters that describe the load operation including:

a) Shiftable or non-shiftable

This depends on the properties of the demand. Some loads with fixed operating durations such as washing machines, microwaves, and dishwashing machines etc. are shiftable, whereas other loads, for instance lighting, cannot be shifted [11].

b) Load flexibility (whole or partial)

Another parameter to be defined is the flexibility of demand profile. The demand profile for a certain load represents the energy use pattern during its operating period. Here the question of whether the total demand or only part of it can be shifted during the control period poses itself. The answer significantly affects the load shifting strategy. The options are available to define part of the demand through the start time to the end time of the profile are provided [12].

c) Shifting increment

This parameter defines how the specified load is shifted, which will affect the results of the match between the total demand and supply curve. The optimal match results of a certain combination of demand and supply are different if the loads are shifted with a smaller increment.

It is more accurate to shift the loads at lower times. However, this means it would take longer to obtain the results [12].

3.4 Economical analyze of the system

The economical analyze is a critical factor in the hybrid power system designing. It's very important to economically optimize each configuration of a hybrid power system. Moreover the economical analyze is very important to evaluate the economic benefit of the proposed DSM. The hybrid power systems and the proposed DSM strategy are economically analyzed according to total net present cost (NPC), as it has a simple mathematical concept and can give a precise overview of the different costs of the system. However before give a definition of the NPC an important parameters influencing the NPC must be defined.

3.4.1 Costs analyze parameters

a) The capital recovery factor

The capital recovery factor is a ratio used to calculate the present value of an annuity (a series of equal annual cash flows). It can be expressed as:

$$CRF(i,N) = \frac{i(1+i)^N}{(1+i)^N - 1} \tag{3.4}$$

Where i is the real interest rate and N is the number of years.

b) The interest rate

It is the discount rate used to convert between one-time costs and annualized costs. The annual real interest rate is related to the nominal interest rate by the equation given below.

$$i = \frac{i' - f}{1+f} \tag{3.5}$$

Where i' nominal interest rate (the rate at which you could get a loan) and f *is* annual inflation rate

c) Sinking Fund Factor

The sinking fund factor is a ratio used to calculate the future value of a series of equal annual cash flows. The equation for the sinking fund factor is:

$$CRF(i,N) = \frac{i}{(1+i)^N - 1} \tag{3.6}$$

d) Salvage Value

Salvage value is the value remaining in a component of the power system at the end of the project lifetime. Usually is assumed linear depreciation of components, meaning that the salvage value of a component is directly proportional to its remaining life. It is also assumed that the salvage value is based on the replacement cost rather than the initial capital cost. This is expressed mathematically as:

$$S = C_{rep} \cdot \frac{R_{rem}}{R_{comp}} \tag{3.7}$$

Where C_{rep} is the replacement cost [$],$R_{comp}$ is the project lifetime [yr] and R_{rem} is the remaining life of the component at the end of the project lifetime and it can be given by:

$$R_{rem} = R_{comp} - (R_{proj} - R_{rep}) \tag{3.8}$$

Where R_{rep} is the replacement cost duration and is given by:

$$R_{rep} = R_{comp} \cdot INT\left(\frac{R_{proj}}{R_{comp}}\right) \tag{3.9}$$

Where R_{proj} is the project lifetime [yr] and INT is the integer function, returning the integer portion of a real value. The integer function does not round up. For example, INT (4.27) = 4, and INT(6.92) = 6.

e) Total Annualized Cost

The annualized cost of a component is equal to its annual operating cost plus its capital and replacement costs annualized over the project lifetime. The annualized cost of each component is equal to the sum of its:

- **annualized capital cost**

The initial capital of each component over the project lifetime is annualized to calculate its annualized capital cost, which can be expressed as:

$$C_{acap} = C_{cap} \cdot CRF(i, R_{proj}) \tag{3.10}$$

Where $C_{cap}$the total is installed cost of all system component at the beginning of the project

- **annualized replacement cost**

The annualized replacement cost of a system component is the annualized value of all the replacement costs occurring throughout the lifetime of the project, minus the salvage value at the end of the project lifetime. It can be calculated as:

$$C_{arep} = C_{rep} \cdot f_{rep} \cdot SFF\left(i, R_{comp}\right) - S \cdot SFF(i, R_{proj}) \tag{3.11}$$

Where C_{rep} is the cost of replacing a component at the end of its lifetime and f_{rep} is a factor arising because the component lifetime can be different from the project lifetime, and is given by:

$$f_{rep} = \begin{cases} \dfrac{CRF\left(i, R_{proj}\right)}{CRF\left(i, R_{rep}\right)} & , R_{rep} > 0 \\ 0 & , R_{rep} = 0 \end{cases} \tag{3.12}$$

- **Annual O&M cost**: which represent all operating and maintenance costs throughout the project.
- **Annual fuel cost (if applicable)**

3.4.2 Total Net Present Cost

The total net present cost of a system is the present value of all the costs that it incurs over its lifetime, minus the present value of all the revenue that it earns over its lifetime. Costs include

capital costs, replacement costs, O&M costs, fuel costs, emissions penalties, and the costs of buying power from the grid. Revenues include salvage value and grid sales revenue.

$$C_{NPC} = \frac{C_{ann,tot}}{CRF(i, R_{proj})} \tag{3.13}$$

3.5 conclusion

This chapter presented the different techniques of demand side management (DSM). The review of the appliance level of DSM for various types of demands from statistical, simulated, and monitored sources was also reported. Moreover an economical analyze of the different economical terms that used in the economic optimization was presented.

3.6 References

[1] Bellarmine G., 2000, Load Management Techniques, Electronic Engineering Technology, Florida A&M University.

[2] Abaravicius, J., 2004, Load Management in Residential Buildings. Considering Techno-Economic and Environmental Aspects. Licentiate thesis. ISRN LUTMDN/TMHP—04/7024—SE, Department of Heat and Power Engineering, Lund University, Lund.

[3] Zhaoguang Hu, Xinyang Han, Quan Wen et al. Integrated Resource Strategic Planning and Power Demand-Side Management. Springer 2013.

[4] Ackermann et al. 2001, Distributed generation: a definition, Electric Power Systems Research 57 (2001) 195-204.

[5] Braithway, S.D., Eakin, K., 2002, the Role of Demand Response in Electric Power Market Design, Edison Electric Institute, Washington DC.

[6] DEFG-CAEM, 2005, A Critical Examination of Demand Response Programs at the ISO Level: End Goals, Implementation and Equity, Distributed Energy Financial Group, LLC and the Center of Advancement of Energy Markets, Washington DC.

[7] DRRC, 2005, Personal communications at the Demand Response Research Center, LBNL. April 2005.

[8] Kiliccote, S., Piette, M.A., 2005, Advanced Control Technologies and Strategies Linking Demand Response and Energy Efficiency,ICEBO 2005 Conference Paper, LBNL58179.

[9] Piette M.A. Development and Evaluation of Fully Automated Demand Response in Large Facilities, California Energy Commission and Demand Response. Research Center PIER Collaborative Report, 2005, Berkeley.

[10] Sernhed, K. 2004. Effects of load. Electricity use and load management in electrically-heated detached (houses from customer and utility viewpoints. Case studies). ISRN LUTMDN/TMHP-04/7025-SE Department of Heat and Power Engineering, Lund University, Lund, Sweden.

[11] Liangyi S. Real-time pricing algorithm considering load identification for smart grid. PES IEEE Conference & Exposition, 2014. National Harbor, 1-5.

[12] Tooraj J. Michael G. The Future of Electricity Demand: Customers, Citizens and Loads. Cambridge University Press 2011.

Chapter 4

Power flow management and dynamic controllers design

4.1 Introduction

This chapter briefly presents the proposed energy management system (EMS). Moreover it describes the dynamic controller's design of the different subsystem components. Firstly the appropriate control of the different DC-DC converters is designed. This is followed by adscription of the proposed energy management system. Finally the validation of the system by simulation is presented, using models implemented in Matlab/Simulink software.

4.2 Hybrid system management and control methodology

In the integrated power system, the power flow between the different sources is controlled by a central controller. It provides overall control of the power system and sets the power reference for the different converters that control the power system components. Moreover, the main controller cooperates with a local loads controller, which controls the different loads, according to the energy balance of the system. It can reduce a part of the home power demand when the system is under stress by disconnecting the offered controllable loads.

4.3 Dynamic controller design

Because of it fast response in the transient power and the possibility of working with a constant or variable frequency, a Sliding Mode Control (SMC) has been chosen for the DC-DC bidirectional battery converter and the MPPT converter of the PV panel. The following section presents an over view of SMC then the specific control of each subsystem will be presented.

4.3.1 SMC general principle

SMC is a nonlinear control solution and a variable structure control (VSC) derived from the variable structure system theory. It was proposed by Vadim UTKIN in (1977) [2]. SMC is known to be robust against modeling inaccuracies and system parameters fluctuations. It was successfully applied to electric motors, robot manipulators, power systems and power converters (Utkin, 1996). The design of the control can be realized in three main steps very dependent on one another:

- The choice of the surface.
- The establishment of existence of the convergence conditions.
- The determination of the control law.

A fairly general form is given by Stalin to determine the sliding surface that ensures the convergence of the controlled variable and it is given by:

$$s(x,t) = \left(\frac{d}{dt} + \beta\right)^{r-1} e(t)\, dt \tag{4.1}$$

Where

e(t): is the error between the variable and its reference to settle, β is a positive constant chosen by the designer and r is the degree relative, (times it takes derive the surface to reveal the Command.

The purpose of the order is to maintain the trajectories on the sliding surface in order to eliminate the error and to impose the chosen dynamics [3]. Let us consider the nonlinear system represented by the following state equation:

$$\dot{x} = f(x,t) + g(x,t)u(t) \tag{4.2}$$

Where x is n-dimensional column state vector, f and g are n dimensional continuous functions in x, u and u is the control input. For the considered system the control input is composed by two components a discontinuous component u_n and a continuous one u_{eq} [4].

$$u = u_{eq} + u_n \tag{4.3}$$

The discontinuous control ensure the attractiveness condition, the simplest form it may take is that of a relay.

$$u_c = s(\dot{x}) = -Ksign(s(x)) \tag{4.4}$$

Where K is a positive constant that represents the gain of the batch command. The continuous component insures the motion of the system on the sliding surface whenever the system is on the surface. The equivalent control that maintains the sliding mode satisfies the condition

$$\dot{S} = 0 \tag{4.5}$$

Assuming that the matrix S is non-singular, the equivalent control maybe calculated as:

$$u_{eq} = -(\frac{\partial s}{\partial x} g(x,t))^{-1}(\frac{\partial s}{\partial t} + \frac{\partial s}{\partial x} f(x,t)) \quad (4.6)$$

The equivalent control is only effective when the state trajectory hits the sliding surface. The nonlinear control component brings the system states on to the sliding surface (Fig 4.1). The nonlinear control component is discontinuous. It would be of the following general form:

$$u_n = \begin{cases} u^+ with\ s > 0 \\ u^- with\ s < 0 \end{cases} \quad (4.7)$$

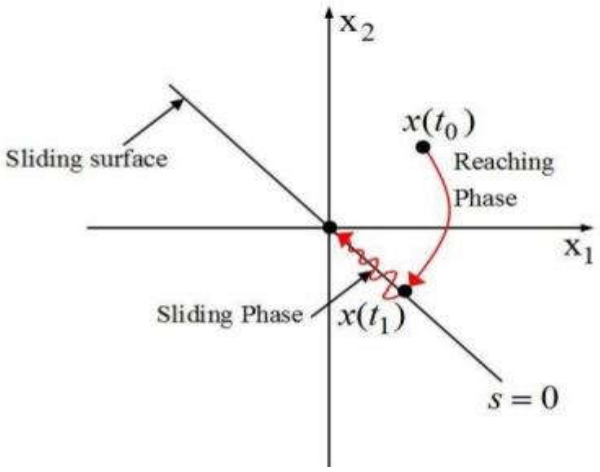

Fig. 4.1. A general overview of SMC

a) Existence condition:

The existence condition of sliding mode implies that both S and $\dot{S}$ will tend to zero when t tend to infinity, which means that the dynamic of the system will stay into the sliding surface. The existence condition of the sliding mode is $\dot{S}S < 0$, the fulfillment of this inequality ensures the existence of sliding mode around the commutation surface.

b) Chattering

The chattering phenomenon is understood to be an oscillatory motion in the neighborhood of the sliding manifold. Possible mechanisms that cause chattering include non- idealities of switching devices for control realization or the existence of parasitic dynamics in series with

the plant. The chattering phenomenon shown in Fig 4.2 is unavoidable in the real application of the SMC.

The chattering caused by un-modeled dynamics may be eliminated in systems with asymptotic observers, in which the observers serve as a bypass for high frequency components. An alternative approach suggestion is a continuous approximation of discontinues control. In many cases, this is not a remedy for the problem since the slop in linear approximations must be adjusted to avoid excitation of the un-modeled dynamics. In addition to that, continuous approximation is unpractical in switching converters related systems, in which the on-off operation is the particular way of operating.

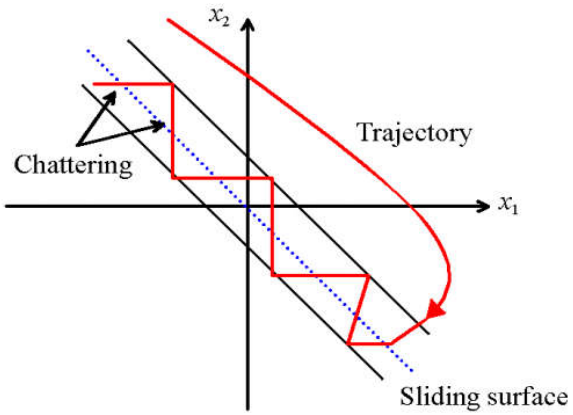

Figure 4.2. Chattering phenomenon in SMC due to non-linearity of the system. The trajectory moves toward the sliding line and oscillates in a defined boundary.

4.3.2 Battery controller

The battery power flow is controlled via a bi-directional DC-DC buck-boost converter. During the battery charging-discharging process the voltage is well regulated and the current is well limited to its maximum reference.

During the battery charging the difference between the reference voltage and the battery voltage (buck mode Fig. 4.3) is supplied to the PI controller to produce the reference current then the battery charging current is adjusted to track this reference current throughout sliding mode controller (SMC). Furthermore during the battery discharging (boost mode Fig. 4.3), the reference current is produced by the difference between the DC bus voltage and the reference voltage then the battery current is limited to its maximum reference value and adjusted using SMC.

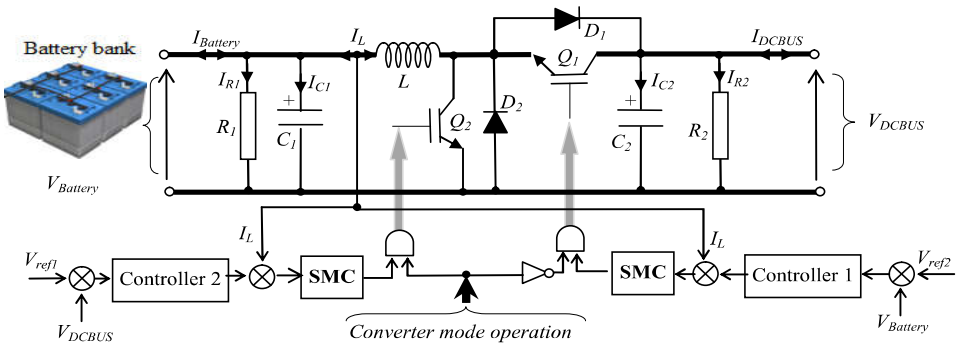

Fig. 4.3. Battery power control, (0: buck mode, 1: boost mode)

a) Discharging mode

The converter mode of operation is determinate by the central controller depending on the power balance within the system, in this mode the battery discharge power to support the DC bus voltage and the converter works in boost mode of operation.

Taking $x_1 = i_L$ and $x_2 = V_{dcbus}$ as the state variables of the system and using the state equations given in(chapter 03-boost converter) with the aim of achieving a desired constant voltage at the DC bus , the state variable x_2 can be obtained as follows:

$$x_2 = V_{dcbus}^* \tag{4.8}$$

$$\dot{x_2} = \dot{V_{dcbus}^*} = 0 \tag{4.9}$$

Determining a suitable switching or sliding surface is the first step to design a sliding mode controller. Here error is denoted as:

$$e = x_{1ref} - x_1 \tag{4.10}$$

The sliding surface S can be defined as:

$$S = Ke = K(x_{1ref} - x_1) \tag{4.11}$$

Where K is the sliding coefficient. Now a switching strategy should be designed to make the system reach sliding surface in finite time. The reference value x_1^* is derived internally to the SM controller from the output of the linear voltage controller. In order to enforce sliding mode in the manifold S=0, the corresponding control signal for the ideal switch can be given as:

$$\mathrm{u} = 0.5(1 - \mathrm{sign(S)}) \tag{4.12}$$

After reaching the surface, the system achieves desired system dynamics and becomes globally asymptotic stable. A positive definite lyapunov function *p* may be defined as:

$$p = \frac{1}{2}S^2 \tag{4.13}$$

Ensuring stability for the system in sliding mode requires derivative of $\dot{P}$ be negative definite and hence the following inequality should be fulfilled:

$$\dot{P} = \dot{S}S < 0 \tag{4.14}$$

Since

$$\dot{S} = \dot{x_1} - \dot{x_1^*} \tag{4.15}$$

The steady state values of the state variables coincide with the corresponding reference values, and they are constant then, $\dot{x_1^*}$=0, replacing Eq (4.15) in Eq (4.14) and solve it we get:

$$x_2 > V_{battery} \tag{4.16}$$

This means that the sliding mode exists if the output voltage is higher than the source voltage.

b) Charging mode

In this case the power is flowing from the dc bus to charge the battery bank and the converter work in buck mode of operation. Taking $x_1 = i_L$ and $x_2 = V_{battery}$ as the state variables of the system, the main aim here is to obtain a desired constant output voltage *to charge the battery*. That is, in steady state the output voltage should be the desired voltage$V^*_{battery}$. Thus,

$$x_2 = V^*_{battery} \tag{4.17}$$

$$\dot{x_2} = \dot{V^*_{battery}} = 0 \tag{4.18}$$

The state variables may be used to construct the sliding function. From the general sliding mode control theory, the state variable error, defined by difference to the reference value, forms the sliding function as:

$$S = Ke = K(x_{1ref} - x_1) \tag{4.20}$$

This means that the control forces the system to evolve on the sliding surface [5]. The reference value $x1^*$ is derived internally to the controller from the output of the linear voltage controller. In order to enforce sliding mode in the manifold $S = 0$, the corresponding control signal for the ideal switch in is:

$$\mathrm{u} = 0.5(1 - \mathrm{sign}(\mathrm{S})) \tag{4.21}$$

Since the aim is to guarantee that the state trajectory of the system is directed to the sliding surface $S = 0$ and slides over it, this is achieved with a suitable design of control law using the reaching condition

$$\dot{S}S < 0 \tag{4.22}$$

Since

$$\dot{\mathrm{S}} = \dot{\mathrm{x}_1} - \dot{\mathrm{x}_1^*} \tag{4.23}$$

The steady state values of state variables coincide with the corresponding reference values and they are constants then, replacing Eq (4.23) in Eq (4.22) and solving it we get:

$$0 < \mathrm{x}_2 < \mathrm{V}_{\mathrm{dcbus}} \tag{4.24}$$

4.3.3 MPPT Control

A nonlinear second order sliding mode control (*SOSMC)* in a boost converter is designed to track the maximum power point with the help of a modified P&O algorithm (Fig. 4.4). The main aim of this algorithm is to generate the voltage reference (V_{ref}) that enters the sliding mode controller.

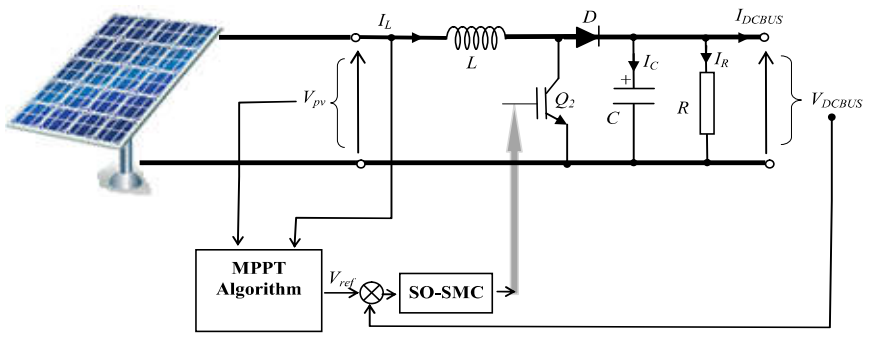

Fig. 4.4. Proposed schematic for P&O modified and MPPT proposed sliding mode control.

In P&O algorithm, the control signal of the converter is periodically perturbed and the resulting effect on the PV power output is observed. If the power increases, the control system moves the PV array operating point in that direction. Otherwise, the direction of the perturbation is reversed. This algorithm can be written as follows [6, 7, 8]:

$$V_{ref}(k) = V_{ref}(k-1) + K.sign(\Delta P) \tag{4.25}$$

with

$$\Delta P = P(k) - P(k-1)$$

If $\Delta P > 0$ **then** increase V_{ref}.

else $\Delta P < 0$ decrease V_{ref}

Generally a fixed step K is used to increase or decrease the reference voltage. The oscillation around the MPP depends highly on that step size. A large step size can improve the dynamic of the algorithm, but it can highly increase the oscillation while using a small step size can reduce the oscillation and slows down the dynamic of the algorithm (it takes much time to reach the MPP). In this work a modified step size P&O algorithm is proposed in order to obtain a fast convergence to the MPP and to reduce the oscillations around it. Equation (4.25) can be rewritten as:

$$V_{ref}(k) = V_{ref}(k-1) + K.|\Delta P|sign(\Delta P) \tag{4.26}$$

The step is adjusted depending on the power variation, when the operating point is far away from the MPP the step is large in order to make fast convergence to the MPP. On the other hand, when the operating point is close to the MPP the step becomes smaller in order to reduce the oscillations.

a) Second order sliding mode controller design

SOSMC based on a super twisting algorithm is used in order to track V_{ref}. Applying SOSMC can improve the transient response of the system for a wide range of a reference voltage or under large parameter variations and load disturbances. Firstly the sliding surface $S(x)$ is defined next, the control law is driven to bring the state trajectory to the desired output [9].

$$\begin{cases} e = (x_2 - x_2^*) \\ S = e + K_1 \int e\,dt \end{cases} \tag{4.27}$$

Depending on the high order sliding mode control theory, the second derivative of the sliding surface could be expressed as:

$$\ddot{S} = (\ddot{e} + K_1 \dot{e}) = \varphi(t, S, \dot{S}) + \phi(t, S, \dot{S})\dot{u} \tag{4.28}$$

With

$$\varphi(t, S, \dot{S}) = \lambda_1\lambda_2 V_{in} u - \lambda_1\lambda_2 x_2 u^2 + K_1\lambda_2 x_1 u - K_1\lambda_3 x_2 - (K_1 \dot{x}_2^* + \ddot{x}_2^*)$$

$$\phi(t, S, \dot{S}) = \lambda_2 x_1$$

The control of the DC-DC converter is a bounded function ($0 \le |u| < 1$). The super twisting algorithm is defined by the following control law:

$$u = u_1 + u_2 \tag{4.29}$$

where

$$\begin{cases} \dot{u}_1 = -k_{11}\,\mathrm{sgn}(S) \\ u_2 = -k_{22}|S|^{0.5}\,\mathrm{sgn}(S) \end{cases} \tag{4.30}$$

and $k_{11} > 0$; $k_{22} > 0$

The use of the second order sliding mode guarantees the finite time convergence to:

$$S = \{x : S = \dot{S} = 0\} \tag{4.31}$$

4.3.4 FC Controller

The central controller determined the fuel cell current reference based on the battery SOC range and load power *Pload* as depicted in Fig. 4.5.

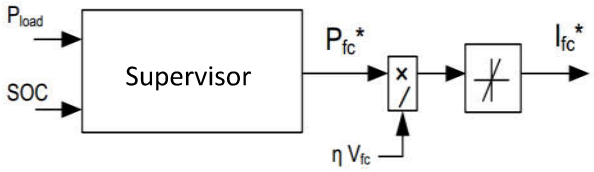

Fig. 4.5. Fuel cell reference current determination

In this case hysteresis current mode (Fig. 4.6) control is used as it is the simplest, most intuitive control strategy for DC-DC converter and it doesn't require a compensation network. In this mode of control, the comparator that compares the inductor current with the reference current (which is set by the controller) has a small amount of hysteresis denoted by ε. The switch of the DC-DC converter is switched ON when inductor current drops below $i_L^* - \varepsilon$ and the switch is turned OFF, when the inductor current exceeds $i_L^* - \varepsilon$.

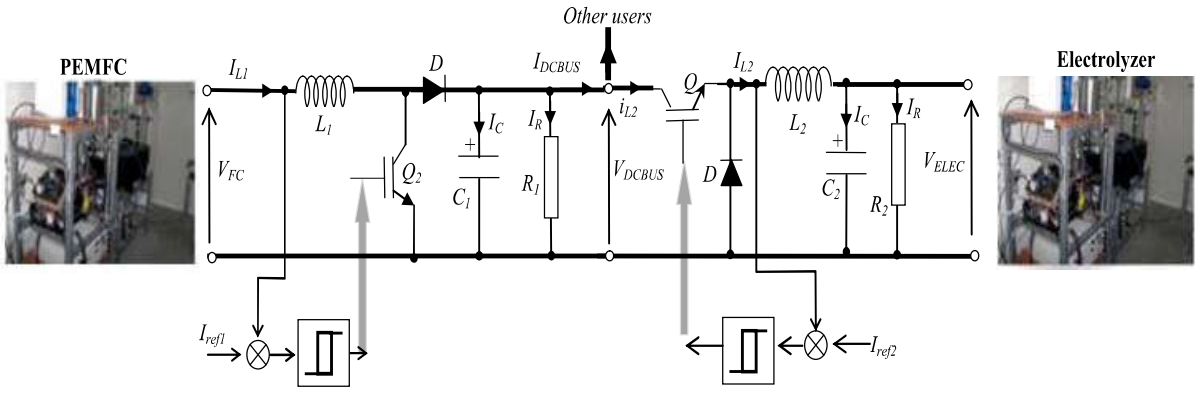

Fig. 4.6. PEMFC power control

4.4 The central power flow controller

The central power flow controller is designed to fulfill many criteria as: a) Manage the power and the energy between the sources, b) Satisfy the load demand even under bad weather conditions. c) Optimize the operation of each power system components and extend its service life, d) Increase the overall system efficiency.

The control is affected through the power converters which are connected to the power system components, with the required measurements and data collecting though the sensors. The operation strategy used in the power flow controller is represented in a form of a decision tree (Fig. 13) and it can be explained as follows:

Firstly the controller measures the power generated by the PV arrays and the power consumed by the loads, then the difference is calculated ($P_d = P_{PV} - P_{load}$). In the case of power deficit, the control strategy defines four modes of operation which are:

Mode 1

This is the case where the PV output power is less than the required load power and the difference between these two powers is lower than the battery rated power ($P_d \leq P_{Batt}$). The lack of energy is provided by the battery, which is mainly sized to support low power demand (P_{Batt}≤1000W). Since the battery will cover the low duration demands, the FC will be turned-on only in the case of the battery bank SOC drops below 45 %(SOC_{min}), or in the case of high load demand. In this way, unnecessary turn-on of the FC is avoided, which increases highly its service life. Moreover, the limitation of battery discharge power ensures that there will be enough energy to support the loads throughout bad weather condition. In addition to that the economical optimization developed in [10, 11] shows that batteries are better to supply low discharged power because the average cost of the power supplied by batteries will be less than the average cost of the power supplied by fuel cells. In this mode, the controller operation is conditioned as follows:

if ($SOC > SOC_{min}$) **then** ($I_{dis} = I_B$)
else
If ($P_{H2} > P_{H2min}$) **then** ($I_{dis} = I_{FC}$)
Else ($I_{dis} = 0$) (total shedding of consumption)
end
end

Firstly the controller will test the battery *SOC*, if it is higher than its minimum threshold ($SOC > SOC_{min}$) then the controller will set the battery discharge current ($I_{dis} = I_B$). In this case, the reference power and current of the battery are given by the following equations:

$$P_{B\_ref} = P_d \tag{4.32}$$

$$I_{Bf} = I_{dis} = \frac{P_d}{V_B} \tag{4.33}$$

On the other hand, if the first conditions are not verified, the *FC* will cover the deficit power if the pressure of the H_2 tank is ($P_{H2} > P_{H2min}$). In this case, the reference power and current of the *FC* are given by the following equations:

$$P_{FC\_ref} = P_d \tag{4.34}$$

$$I_{FC} = \frac{P_d}{V_{FC}} \tag{4.35}$$

Moreover, if the last two conditions are not verified the total shedding mode will be activated to prevent the overall system failure.

Mode 2

It's the state when ($P_{Batt} < P_d \leq P_{FC}$), which indicates that the power deficit is higher than the rated power of the battery but lower than the *FC* rated power. In this mode the controller operation is conditioned as follows:

if ($P_{H2} > P_{H2min}$) **then** ($I_{dis} = I_F$)

else

If ($SOC > SOC_{min}$) **then** ($I_{dis} = I_B$)

Else ($I_{dis} = 0$) (total shedding of consumption)

end

end

Firstly the controller will test the pressure of the H_2 tank, if it is higher than its minimum threshold ($P_{H2} > P_{H2min}$), then the controller will set the FC current ($I_{dis} = I_F$). Moreover, if the first condition is not verified, the battery will cover a part of the power deficit with partial shedding of controlled loads. On the other hand, if the battery charge state is ($SOC \leq SOC_{min}$), the total loads shedding mode will be activated ($SOC \leq SOC_{min}$) to prevent the system failure under heavy load consumption.

Mode 3

This mode is activated in the case of extra power deficit ($P_d \leq P_{FC} + P_{Batt}$), when the power deficit is greater than the rated power of the battery and the *FC*. In this mode, the controller operation is conditioned as follows:

if ($P_{H2} > P_{H2min}$) **&** ($SOC > SOC_{min}$) **then** ($I_{dis} = I_F + I_B$)

if ($P_{H2} > P_{H2min}$) **&** ($SOC \leq SOC_{min}$) **then** ($I_{dis} = I_F$)

if ($P_{H2} \leq P_{H2min}$) **&** ($SOC > SOC_{min}$) **then** ($I_{dis} = I_B$)

if ($P_{H2} \leq P_{H2min}$) **&** ($SOC \leq SOC_{min}$) **then** ($I_{dis} = 0$)

If H_2 tank pressure and the battery *SOC* are greater than their minimum threshold, the battery and the *FC* will support the heavy load consumption at the same time. In this case, the reference powers and current of the FC and the battery are given by the following equations:

$$P_{B\_ref} = 1000kW \tag{4.36}$$

$$I_B = \frac{1000}{V_B} \tag{4.37}$$

$$P_{FC\_ref} = P_d - P_{B\_ref} \tag{4.38}$$

$$I_{FC} = \frac{P_{FC\_ref}}{V_{FC}}$$

$$I_{dis} = I_F + I_B \tag{4.39}$$

On the other hand, if the H_2 tank pressure is greater than its minimum threshold, but the battery SOC is lower than its minimum threshold, then the FC will cover a part of the power deficit with partial shedding of controlled loads. Moreover, if the H_2 tank pressure is lower than its minimum threshold, but the battery SOC is greater than its minimum threshold, then the battery will cover a part of the power deficit with partial shedding of controlled loads. Finally, if the H_2 tank pressure and the battery SOC are lower than their minimum threshold, then the total shedding of consumption mode will be activated. In this way, the controller ensures highly the energy balance of the power system, as it shifts the power consumption during the heavy consumption and low energy production.

Mode 4

During the power surplus ($P_{net} > 0$), the excess power is transferred to the battery bank. Moreover, if the battery bank *SOC* reaches its maximum level, the electrolyzer will turn-on, unless maximum tank pressure P_{max} is reached. If the H_2 tank is full then the surplus power will be transferred to the dump load.

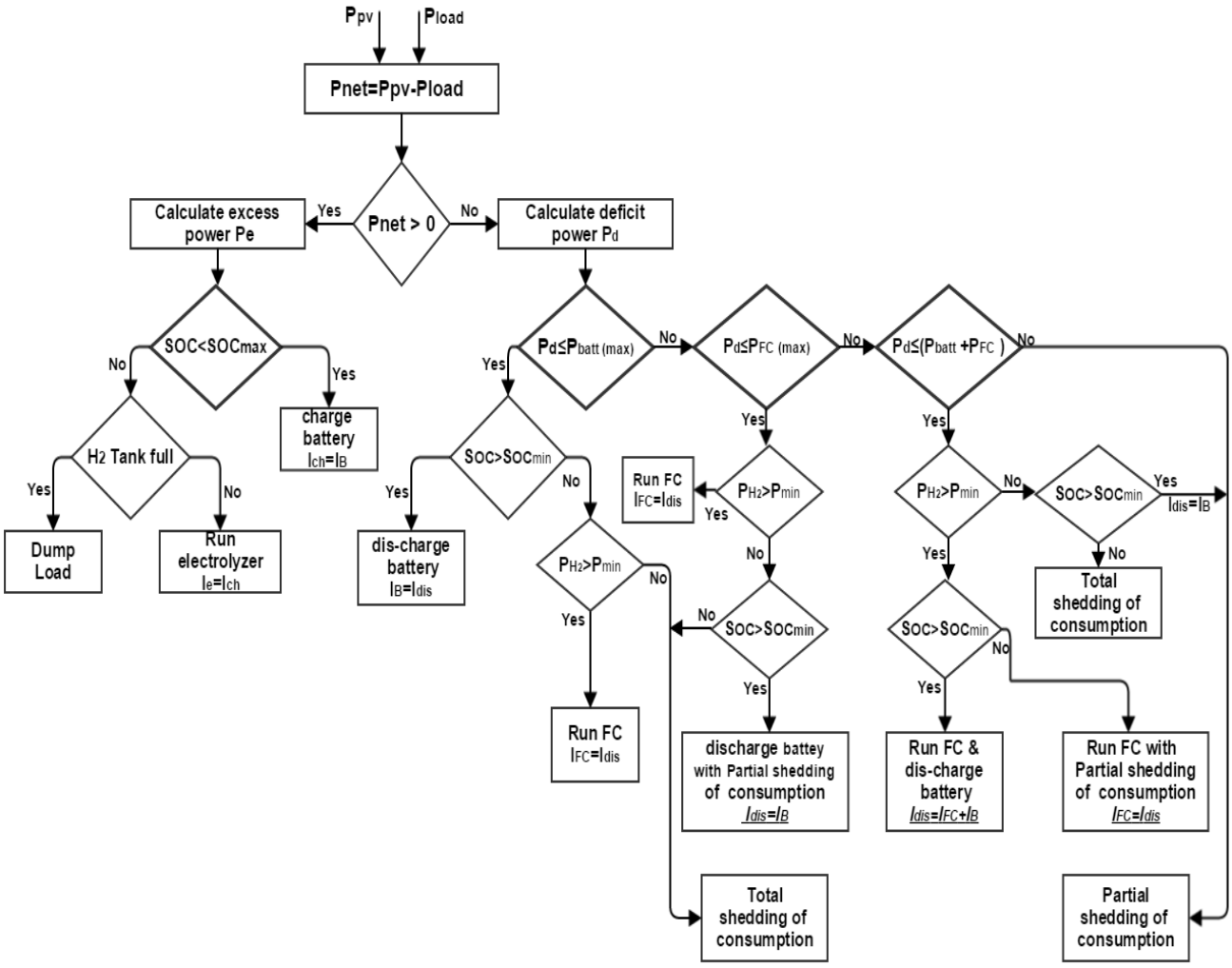

Fig. 4.7. Decision tree of the power flow controller

4.5 Dynamic control simulation

The hybrid power system has been simulated over a short and a long period of time in order to evaluate the performance of the dynamic controllers and the effectiveness of the management strategy. Fig. 4.8 presents the behavior of PV output power under sudden variation in the irradiance (Fig. 4.9). The result confirms the efficiency of the MPPT controller as the output power perfectly follows the power reference.

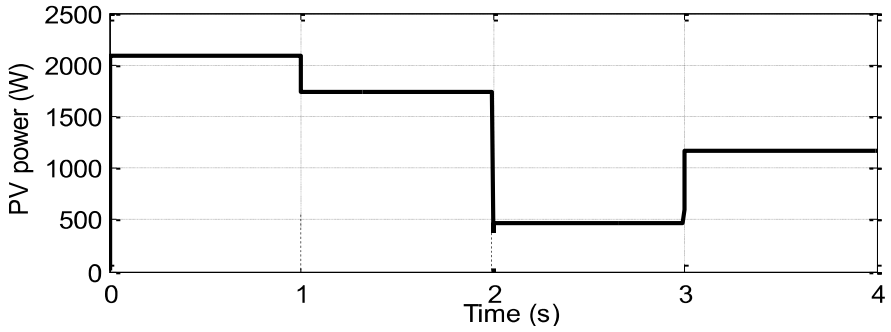

Fig. 4.8. PV output power (W)

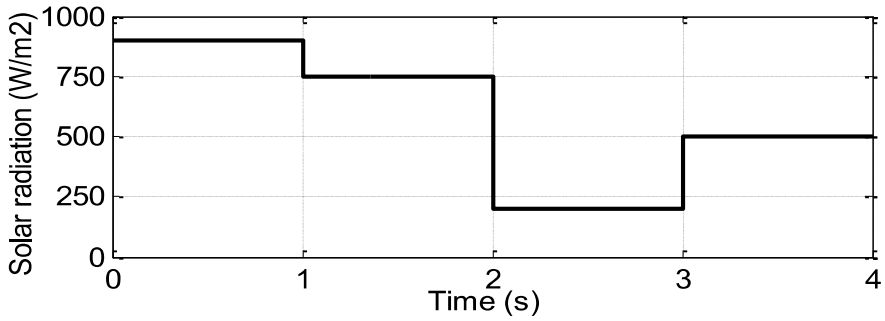

Fig. 4.9. Solar irradiance (W/m^2)

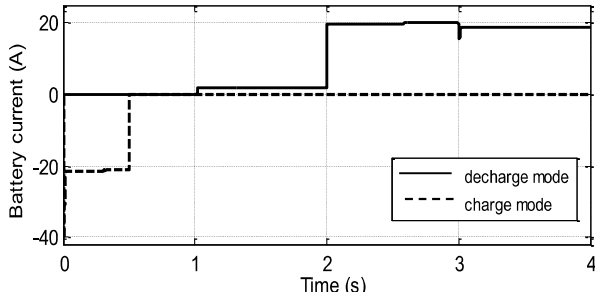

Fig. 4.10. Battery current (A)

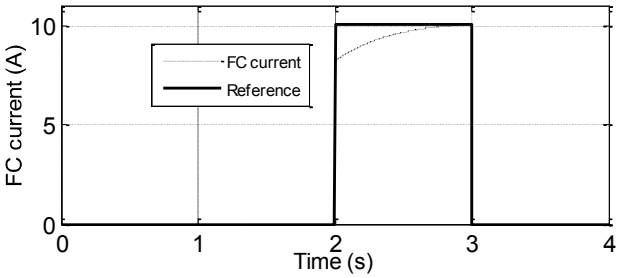

Fig. 4.11. FC current (A)

Fig 4.10, 4.11 and 4.12 present battery, FC and electrolyzer current respectively for transient responses obtained for a transition from different operating mode. The test is performed by changing the irradiance level and the load current. During the first interval (0s≤t<1s) the power difference is positive ($P_{PV} - P_{Load}$) and the excess power is transferred to the battery. At t=0.5s, the battery is fully charged and the excess power is transferred to the electrolyzer. At t=1s, the PV output power changes from 2200W to 1750W (due to the last change in the irradiance level Fig. 4.9) and the load demand (Fig. 4.13) increases from 1000W to1800W. The power difference is negative and the power deficit is less than the battery maximum discharge power, the controller sets the reference discharge current of the battery boost converter and the required power is

drawn from the battery to supply the load. At t=2s, the PV power decreases from 1750W to 450W respectively, in this case, the power deficit is greater than the battery maximum discharge power and the FC starts to support the battery and the controller sets the reference discharge current of the FC and the battery boost converter. The required power is drawn from the battery and the FC to supply the load.

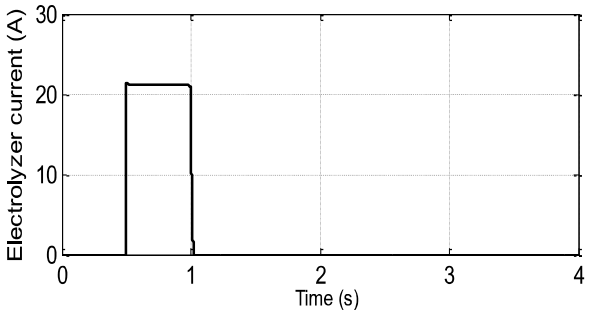

Fig. 4.12. Electrolyzer current (A)

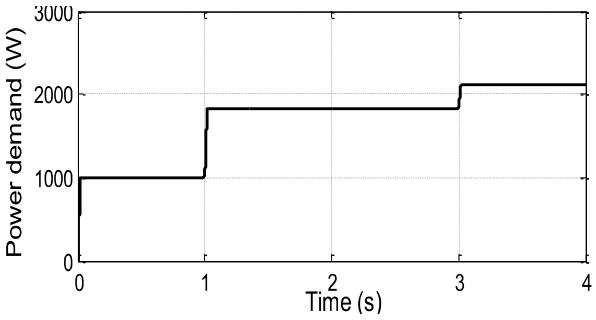

Fig. 4.13. Power demand (W)

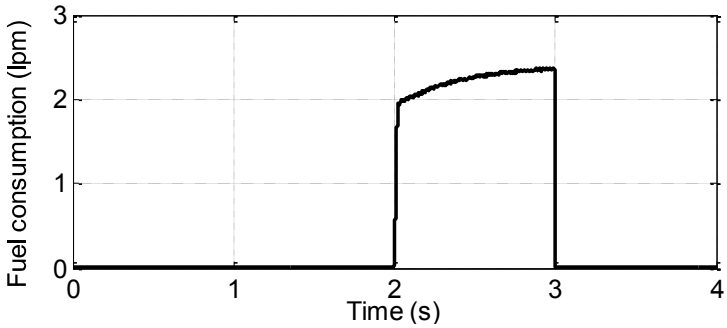

Fig. 4.14. Fuel consumption (lpm)

During the load variation and mode fluctuations, the power imbalance of the system is increased which increases the stress on the battery and the FC. Connecting the SC to the DC bus improves highly the balance of the system, since the super capacitor can react faster to quick fluctuations and could compensate the slow dynamic of the FC. Fig. 4.15 shows the SC output (DC bus) voltage. The fast rate of charge-discharge of the SC handle the load variation and help to maintain the DC voltage close to its reference 120V level, which reduces the stress on the battery and increases its service life.

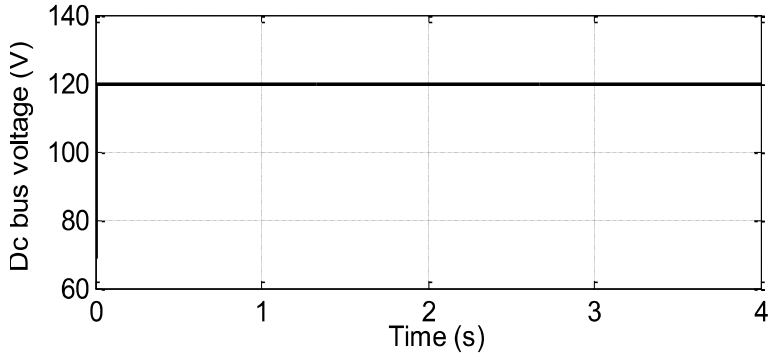

Fig. 4.15. DC bus voltage (V)

4.6 Conclusion

This chapter briefly presented the system power flow management and dynamic controllers design of the different subsystem components. It developed an optimal strategy for controlling the energy flow within the system based on the energy availability. The performance of the dynamic controller was tested by the mean of simulation under MATLAB Simulink Environment , the result assume the effectiveness of the proposed control method and the intelligent management of the power flow management over a short period time.

4.7 References

[1] Gao L, Dougal R.A, Liu S. Power enhancement of an actively controlled battery/ ultracapacitor hybrid. IEEE Transactions on Power Electronics 2005; 20:236–43.

[2] Utkin V,Guldner J ,Shi J. Sliding mode control in electromechanical systems. Taylor & Francis 1999.

[3] Kercha Mébarka. Commande par mode de glissement d'un Moteur pas à pas à Aimant Permanent. Faculté des Sciences de l'Ingénieur. Universite De BATNA, 2005.

[4] Kamel Ben Saad, Abdelaziz Sahbani and Mohamed Benrejeb (2011). Sliding Mode Control and Fuzzy Sliding Mode Control for DC-DC Converters, Sliding Mode Control, Prof. Andrzej Bartoszewicz (Ed.), ISBN: 978-953-307-162-6, InTech, Available from: http://www.intechopen.com/books/sliding-mode-control/sliding-modecontrol-and-fuzzy-sliding-mode-control-for-dc-dc-converters

[5] Md. Shamim-Ul-Alam*, Muhammad Quamruzzaman and K. M. Rahman. Fuzzy Logic Based Sliding Mode Controlled DCDC Boost Converter. 6th International Conference on Electrical and Computer Engineering
ICECE 2010, 18-20 December 2010, Dhaka, Bangladesh.

[6] Drid S, Chrifi-Alaoui L, Bussy P, Ouriagli M. Robust Control of the Photovoltaic System with Improved Maximum Power Point Tracking. Ninth International Conference on Ecological Vehicles and Renewable Energies (EVER) 2014, Monte-Carlo,1-7.

[7] Kollimalla SK, Mishra MK. Variable Perturbation Size Adaptive P&O MPPT Algorithm for Sudden Changes in Irradiance. IEEE Transactions on Sustainable Energy 2014; 5(3): 718 - 728.

[8] Sahraoui H, Drid S, Chrifi-Alaoui L. Robust control of DC-DC Boost converter applied in photovoltaic systems using second order sliding mode. The 15th International conference on Sciences and Techniques of Automatic control & computer engineering 2014, Hammamet-Tunisia, 719-724.

[9] Levronand Y, Shmilovitz D. Maximum power point tracking employing sliding mode control. IEEE transaction on circuit and systems 2013; 60(3): 724 - 732.

[10] Dufo-Lopez L, Bernal-Agusto J, Contreras J. Optimization of control strategies for stand-alone renewable energy systems with hydrogen storage. Renewable Energy 2007; 32:1102- 1126.

[11] Kang KH, Won DJ. Power Management Strategy of Stand-Alone Hybrid System to Reduce the Operation Mode Changes. IEEE Conference on Transmission, Distribution & Exposition 2009, Seoul, 1-4.

Chapter 5

The first case study on the proposed demand side management and control algorithm

5.1 Introduction

The chapter five describes the DSM methodology developed for this study in detail. Moreover the optimization process of the hybrid energy system is presented. In addition to that a case study is presented to assume the effectiveness of the developed DSM. The proposed DSM strategy is applied for zero emissions hybrid system for off grid house.

5.2 General description and objectives

The concept of DSM involves using control devices to manipulate individual demands. The aim is to achieve a favorable aggregated demand for better energy supply system operation over a certain time period based on the availability of supply resources. The DSM algorithm developed in this chapter has been dedicated to this concept. This DSM algorithm is generic enough to be suitable for the demands from various sources, such as statistical demand, simulated demand and monitored demand. Based on the source of available demand data, different types of DSM algorithm will be invoked. Therefore, the DSM algorithm can be applied at different stages, from initial feasibility study, to detailed design stage, even to the operational level in practice. The DSM algorithm can be regarded as a means to improve the demand/supply matching rate and thereby optimize the performance of energy supply systems such as RE technologies etc. The objective of the DSM algorithm is to minimize the impact on users and at the same time maximize the match between demand and supply through identifying the best combinations of different demand side control options such as load shifting, load control (on/off control and proportional control) and load recover for various demand loads. Utilizing these demand side measures will improve energy efficiency (e.g. by reducing the total demand magnitude), change the pattern of use (e.g. load shift), and achieve optimal switching strategies (e.g. on/off or proportional control) etc. The objectives of DSM control algorithm can be summarized as follows.

- To maximize the efficiency of energy use, so that energy wastage is reduced;
- To facilitate the integration of renewable sources;

- To create optimal demand profiles for the operation of RE.
- To maximize the system reliability
- To maximize the service life of the system components

The implemented overall control managing both energy sources and loads based on the comparison of demand and available supply resources and generating optimal DSM strategies. The strategy links between different DSM techniques mainly load shifting, energy efficiency and demand response. The management time are classified into two main time step: a dynamic real time control and an hourly optimization. The proposed strategy employs DR technique that normally responds to "emergency" situations in the system ,or in the another word it's a dynamic real time loads control that takes place when there is a specific situation at the production or transmission side. Moreover the proposed strategy employs a LM techniques that operates on a regular hourly basis. In addition to that a real time energy efficiency optimization is done which provide the same level of service throughout an efficient use of energy. In this way the advantages of each DSM can be employed which results in many benefits. In this study the load curves are time-series data known in advance. It's mainly constructed based on a real load profile.

5.3 DSM Concept

The concept of the proposed management strategy essentially depend on defined several parameters that describe the demand and the energy state of the system such as.

a) Energy availability

The energy availability consider to be one of the most important factor that affect in the control algorithm. The energy availability can be determined depending on the state of the storage elements in the system such as the battery bank state of charge and the pressure in the hydrogen tanks.

b) Weather condition

The weather conditions have a major effect both in the energy demand and generation of the system.

c) Load type (Shiftable or non-shiftable)

This depends on the properties of the demand. Some loads with fixed operating durations such as washing machines, microwaves, and dishwashing machines etc. are shiftable [1], whereas other loads, like lighting, cannot be shifted.

d) Load flexibility (whole or partial)

Another parameter to be defined is the flexibility of demand profile. The demand profile for a certain load represents the energy use pattern during its operating period. Here the question of whether the total demand or only part of it can be shifted during the control period poses itself. The answer significantly affects the load shifting strategy. The options are available to define part of the demand through the start time to the end time of the profile are provided.

e) Load importance

The different loads can be classified based on their priorities in two types: non-critical loads, and critical loads. The on/off control can be applied on the non-critical loads depending on the different situation of the system while the command algorithm must ensure continuous supply of critical loads.

After the different loads are classified, the different DSM techniques mainly load shifting, energy efficiency and demand response will be applied depending in the load category and the energy situation. The proposed strategy employs DR technique to responds to “emergency” situations in the system, this technique will applied mainly on the non-critical, non-shiftable loads in the case of the energy misbalance of the system or in the dynamic optimization of the energy demand. Moreover the proposed strategy employs a LM techniques that operates on a regular hourly basis, this technique will applied mainly on the non-critical, shiftable loads, to shift the demand of these loads throughout the normal operation. In addition to that a real time energy efficiency optimization is done which provide the same level of service throughout an efficient use of energy. In this way the advantages of each DSM can be employed which results in many benefits. To assume the effectiveness of the proposed DSM strategy, it will be applied for two different case study.

5.4 Load profile

Deep analysis of the different loads lead to improve the energy balance of the hybrid system, a real investigation must be done on daily electricity consumption throughout the year. These electrical loads drive energy consumption and costs, but also facilitate the different critical services that take place in building; understanding the best way to support, protect and expand those services starts with an analysis of those loads. A basic electric load assessment involves creating a table showing power ratings, or loads (in Watts), of all electrical devices in the building along with an estimate of the number of hours each device will operate on a daily basis (Table 5.1). This results in an estimate of facility consumption, the number of Watt-hours used by the building per day, and the total facility electrical load, the sum of all inventoried loads.

More over the consumption must be modified during the year, because it highly affected by the weather change between the different season. When properly executed, a load analysis can yield valuable insights into building energy usage that can be used to save on energy costs, increase productivity and protect critical assets.

Table 5.1. Hourly load consumption exemplary

Operating time (h) / **Power (W)**	**00-01**	**01-02**	**02-03.....**	**22-23**	**23-00**
Lights Air conditioner Fan					

.

5.5 Hybrid system optimization

The system optimization is very important part of hybrid system management, before the application of the proposed DSM strategy the best combination and size of the electrical generation must be sited to satisfy the different load with tacking in the consideration its life-cycle cost. Many different design options must be compared based on their technical and economic merits. For example the best size of the PV generator, the battery bank and the fuel cell must be carefully determined

5.5.1 Application of HOMER program for the optimization

a) Program representation

The HOMER Micro power Optimization Model is a computer model developed by the U.S. National Renewable Energy Laboratory (NREL) to assist in the design of micro power systems and to facilitate the comparison of power generation technologies across a wide range of applications [2, 3]. HOMER performs three principal tasks: simulation, optimization, and sensitivity analysis. In the simulation process, HOMER models the performance of a particular micro power system configuration each hour of the year to determine its technical feasibility and life-cycle cost. In the optimization process, HOMER simulates many different system configurations in search of the one that satisfies the technical constraints at the lowest life-cycle cost. In the sensitivity analysis process, HOMER performs multiple optimizations under a range of input assumptions to gauge the effects of uncertainty or changes in the model inputs. Optimization determines the optimal value of the variables over which the system designer has control such as the mix of components that make up the system and the size or quantity of each.
HOMER can simulate a wide variety of micro power system configurations, comprising any combination of a PV array, one or more wind turbines, a run-of-river hydro-turbine, and up to three generators, a battery bank, an AC–DC converter, an electrolyzer, and a hydrogen storage tank. The system can be grid-connected or autonomous and can serve AC and DC electric loads and a thermal load. Figure 5.1 shows schematic diagrams of some examples of the types of micro power systems that HOMER can simulate.

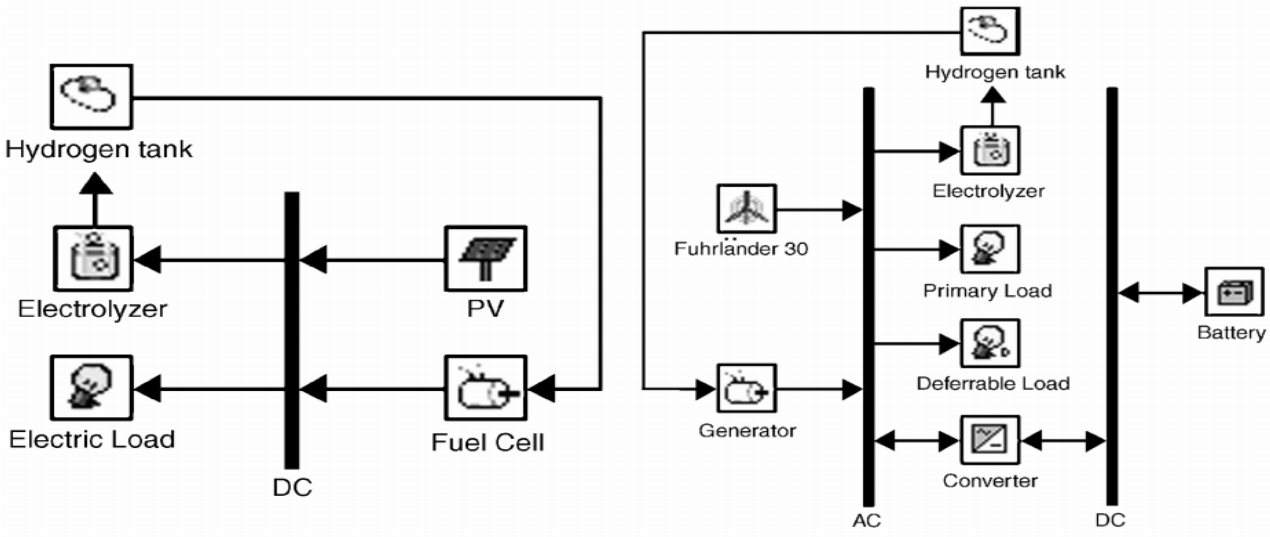

Fig 5.1. Schematic diagrams of some micro power system types that HOMER models

b) Program input and output

The different resources must be entered to the program, the term resource applies to anything coming from outside the system that is used by the system to generate electric power. That includes technology options, component costs, and resource availability.

Renewable resources vary enormously by location. At any one location a renewable resource may exhibit strong seasonal and hour-to-hour variability. The nature of the available renewable resources affects the behavior and economics of renewable power systems, since the resource determines the quantity and the timing of renewable power production.

Moreover for the different renewable technologies costs must be entered, the user must specifies the initial capital cost in dollars, replacement cost in dollars, and operating and maintenance (O&M) cost in dollars per year Figure 5.2 .

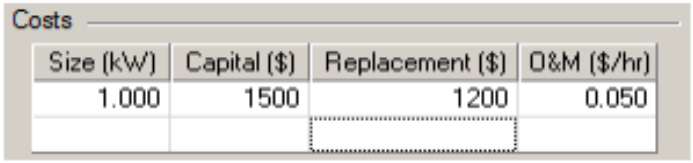

Fig 5.2. Homer cost inputs

The replacement cost is the cost of replacing the renewable technology at the end of its useful lifetime, which the user specifies in years. By default, the replacement cost is equal to the capital cost, but the two can differ for several reasons. For example, a donor organization may cover some or all of the initial capital cost but none of the replacement cost. In addition to the hourly average load profile for each month must be entered to show the effect of the weather condition on the demand pattern Figure 5.3.

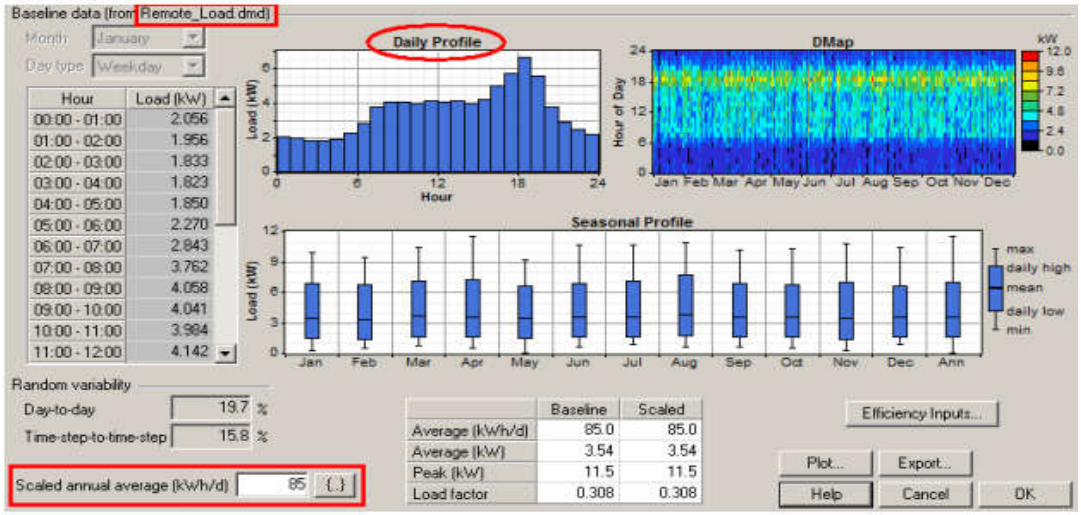

Fig. 5.3. Homer profile input

HOMER uses these inputs to simulate different system configurations, or combinations of components, and generates results that you can view as a list of feasible configurations sorted by net present cost. HOMER also displays simulation results in a wide variety of tables and graphs that help you compare configurations and evaluate them on their economic and technical merits.

5.6 The first case study on the operational application of DSM control algorithm

The first case is described to demonstrate the feasibility of applying the proposed DSM algorithm to the power supply for an individual appliance base on a real-data. This case study applied for a (PV-FC-EL-Battery) hybrid system for a rural house located in the high plateaus region. This case study will look at the viability of using DSM algorithm for a strategic solution to design zero carbon energy systems in the context of a grid off house. In this case the hybrid energy system has zero carbon emission and depend mainly on the renewable energy source. The proposed DSM has to be able to optimize the operation of such a hybrid system and to eliminate any energy deficit

5.6.1 Geographic and climate data of the region

This work takes a rural house located in the high plateaus region **(**province of Batna (35°33′N 6°10′E)) as a case study. The location characterized by high solar potential, the yearly average value of daily solar irradiance is about 4.87 kW/m^2. The area climate is characterized with Mediterranean climate with dry hot summers and mild winters, it has an annual average temperature of 15.5°C. The monthly averaged global solar radiation on a horizontal surface (W/m^2) and the ambient temperature for the location, is shown in Figures 5.4 and 5.5 respectively.

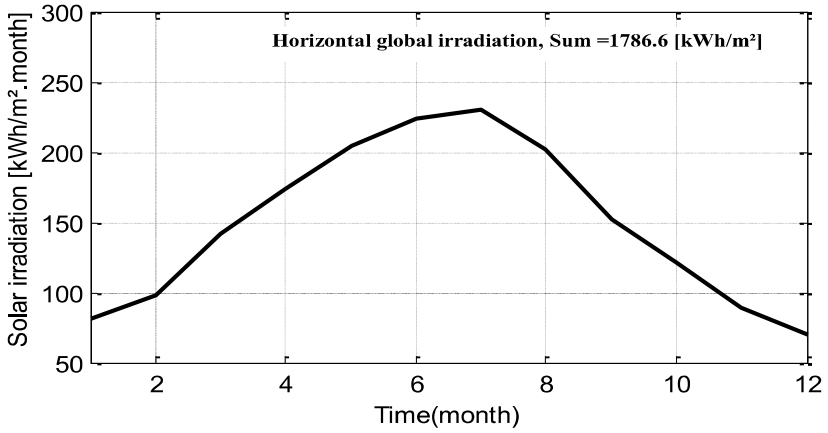

Fig. 5.4. Horizontal global irradiation, [kWh/m².month]

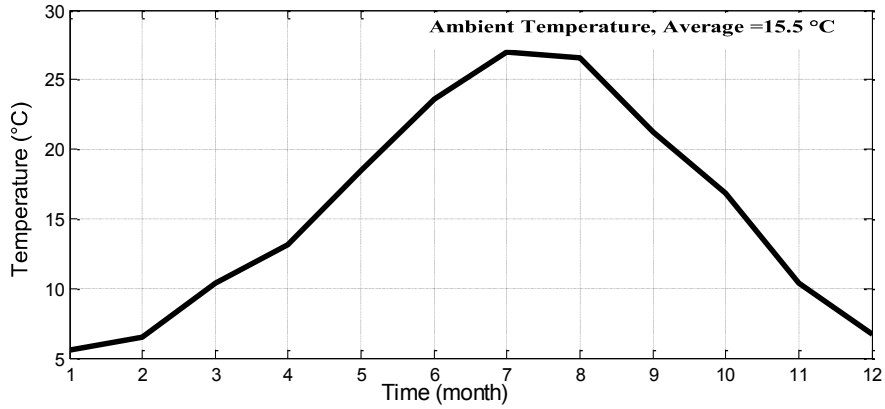

Fig. 5.5. Ambient temperature °C

5.6.2 Electricity Load Estimation of the site

For testing the effectiveness of the proposed management strategy, a deep study is accomplished on a real load profile for an average house (house is approximately 100m^2 and includes all household electrical devices) in the location.

It is important to choose an economic devices for such remote sites, that for minimizing the costs of the installation. Table (5.2) shows a list of the typical electricity consumption of household appliances in the location. The second column notes the electricity power (W) of each appliance. Appliance power is usually given on the appliance itself. However, this often indicates maximum power use, which can be much higher than average power use. Column 3 record (in hours) how long each appliance is used per day, we mainly used the daily average value throughout the year considering the consumption differences between the different seasons. Moreover some appliances switch on intermittently such as fridges so mainly we use the hourly average consumption for such appliances.

Table 5.2. List of the typical electricity consumption of household appliance in the location

Equipment	quantity	Power(w)	Hour used per day	Total energy Kwh/day
Lights	4	40	6	0.96
Refrigerator	1	300	8	1.5
Iron	1	900	0.1	0.09
Washing machine	1	2000	0.25	0.5
Television	1	110	4	0.44
Hair drier	1	647	0.1	0.064
Desktop computer	1	230	7	1.6
Air conditioner	1	1500	2	3
fan	1	45	2	0.090

After the construction of the first table, the hourly consumption throughout the day must be defined as showing in the table (5.3). Basically a 12 table must be constructed covering the different months of the year and taking into consideration the climate condition different among these months. Then the different table will be to the homer program which generated an hourly time series covers all the year.

Table 5.3. Hourly consumption of the house

hour	**00-01**	**01-02**	**02-03**	**03-04**	**04-05**	**05-06**	**06-07**	**07-08**	**08-09**	**09-10**
Load	102	105	100	95	100	100	210	300	450	300
hour	**10-11**	**11-12**	**12-13**	**13-14**	**14-15**	**15-16**	**16-17**	**17-18**	**18-19**	**19-20**
Load	290	430	460	480	460	485	500	550	560	580
hour	**20-21**	**21-22**	**22-23**	**23-24**						
Load	600	550	350	220						

Figure 5.6 shows a daily average exemplary load profile for summer. It is associated with a huge energy consumption and represents a real challenge to our proposed strategy.

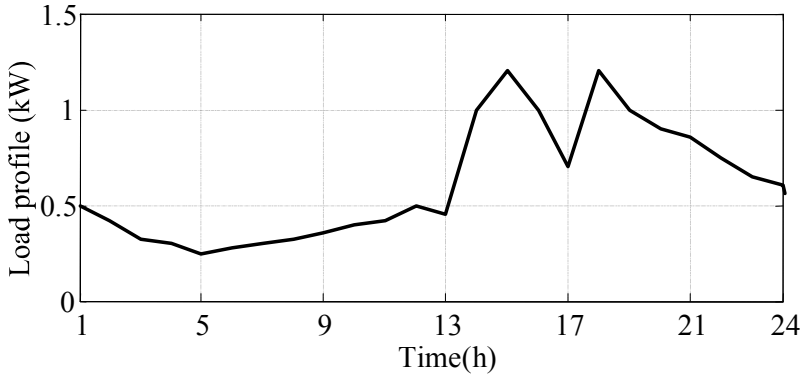

Fig. 5.6. An exemplary load profile

5.7 Optimization of the hybrid power system

The drawbacks of using renewable sources as off-grid/standalone power systems, it has intermittence nature that makes difficult to regulate the output power to manage with the load sought. To make sure for the reliability and affordability of the supply the optimal size and configuration of the system must be carefully sited based on technical, environmental and economic criterions. The proposed energy system should meet the load demand of the house with the minimum cost of energy. Figure 5.7 presents the schematic representation of HOMER simulation model of the hybrid system architecture.

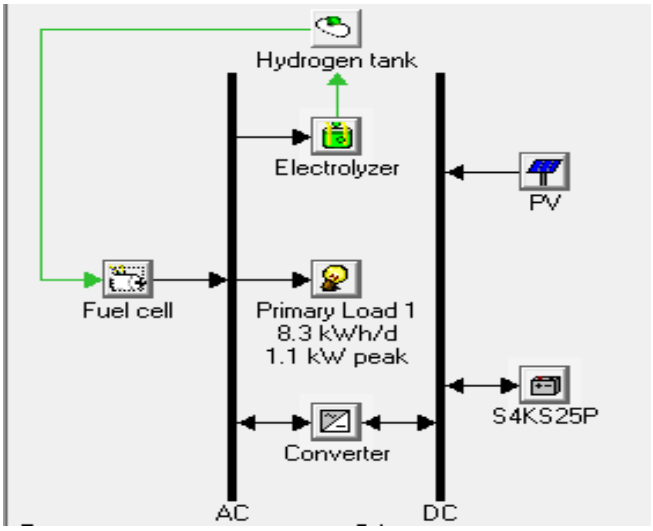

Fig. 5.7 Architecture of the Selected Technologies of the Hybrid System Produced by HOMER

5.7.1 Model input

a) The electricity load

Next to the selection of the components technology from the library of HOMER software, the electricity load is the first to be entered in to the modeling tool. The primary load input, which was determined in section 5.6.2, has entered on hourly basis (24 hours data) and thereafter the software modeled the peak load.

b) Solar Source

The solar resource raw data inputting to the software is the average global horizontal radiation measured in 10 minute time interval over the two years. On top of the solar resources data the latitude and longitude of this area would also be used as an input. The time zone is another parameter to be set. The area under study is located at latitude: 35.33 longitude: 6.10E, and with time zone of GMT +1:00. In order to get how much power is generated by the solar PV it requires inputting measured solar resources data in units of kW/m^2 into HOMER software.

c) Cost Data and Size Specifications of Each Component

The basic criterion related to the selection of the power system components in this work is the cost of components, as the main purpose of the work is searching the optimum power system configuration that would meet the demand with minimum NPC and COE. The estimation of the components cost was made based on the current cost available on market. Table (5.4) summarized the model economic inputs, which describe the Initial capital cost of components, the operating and maintenance and Replacement cost: Homer uses these inputs to simulate the different designs and the combinations of components, the results are displayed in wide diversity of tables and graphs.

Table 5.4. Model economic inputs

Component	Size variation rang (Kw)	Capital cost for 1Kw of power	operating and maintenance ($/yr)	Replacement cost ($)
PV	1-18	1500	30	1500
Fuel cell	1-6	4000	100	4000
Converter	5-10	175	20	175
Electrolyzer	1-6	4000	100	400

5.7.2 Optimization results

Various configuration and combinations of components of the hybrid system have been simulated, the different combinations is evaluated by three important parameters. The first is the total unmet load which is total amount of unmet load that occurs throughout the year, the unmet load occurred when the power supply don't cover the load demand. The second is the total net present cost, which is the present value of all the costs that it incurs over its lifetime, minus the present value of all the revenue that it earns over its lifetime [4], the third is the renewable fraction that is fraction of the energy delivered to the load that originated from renewable power sources. The selected configuration must have unmet load equal to zero with the lowest value of the capital cost and high value of renewable fraction. HOMER evaluated more than 117306 configurations, the first six optimized configurations are summarized in Table 5.5, according to the lowest NPC.

Table 5.5. Optimized configurations of the system

Combination	PV capacity (kW)	FC Capacity (kW)	EL Capacity (kW)		Number of batteries	Inverter Capacity (kW)	Total NPC $	REF %	Total unmet load %
1	3	1	1		3	5	22.725	100	0
2	2	1	1		4	5	22.800	100	0.03
3	3	1	1		3	7	23.300	100	0
4	2	1	1		4	7	23.400	100	0
5	3	1	1		3	10	24.000	100	0
6	2	1	1		4	10	24.220	100	0

Among the various configurations the first one is selected, because it satisfies all the requirements, it has total unmet load equal to zero with the lowest NPC, which make a balance between economic, environmental and technical standers. It consist of a field of solar panels of power of 3 kW,2 fuel cell of 1kW,1 Electrolyzer of 1 kW ,1 inverter of capacity 5 kW and 3 solar batteries .

5.8 Load management strategy

In this work, a load management unit is added to improve the system reliability and to increase the energy balance of the system. The residential loads is classified based on their priorities in two main types:

- Non- Controlled loads: as lamps of rooms and toilets, refrigerator, and freezer.
- Controlled loads: such as space cooling and heating, water heating, outdoor lighting, corridor lighting, fans, dryer, washing machine, kitchens lighting, and others.

The load management unit has five inputs which are: the hydrogen tank pressure (P_{H_2}), the charge state of the battery (SOC), the natural irradiance (Ga), the ambient temperature (Ta) and the occupancy (O_c).These inputs are intended to control the controlled loads especially the lights, the washing machine, the air conditioning system and the fans. The strategy flowchart is shown in Fig. 5.8 and can be explained as follows: the air conditioning (A/C) system is considered to be one of the largest energy consumer in the house and represents a real challenge for such isolated power system, its operation is submitted to three main conditions which can be expressed as:

$$\begin{cases} T_a \geq T_{a,ref} \\ O_c = 1 \\ P_{H2} > P_{H2\min} \end{cases}$$

The first condition represents the comparison between the reference temperature and the ambient temperature, if it is verified the controller will pass to the second condition, which indicates the occupancy of the place. Finally, the third condition is associated with the amount of hydrogen storage in the tank. This condition ensures that the hydrogen storage will not be depleted by the huge consumption of the A/C system and there will be enough H_2 to back up the system in different conditions. Moreover, if the H_2 storage is under its minimum security level, the controller will activate the fan, if the charge state of the battery is (SOC>SOC_{min}). In this way the controller balances between the maximum available comfort of the consumer and the energy balance of the system.

The operation of the lighting is subjected to manual control, natural irradiance and the occupancy of the place, for this, the operation of the controlled lighting was conditioned as follows:

if ($G_a \leq G_{a,ref}$) **&** (O_C =1) **then** (Turn on lamps)

if (G_a > $G_{a,ref}$) **then** (Extinct lamps)

The first condition signifies that the light that enters the house through the windows is not enough to light up the place and the second is associated with the occupancy of the place. The washing machine is controlled according to the H_2 tank pressure measured at the time of the deciding, which gives an idea about the availability of the energy produced during the day.

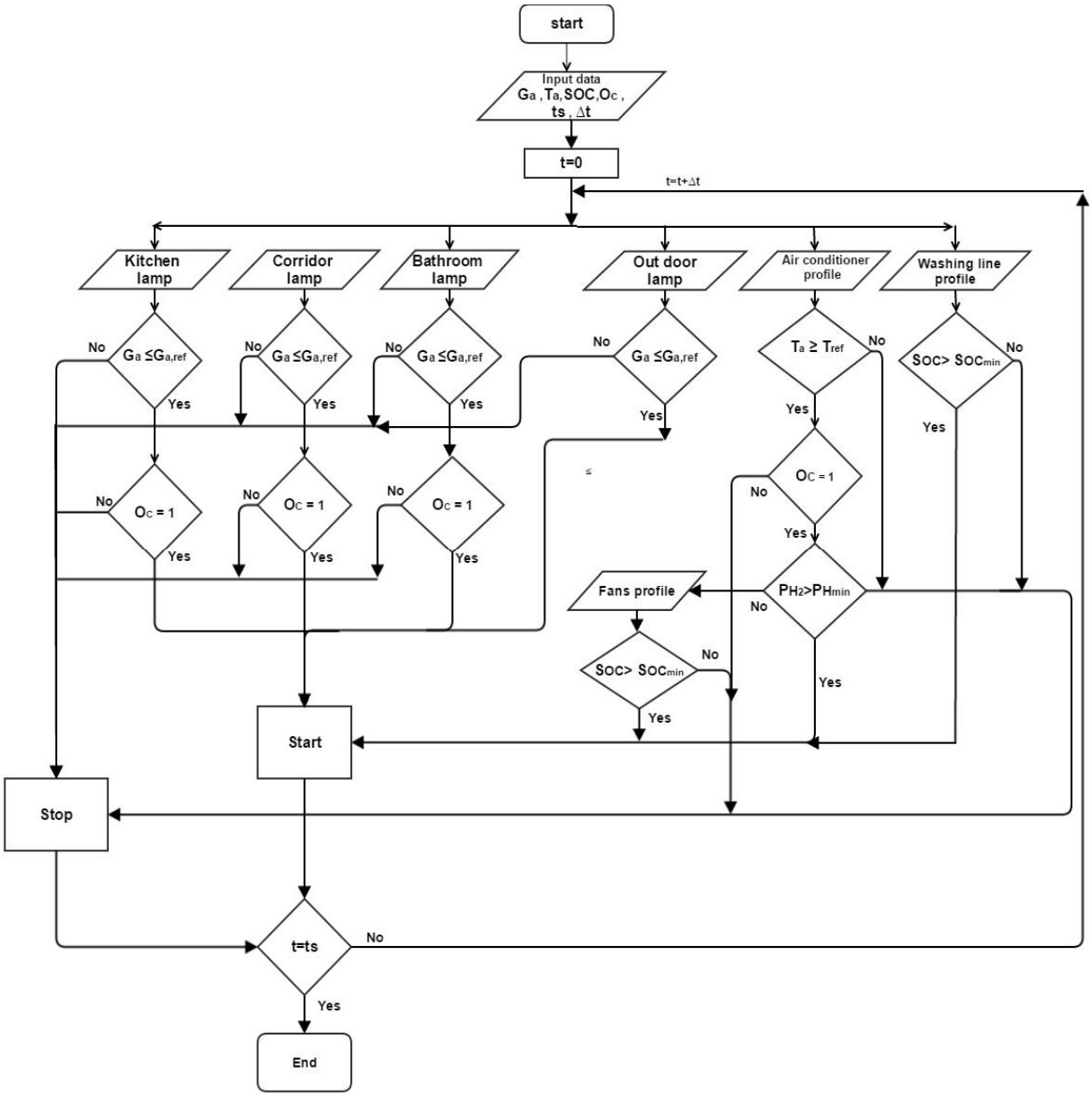

Fig. 5.8. The load management strategy flowchart

5.8.1 Load management strategy simulation

The main objective of the simulation process is to test the performance of the proposed system over a long period of time and under different stresses on the system like bad weather condition and heavy load consumption. The load management parameters are shown in Table 5.6.

Table 5.6. Load management parameters

Parameter	Value	Unit
$G_{a,ref}$	400	W/m^2
$T_{a,ref}$	25	°C
SOC_{min}	45	%
SOC_{max}	98	%
H_{2min}	3000	Pa
H_{2max}	14000	Pa
Δt	1	hour

The energy balance of the system affected deeply by the availability of the renewable resources. Fig. (5.9-a) shows the hourly averaged global solar radiation on a horizontal surface (W/m2) for four days of summer, these days coincide with low irradiance level. In the third day and as a result of the low irradiance during the previous days the battery state of charge (Fig 5.9-b) and the hydrogen tanks pressure (Fig 5.9-d) reach their minimum level and the energy balance of the system shows an exorbitant deficit (Fig 5.9-c).

On the other hand, using the proposed management strategy can improve highly the energy balance of the system as it minimizes the discharge level of the battery (Fig 5.10-b) and eliminates any energy deficit during the same period (Fig 5.10-c). Moreover, the proposed strategy ensures that there will be sufficient amounts of hydrogen inside the tanks (Fig 5.10-d) during the different conditions.

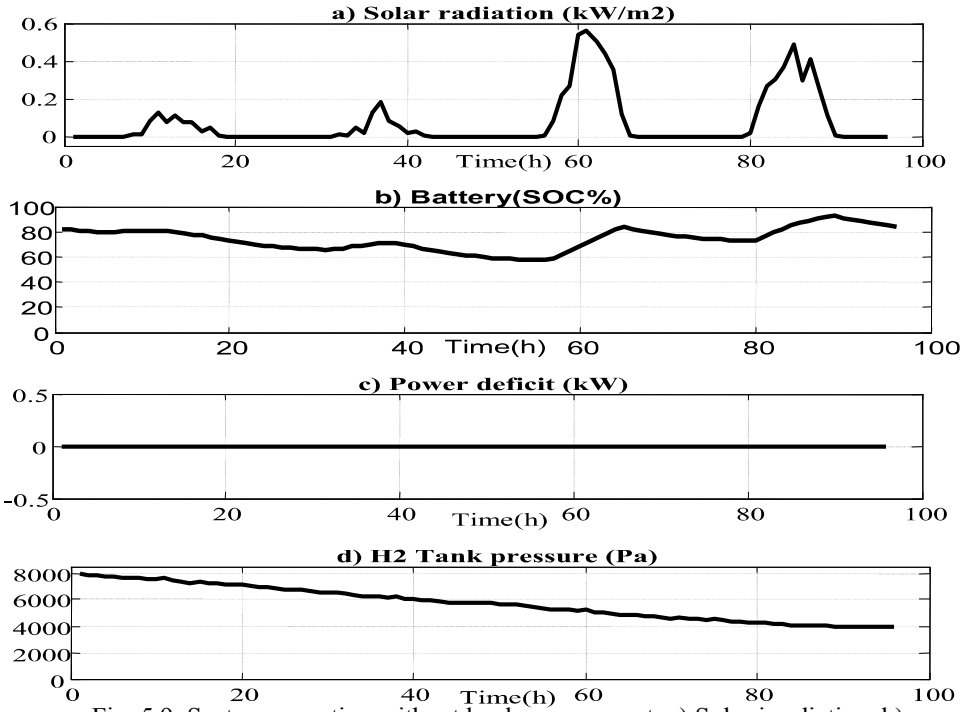

Fig. 5.9. System operating without load management: a) Solar irradiation, b) Battery (SOC %),c) Power deficit (kW),d) H_2 Tank pressure (Pa)

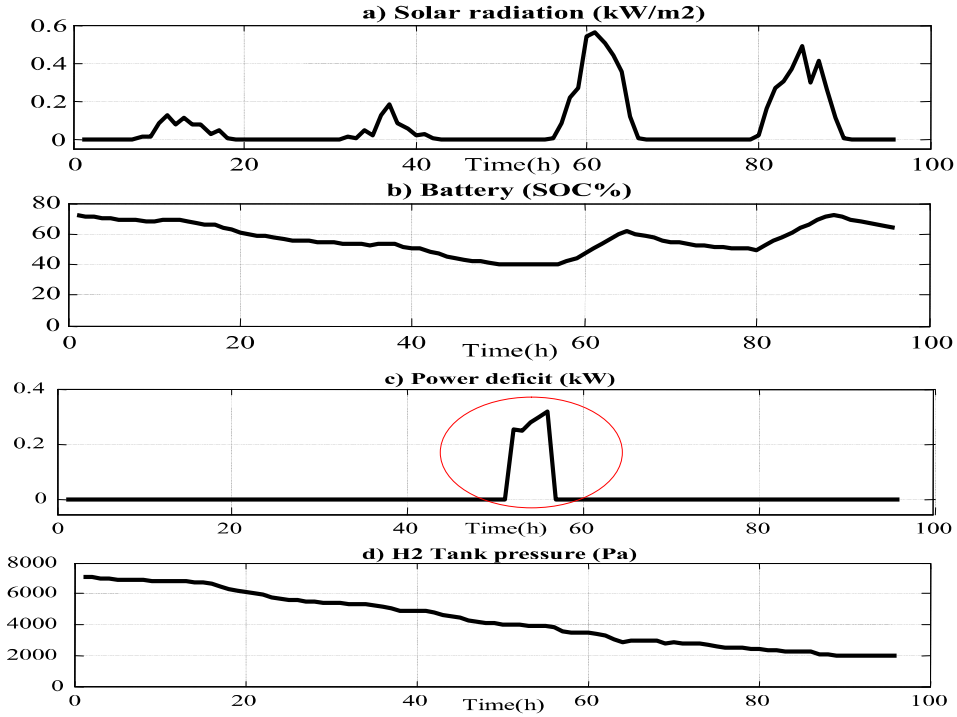

Fig. 5.10. System operating with load management: a) Solar irradiation, b) Battery (SOC %),c) Power deficit (kW),d) H_2 Tank pressure (Pa)

5.9 Conclusion

This chapter described the DSM methodology developed for this study in detail. Moreover the optimization process of the hybrid energy system was presented. The proposed DSM strategy was applied for zero emissions hybrid system for off grid house. It takes a house located in the province of Batna (35°33′N 6°10′E) as a case study with a deep study on a real load profile for an average house with all required weather data of the location. The simulation result illustrates the effectiveness of the proposed control strategy. The proposed control strategy increases the service life of the battery and fuel cell, as it reduces the ON-OFF switch cycle of the FC and prevents battery deep discharge under heavy loads consumption and bad weather condition. In addition to that, it improves the reliability of the system, as it disconnects the non-critical loads in case of extra heavy loads consumption and power deficit which increases largely the overall system efficiency.

5.10 References

1. Newborough M, Augood P. Demand-side management opportunities for the UK domestic sector. IEE Proceedings: Generation, Transmission and Distribution, 1999, vol. 146, no. 3, pp. 283-293.
2. T lambert. Micro power system modeling with HOMER. National renewable energy laboratory,2006.
3. Getting Started Guide for HOMER, National Renewable Energy Laboratory.2005.

Chapter 6

The second case study on the proposed demand side management and control algorithm

6.1 Introduction

As the previous chapter is applied the proposed DSM strategy for zero emissions hybrid system, the main aim of the presented chapter is to test the efficacy of the proposed DSM for hybrid power system that consist of a conventional and a renewable energy sources. The second case study focuses on applying a modified DSM on a (photovoltaic–wind–diesel) hybrid energy system for medium rural health building located in the Sahara region. Designing a suitable DSM for such facility is a critical issue because of the activity nature of such important facility. The modified version of the proposed DSM employ a combination of ON/OFF direct load control and fuzzy logic control strategy. Using these combinations of control minimize highly the impact on users and at the same time maximize the match between demand and supply through identifying the best control depending on many standers such as energy availability and occupancy. In addition to that the proposed DSM must be able to reduce effectively the harmful emissions of the system with keeping the energy balance of the system.

6.2 General overview

The main objective of the DSM is to improve the health facility energy system with maintain a certain thermal comfort level. As inertial features of these types of demand systems, they have a certain extent of flexibility. This flexibility can be used for better operation of the demand devices and to facilitate the usage of intermittent renewable energy without violating user convenience. This strategy is based on the control of air conditioning system depending on the battery state of charge (SOC), the occupancy (O_C) level, and the temperature difference between the setting and the indoor temperature. The control aspect of lighting is added, which is based on the O_C level and the comparison between the reference and the natural lighting that enters the facility through the windows, taking into account the visual comfort. Fuzzy logic control will be employed to control the A/C system which represents many advantages over the previous ON/OFF control.

6.3 Geographic and climate data of the region

The Algerian Desert is part of the Sahara desert, it is located in north-central Africa and cover about 80% of the Algerian territory. The province of Tindouf covers the northern part of the Algerian Sahara (Fig 6.1), with a surface of 159,000 km^2. Due to it remote location and wide surface several thousands of the consumers don't have access to the electricity grid, which has a large effect on prosperity and economic development of the local society. On the other hand the location benefits from enormous renewable energy sources which can be the best solution to provide energy to these remote area.

Fig 6.1. Geographical position of Tindouf

a) Temperature

Fig 6.2 shows the daily average temperature of the location, the area climate characterized with two main seasons: one very hot extends about four months from April to August and another temperate season extend about three month from December to March. The temperature has large influence in the energy consumption throughout the year, during the two distinct seasons the air conditioning system is necessary and often used either for cooling or heating.

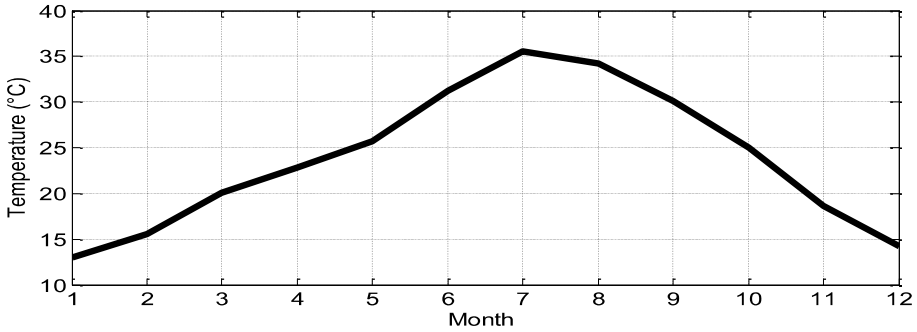

Fig. 6.2. Ambient temperature °C

b) Solar irradiance

Tindouf receives an average of 9:51 hours of sunlight per day. The shortest day is December 21 with 10:23 hours of daylight; the longest day is June 20 with 13:54 hours of daylight. It is sunny 82.2% of daylight hours.

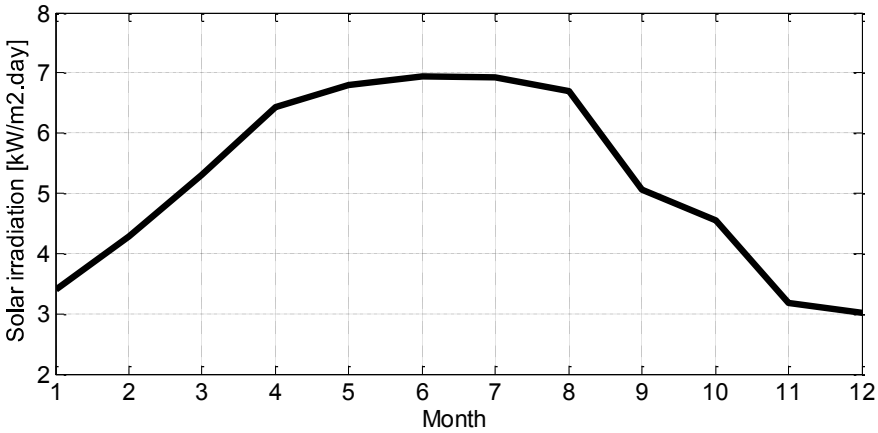

Fig. 6.3. Horizontal global irradiation, [kWh/m².month]

It receives high Level of radiation; the yearly average value of daily solar irradiance is about 5.89kw/m^2 [1]. The Monthly average values of solar data are shown in the fig 6.3.

C) Wind speed

The wind speed data for Tindouf site have been use to estimate the amount of generated energy during the year, Fig 6.4 shows the monthly average wind speed of the location. The highest monthly wind speed is in April (7.6 m/s), with the average daily maximum wind speed is 11.6 m/s. The lowest monthly wind speed is in December (4.2 m/s) with and the average daily maximum wind speed is 6.7 m/s. [2].

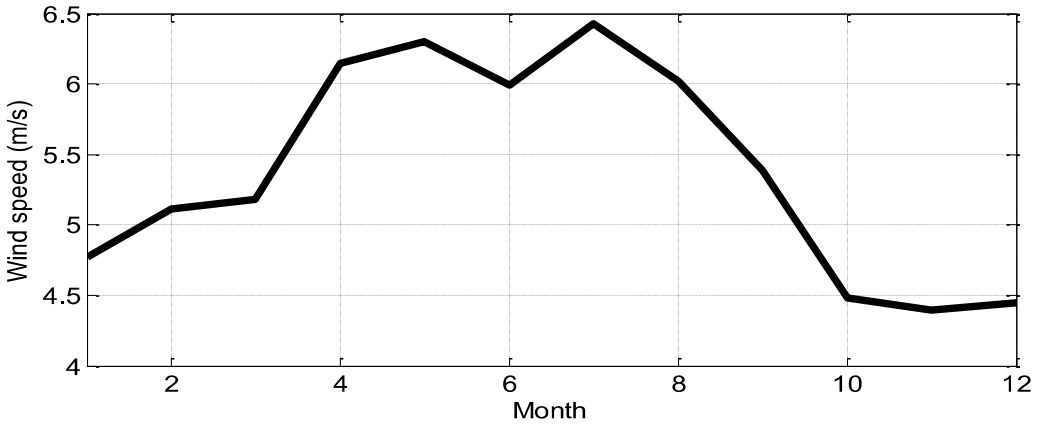

Fig. 6.4. Yearly average wind speed (m/s)

6.4 Load profile

Deep analysis of the different loads lead to improve the energy system of the health facility, areal investigation is done on daily electricity consumption throughout the year. These electrical loads drive energy consumption and costs, but also facilitate the critical health services that take place in such facilities; understanding the best way to support, protect and expand those services starts with an analysis of those loads. A load analysis can yield valuable insights into facility energy usage that can be used to save on energy costs, increase productivity and protect critical assets.

Health facility loads can be divided in two ways: non-critical loads, and critical loads. Non-critical loads are those loads, which have any effect in the patient life, such as air conditioners and security lights [3].

Critical loads are defined as equipment that is essential to the operation of the facility as vaccination refrigeration, Sensitive laboratory instruments, medical equipment such as x-rays, and data acquisition systems [3]. Table 6.1 shows example of load inventory for a medium health clinic, the information is collect with the help of the ministry of public health and population showing the load distribution and the different equipment used in health facilities.

Table 6.1.Example of load inventory for a medium health clinic

Equipment	quantity	Power(w)	Hour used per day	Total energy Kwh/day	Type of loads
Lights	15	40	10	6	Non-critical Non-shiftable
Vaccine Refrigerator	2	60	10	1.2	Critical
Refrigerator Non-med	2	300	8	2	Critical
centrifuge	4	242	4	3.87	Critical
Microscopes	3	40	4	0.48	Critical
Hematology Analyzer	2	230	4	1.840	Critical
Blood chemical analyzer	2	88	4	0.704	Critical
CD4 machine	2	200	4	1.6	Critical
x-ray	1	3000	1	3	Critical
Desktop computer	2	230	7	3.222	Critical
Air conditioner	3	1500	3	13.5	Non-critical shiftable
fan	2	45	2	0.18	Non-critical shiftable

The example laboratory loads in the tables above demonstrate the importance of developed an advanced DSM strategy for non-critical load. The non-critical air conditioning load increases total daily consumption considerably, at the basic laboratory it accounts for over half. Moreover the size and cost of the system will be highly augmented. ON-OFF-fuzzy logic control can be applied on non-critical non-shiftable loads while a combination of load direct control and load shifting strategy can be applied on non-critical shiftable loads, in this way we can benefit of the advantages of the tow method at the same time.

6.5 Design and optimization of the hybrid power system

HOMER software is used to get the optimal configuration of the hybrid system .The tested hybrid system configuration is shown in Fig 6.5. Table 6.2 summarized the model inputs, which describe technology options, component costs, and resource availability. Concerning the diesel price, Algeria has very low price rang varying between 0.19-0.17 $/L (2004-2014) [4]. Concerning the batteries, 6V- 1.156Ah lead acid battery is selected, the variation of the batteries numbers in the range of 1-20.

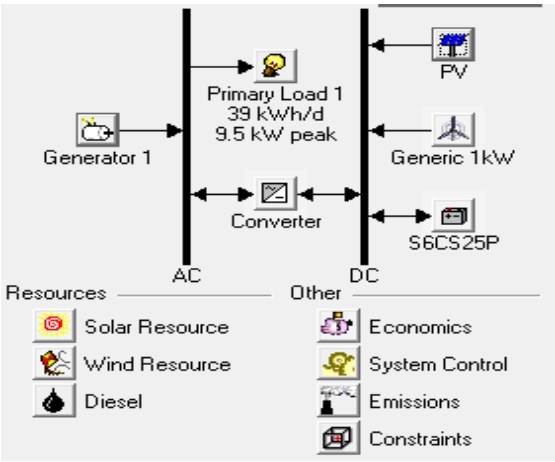

Fig 6.5. Tested hybrid system configuration

Table 6.2.Homer model input

Component	Size variation rang (Kw)	Capital cost for 1Kw of power
PV	1-18	2000
Wind turbine	1-6	1000
Converter	5-10	175
Diesel generator	1-5	350

Homer uses these inputs to simulate the different designs and the combinations of components, the results are displayed in wide diversity of tables and graphs.

6.5.1 Optimization results

HOMER evaluated more than 117306 configurations, the first six optimized configurations are summarized in Table 6.3, according to the lowest NPC.

Table 6.3. Parameters of feasibility analysis

Combination	PV capacity (kW)	WG Capacity (kW)	DG Capacity (kW)	Number of batteries	Inverter Capacity (kW)	Total NPC $	REF %	Total unmet load %
1	3	2	4	4	7	28.599	54	0
2	3	3	3.5	4	8	30.860	58	0.03
3	4	2	4	5	8	31.021	54	0
4	4.5	3	4	4	7	31.174	55	0
5	4	4	4.5	4	10	32.322	57	0
6	5	4	5	4	9	34.155	59	0

Among the various configurations the first one is selected, because it satisfies all the requirements, it has total unmet load equal to zero with the lowest NPC and high value of

renewable fraction, which make a balance between economic , environmental and technical standers. It consist of a field of solar panels of power of 3kW,2 wind turbine of 1kW,1 diesel generator of 4 kW ,1 inverter of capacity 6 kW and 4 solar batteries .

The cash flow summary of the selected system is shown in Fig 6.6, diesel generator has the highest NPC, the price of fuel occupies more than 50% of it NPC. The battery bank has the second highest NPC rate; battery replacement occupies about 40 % of its total NPC, the expected life of the battery bank is 12 year.

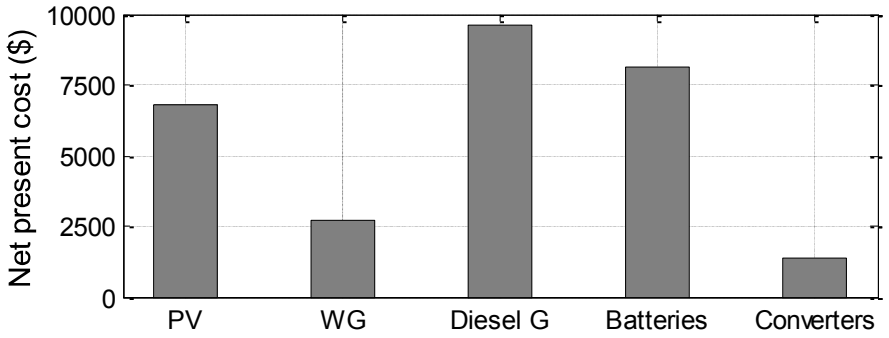

Fig 6.6. Cash flow summary of the PV-Wind-Diesel hybrid system components

6.6 DSM Concept

Depending on the optimization results the configuration comprise a PV panel, a small wind turbine, a diesel generator and a battery bank. In this configuration the renewable energy source is integrated with the traditional system (group of diesel generator system) which is often used to supply power to remote area. However an advanced DMS is more than necessary to optimize the operation of such power system. The main aim of the LSM strategy is to control the non-critical load especially the air conditioning (A/C) system, as it consumes about 35% of the total power consumption. The control aspect of lighting is added, in order to control the non-critical lights (kitchen, bathrooms, and security lights). ON-OFF control can be applied on lights control (non-critical non-shiftable loads) while a combination of load direct control and load shifting strategy will be applied on air conditioning (A/C) system (non-critical shiftable loads), in this way we can benefit of the advantages of the tow method at the same time.

The DSM algorithm has four inputs, which are the battery state of charge (SOC), the ambient temperature (T_A), the irradiance level (G) and the occupancy level (O_{CC}).

The working level of the AC units is controlled depending on the battery SOC, the temperature T_A and the O_{CC} level, the non-critical lights working time are controlled according to the O_{CC} and

nature irradiance level G_a, which enters the facility throughout the windows. Figure 6.7 shows the proposed structure of the load management unit.

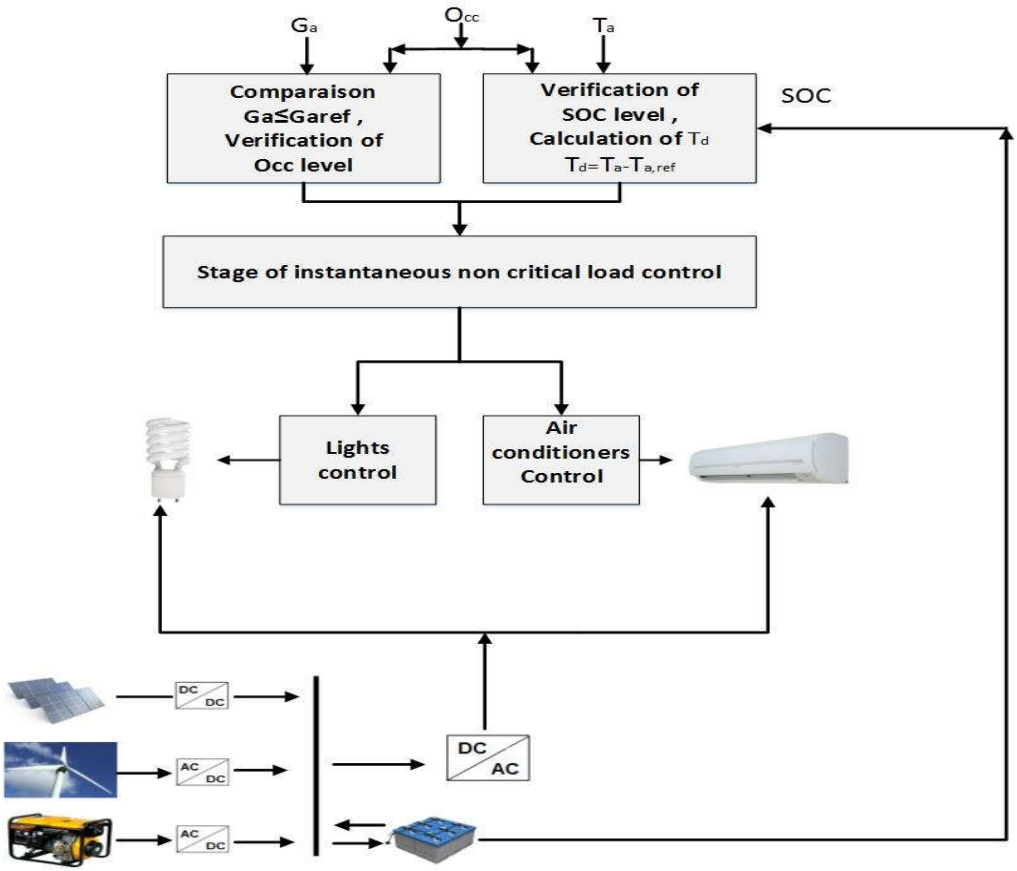

Fig. 6.7.The proposed structure for load management units

6.6.1 Load management unit for non-critical lights

As the lighting consumes about 15% of the total energy consumption of the facility, the DSM strategy for the lighting is necessary without affecting visual comfort. Non-critical lights of the facility can be divided into kitchen, corridor, bathrooms and security lights. The kitchen, the corridor and the bathroom lamps are controlled according to nature irradiance (that enters the facility throughout the windows) which is compared to a reference irradiance G_{aref} and according to the occupancy of the building (O_{CC}). The security lamps located outside of the building are controlled according to the nature outside irradiance which is compared to a reference irradiance $G_{aref,}$ the organization chart of the non-critical light power management is shown in Figure. 6.8.

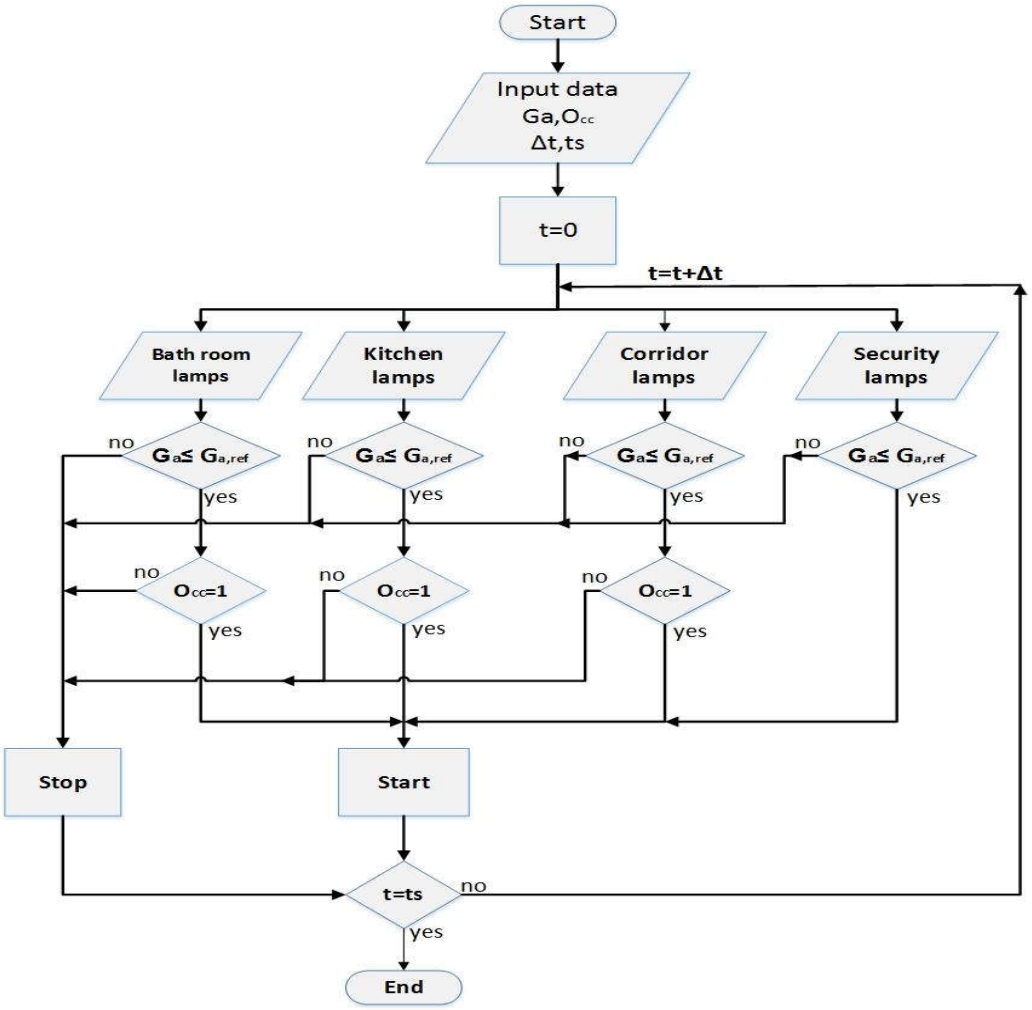

Fig 6.8.The organization chart of Non critical lights power management

6.6.2 Load management unit for air conditioners

The A/C units consume about 35% of the total energy consumption during the hot summer. The utilization of air conditioning system results in peak consumption during the mid-day's hours, an efficient load management strategy is needed to limit or shift the peak load from on-peak to off-peak time periods, and to use the load in an active and intelligent way.

The facility is divided into four thermal zones depending on heating and cooling requirements, which are the waiting room (zone 01), the checking room (zone 02), the patient's room (zone 03) and the laboratory (zone 04), each zone is connected to a split AC unit. Each thermal zone is connected to a local load management device (LMD), to control the flow of the AC refrigerant, depending on the indoor temperature and the O_{CC} level. The four local LMD are wired via one

master controller, which makes the necessary balance between the A/C units demand and the available power of the hybrid system. For example in the case of low batteries SOC, the master LMD will send a signal to the local LMD to completely turn off the A/C units for some thermal zones or for all thermal zones, depending on the batteries SOC level as explained later.

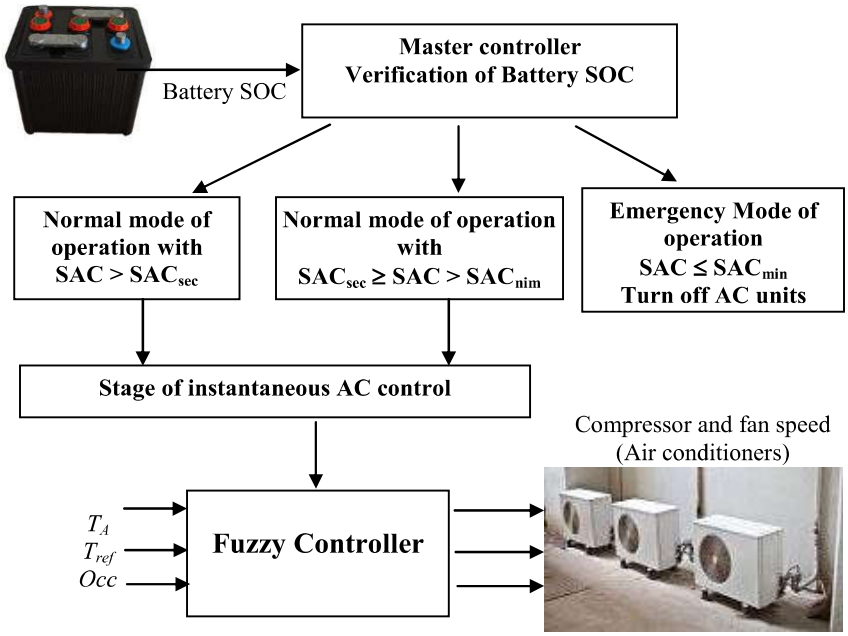

Fig. 6.9. Operation mode of LMD for AC units

Fig. 6.9 shows the operation mode of the LMD of the A/C units, the master controller switches between three modes of operation which are: normal, partial and emergency mode. The switch between these modes is made, according to the battery SOC level and the importance degree of the thermal zone. Table 6.4 summarizes the principal operation of each mode.

Table 6.4. The principle of operation of the master controller modes.

Modes	SOC	AC unit of (zone-01)	AC unit of (zone-02)	AC unit of (zone-03)	AC unit of (zone-04)
Normal	SOC>SOC_{sec}	ON	ON	ON	ON
Partial	SOC_{sec} ≥SOC>SOC_{min}	ON	ON	OFF	OFF
Emergency	SOC≤ SOC_{min}	OFF	OFF	OFF	OFF

SOC_{sec} is defined as a value of battery state of charge located between SOC_{min} and SOC_{max}, it's generally equal to (SOC_{min} + 10%). The main objective of determining this value is to ensure that the battery state of charge will not fall down under its minimum level, under the huge energy consumption of the A/C units and to guarantee a non-interruptible power supply for the critical loads under any circumstance. Essentially the master controller works in the normal mode as the

condition SOC > SOC_{sec} is verified. The partial mode is activated when SOC_{sec} ≥ SOC > SOC_{min}, the AC units for waiting room and checking room is completely turned off, while the AC units for laboratory and patient room is still working at the normal level. This decision is made, depending on the importance of maintaining the proper temperature within these two rooms, to ensure maximum comfort of patients and to protect the sensitive equipment's in the laboratory.

In the case of SOC ≤ SOC_{min}, the controller will enter the emergency mode of operation and the A/C units of all thermal zones will be turned off, in order to supply all available power to serve the critical load.

6.6.3 The local load management device

The operation of each A/C unit is controlled, according to the T_A and the O_{CC} level by a local LMD. At this level of command, a fuzzy logic controller FLC is proposed, in order to adjust and control the AC compressor speed [5, 6]. This type of control adjusts the flow of refrigerant to adapt the variation of its load, resulting in many advantages such as low energy consumption and a much steadier temperature control. The measured indoor temperature difference and the O_{CC} level are used as fuzzy inputs in order to control the A/C compressor/fan speed, which is the fuzzy output. Using this type of command can increase the amounts of energy savings range from 10% to 30%, comparing with On-off cycling controller [7].

6.6.3.1 Fuzzy logic controller

a. Fuzzy input and output variable

Temperature Difference (T_d): The temperature difference (*Td*) between the indoor temperature and the setting temperature, has direct impacts on the electricity consumption of air conditioner units. According to ACEEE (American Council of Energy Efficiency Economy), an increase of 1°C can saves to 5 % of the energy consumption of the air conditioning system. Each thermal zone has a specific setting temperature, depending on the kind of the zone activity and the difference between indoor/outdoor temperatures. In our case, the setting temperature varies in the range of [22.5, 25] °C.

The *Td* varies in the range of [-7, +7]°C which is divided into: negative high (NH), negative medium (NM), zero (ZE), positive medium (PM), and positive high (PH), the membership function of the temperature difference Td is given in Figure 6.10.

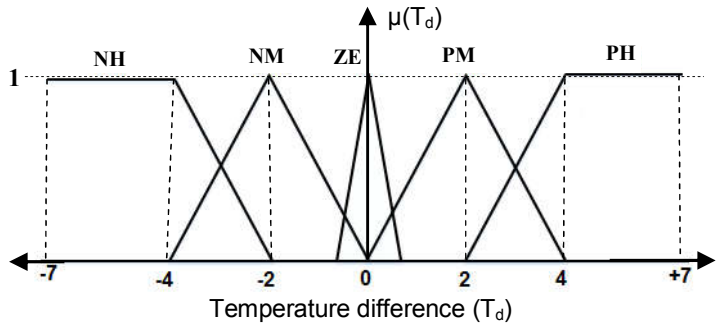

Fig. 6.10. Membership function for temperature difference

Occupancy (O_{CC}): The occupancy level has a direct effect on the indoor temperature by the people, which enter and leave the facility through the doors or by the body heat flow. Each thermal zone can be characterized with different O_{CC} level according to its activity, Table 6.5 summarizes the O_{CC} rang of the different thermal zones with the help of AMHP (Algerian Ministry of Health and Population). The occupancy level is determined, according to the range of people as low (L), medium (M) or high (H). In the absence of people, the compressor/fan remains off. The membership function of the O_{CC} level example of the waiting room is shown in Figure 6.11.

Table 6.5. Occ rang of the facility thermal zones

Thermal zone	waiting room	checking room	Patient room	The laboratory
O_{CC} rang	1-15	1-7	1-12	1-6

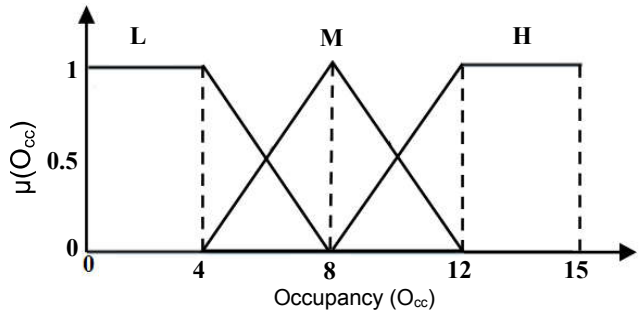

Fig 6.11. Membership function of O_{CC} level example of the waiting room.

b. ***Output variable and fuzzy base rule***

Compressor/Fan speed : The speed of the compressor and fan of the A/C units varies in the range of (25-100)%, Figure 6.12 shows the membership function for compressor and fan speed.

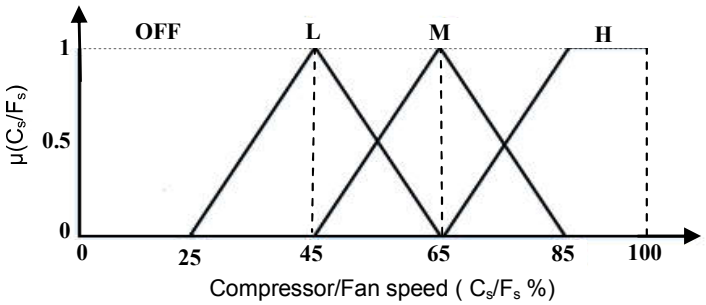

Fig 6.12. Membership function for compressor and fan speed.

Fuzzy base rule: The temperature difference *Td* has five fuzzy variables and the occupancy level O_{CC} has four fuzzy variables. Thus, we have twenty control rules (Table 6.6), the output operation control of the compressor and the fan speed can be summarized in six output variables, namely, A, B, C, D, E and F. (Table 6.7)

Table 6.6. Fuzzy control rules of the system

	NH (negative high)	NM (negative medium)	ZE (zero)	PM (positive medium)	PH (positive high)
ZE (zero)	A	A	A	A	A
L (Low)	A	A	B	C	D
M (medium)	A	A	B	D	E
H (high)	A	A	C	E	F

Table 6.7. The output variable definition

	A	B	C	D	E	F
Fan speed (Fs)	OFF	L (low)	L (low)	M (medium)	H (high)	H (high)
Compressor speed (Fc)	OFF	OFF	L (low)	M (medium)	M (medium)	H (high)

6.7 Result and discussion

6.7.1 Load management results

The simulation is carried out, to compare the system with and without load management. The comparison criterions are the limitation of peak consumption throughout the on-peak period and the minimization of the dependence on the DG throughout this period. The load management simulation parameters are given in Table 6.8.

Table 6.8. Parameters of load management simulation

Parameter	Value	Unit
G_{aref}	400	W/m^2
T_{aref}	25	°C
SOC_{min}	45	%
SOC_{max}	98	%
SOC_{sec}	55	%
Δt	1	hour

The DG works at its rated capacity during the mid-day's hour, in order to cover the high power consumption during this period, which cannot be covered by the total renewable energy production. Figure 6.13 shows that using our LSM strategy can shift the peak load in rang of 20%, resulting in a reduction of the DG capacity during the peak period. The reduction is about 18% compared to the system without LSM (Figure6.14), which has significant economic and environmental benefits.

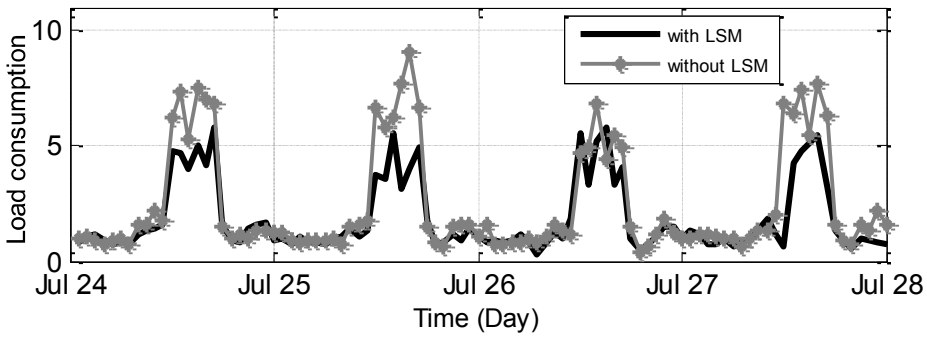

Fig 6.13.Load consumption

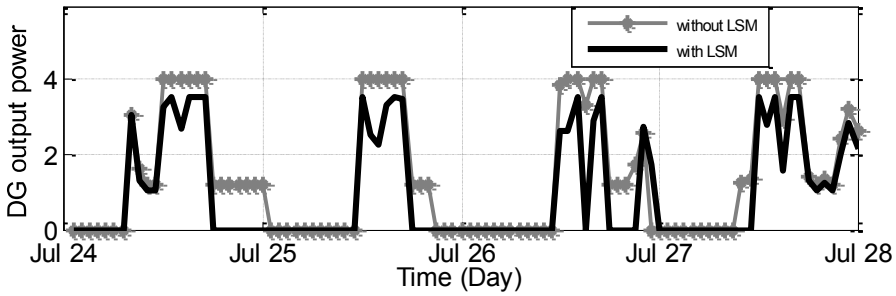

Fig 6.14. DG output power

As mentioned earlier the partial operation mode occurs when there is not enough energy to charge the battery under bad weather condition or high consumption level, our LSM strategy improves the performance of the battery banks and increases the reliability of the system.

Figure 6.15 compares the battery SOC between the systems with and without load management. Figure 6.16 shows that as there is not enough renewable energy, the battery SOC reaches its minimum level under huge consumption during peak period. Moreover using our LSM strategy minimizes the storage use over the year and increases the batteries lifetime.

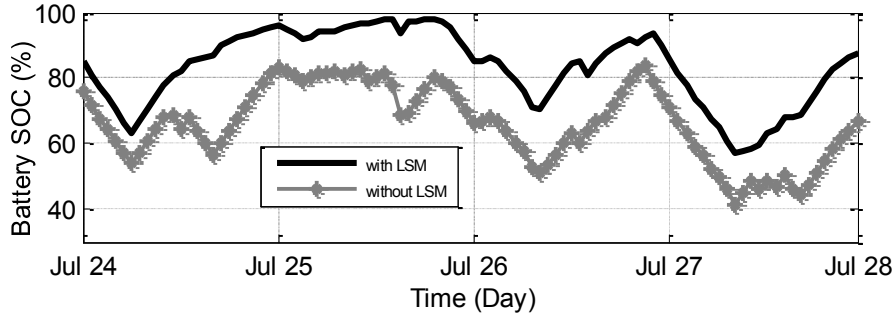

Fig 6.15. Battery state of charge (%)

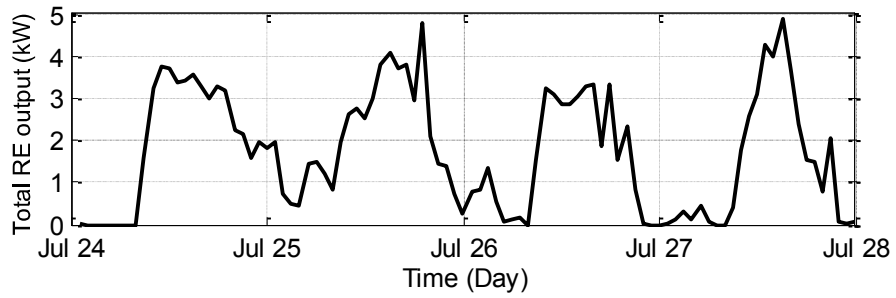

Fig 6.16. Total RE output (kW)

6.7.2 Environmental evaluation

Table 6.9 compares CO_2 emission between the two studied systems (with and without LSM), the comparison reference is the traditional system (group of diesel generator system) which is often used to supply power to remote area.

Table 6.9. Environmental evaluation of the two studied systems

Systems	DG hours of operation (hr/year)	Fuel consumption (L/year)	CO_2 Emission (kg/year)	The reduction in CO_2 Emission (%)
Traditional	6895	5784	16251	00%
Without LSM	2643	2441	6427	60%
With LSM	2121	1921	5058	70%

The system with LSM has the lowest CO_2 gas emission, the reduction is about 10% compared to the free LSM case, which makes our facility ecological at a high level.

6.8 Conclusion

The second case study focuses on applying a modified DSM on a (photovoltaic–wind–diesel) hybrid energy system for medium rural health building located in the Sahara region. The proposed DSM was tested by simulation. The result showed that the reduction in the peak consumption is about 20% using the proposed management strategy, which has significant economic and environmental benefits. The reduction of diesel capacity throughout the peak period was about 18%, which leads to a reduction in the fuel cost and CO_2 emission at the same time. In addition, the proposed strategy minimizes the storage use over the year and increases the battery lifetime.

6.9 References

1. S. Bentouba, M. Hamouda, A. Slimani, C.Pere Roca, M.Bourouis,A. Coronas,B. Draoui, M.S.Boucherit « Hybrid System and Environmental Evaluation Case House In South of Algeria » Energy Procedia 36 (2013) 1328 – 1338
2. http://www.tindouf.climatemps.com
3. Powering health electrification options for rural health centers report, USAID (2010)

4. B.S. Borowy B, Salameh Z. Methodology for Optimally Sizing the Combination of a Battery Bank and PV Array in a Hybrid Wind/PV System. IEEE Transaction on Energy Conversion 1996; **11**(2):367 – 488.
5. Kazuo Tanaka. An Introduction to Fuzzy Logic for Practical Applications 1996.
6. Jerry M. Mendel.Uncertain Rule-Based Fuzzy Logic Systems: Introduction and New Directions University of Southern California, Los Angeles, CA.
7. Funami K, Nishi H. Evaluation of power consumption and comfort using inverter control of air-conditioning. 37th Annual Conference on IEEE Industrial Electronics Society (IECON) 2011, Melbourne, 3236 – 3241.

Appendix

Energy Conversion and Management 105 (2015) 377–392

Contents lists available at ScienceDirect

Energy Conversion and Management

journal homepage: www.elsevier.com/locate/enconman

Dynamic control and advanced load management of a stand-alone hybrid renewable power system for remote housing

Tareq Alnejaili [a,*], Said Drid [a], Driss Mehdi [b], Larbi Chrifi-Alaoui [c], Rafik Belarbi [d], Aziz Hamdouni [d]

[a] Laboratoire LSPIE, University of Batna, Rue Chahid M[ed] El-Hadi Boukhlof, Batna, Algeria
[b] Laboratoire LIAS, University of Poitiers, Bât. 25, 2 Rue Pierre Brousse, BP 633, 86022 Poitiers, France
[c] Laboratoire LTI, Université de Picardie Jules Verne, GEII, IUT de l'Aisne, 02880 Cuffies, France
[d] Laboratoire LaSIE, Université de La Rochelle, Avenue Michel Crépeau, 17042 La Rochelle, France

ARTICLE INFO

Article history:
Received 5 March 2015
Accepted 29 July 2015

Keywords:
Power management
Dynamic control
Hybrid power system
Load profile
Energy efficiency

ABSTRACT

This paper proposes an advanced energy management strategy for a stand-alone hybrid energy system. The considered hybrid system includes a photovoltaic panel, a fuel cell, an electrolyzer, a battery bank and a supercapacitor. The proposed power management system aims to control the energy flow within the system and decides the amount of the load power shared with each power source. The system control is implemented in two parts: a central power flow controller that provides overall control of the power system and a local loads controller, which controls the different loads according to the energy balance of the system. The hybrid power system has been tested by simulation using models implemented in Matlab/Simulink software. The simulation is performed over a short and a long period of time in order to evaluate the performance of the dynamic controllers and the effectiveness of the management strategy. For a long simulation period, a house located in the province of Batna (35°33′N 6°10′E) has been taken as a case study with a deep study on real load profile for an average house with all required weather data with respect to the location. The simulation results confirm the efficiency of the proposed control strategy, as it increases the reliability of the system and improves its energy balance.

1. Introduction

During the last two decades, the electrical energy consumption in the world has increased significantly. That enormously increasing in the energy demand brought renewed interest in renewable energy (RE) sources such as solar, wind, hydro power, biomass and hydrogen.

Among the different RE technologies, solar and hydrogen energy sources are considered to be one of the most favorable options, as they can work in a complementary way. The solar energy technology as the photovoltaic (PV) system can be employed effectively in a different hybrid energy systems On the other hand, the output power of a PV system depends strongly on the fluctuating weather conditions. Consequently, the cloudy and night periods represent a real challenge to their utilization in hybrid energy systems. Moreover, there are a lot of difficulties related to the storage of the generated PV power. The performance of the PV system can be improved; by its integration with other power sources and/or storage systems as battery bank, fuel cell (FC), wind, electrolyzer (EL) and diesel generators.

An FC power plant is a power generation system that generates electricity, heat, and water from oxygen and hydrogen, it can be used for different application such as residential, vehicles and commercial applications [1–3]. The hydrogen could be obtained throughout proton exchange membrane (PEM) electrolyzer system. PEM electrolyzer cells offer many advantages like being environmental friendly and high hydrogen purity, compared with conventional hydrogen production processes including fossil fuel reforming and alkaline water electrolysis [4,5]. Generally the FC is characterized by its high efficiency and reliability, but its dynamics are limited by the hydrogen/oxygen delivery system. Therefore, a fast response auxiliary power source is needed to compensate its slow dynamic which can be achieved by the utilization of a supercapacitor bank.

A different hybrid renewable power production structures have been studied in many research papers. Khanand Iqbal [6] presented an investigation on a standalone wind-hydrogen hybrid energy system. The aim of their work was the analysis of the system behavior under sudden load variation and wind speed change. Carapellucciand Giordano [7] developed a simulation tool for

* Corresponding author. Mobile: +213 797358743.
E-mail address: tareq.elnejaili@univ-batna.dz (T. Alnejaili).

http://dx.doi.org/10.1016/j.enconman.2015.07.080
0196-8904/

testing energy and economic performance of renewable energy islands. An economic optimization approach was also proposed to minimize the unit cost of electricity. Castañeda et al. [8] discussed a new sizing method for a stand-alone PV/FC/EL hybrid system. The technical optimization was performed to efficiently utilize the energy sources integrated with the hybrid system.

The utilization of renewable energy technology requires a comprehensive energy management strategy (EMS) that achieves an optimal fuel economy with a minimum impact on the life cycle of a hybrid power system.

Semaoui et al. [9] proposed a new EMS for a stand-alone PV system, the control strategy was intended to control washing machine, fans and lights. Their results showed that the suggested load management strategy improves the performance and the reliability of the stand-alone PV system. In the same line, Clastres et al. [10] presented an advanced energy management for residential application, their management strategy relies on data forecasts on the operating plan for a 24 h period. To improve the reliability of a PV hybrid system, Alnejaili et al. [11] proposed a new EMS for a stand-alone PV-Wind-Diesel power system. The control strategy was intended to control air conditioning system and lights. Their result showed that the reduction in the peak consumption is about 20% using the proposed management strategy.

Concerning load management for a standalone Renewable/Fuel Cell Hybrid energy system, Uzunoglu et al. [12] presented a modified power flow controller for PV/FC/EL hybrid power system. Their control strategy manages the power flow among the power source and optimizes the operation of the hydrogen storage system. In [13], Behzadi and Niasati evaluated the performance of three different power management strategies with three different sizing methods for a standalone PV/FC/Battery hybrid energy system. The best combination of a power management strategy and sizing method has been outlined depending on the battery state of charge and hydrogen tank pressure. Dursun and Kilic [14] presented a three different power management strategies for an isolated PV/FC/Wind/Battery hybrid energy system. The main aim of the different strategies was the evaluation of the battery energy efficiency.

In this paper, we propose a stand-alone hybrid power system made up of a PV panel and a FC as energy sources, an EL as a hydrogen storage system, a lead acid battery bank as a long term storage element and a supercapacitor (SC) as a short term energy storage element. The main contribution of this work is to present an energy management algorithm according to the following constraints: (i) weather condition fluctuations, (ii) load demand, (iii) battery state of charge (SOC), (iii) pressure of the hydrogen tank, (v) energy balance of the system. The considered strategy offers many power flow possibilities according to four operating modes of the hybrid system. Each operating mode contains several sup-mode to cover all the circumstances. In addition to that, an advanced load management strategy is developed in order to meet the energy constraints and to increase the overall efficiency of the system. This paper is organized as follows. Section 2 describes the fundamentals of hybrid systems. Section 3 describes the modeling of the system components. Section 4 presents the design of the system dynamic controller. Section 5 describes the proposed management strategy. Section 6 presents the dynamic simulation results and discuss a case study.

2. Hybrid system description

2.1. System representation

Fig. 1 shows the proposed structure of the hybrid power system (HPS), which comprises a solar module, a PEM fuel cell stack, an electrolyzer, a lead acid battery bank, and a super capacitor. The system specifications are summarized in Table 1. The components of the system are linked to a common DC bus through appropriate DC–DC power converters and assumed to be controlled by independent control system. The PV array is the primary source of the HPS, it is connected to the DC bus through DC–DC boost power converter, which achieves the PV Maximum Power Point Tracking (MPPT) control. The FC is sized to be the main backup source when the power generated by the PV or stored in the battery is insufficient to support the loads. It is connected to the DC bus through DC–DC boost converter Generally a FC is characterized by its high efficiency and reliability, but its dynamic is limited by the hydrogen/oxygen delivery system. Therefore, a fast response auxiliary power source is needed to compensate its slow dynamic, which can be achieved by the utilization of supercapacitor bank. The electrolyzer is connected to the DC bus via DC–DC buck converter, when the battery is fully charged the excess power is transferred to the electrolyzer unless the H_2 storage tankis full. The battery bank is mainly sized to support the low power demand, it is connected to the DC bus via bidirectional converter, which is controlled to follow the reference of charge or discharge current and to regulate the DC bus voltage (or super-capacitor SOC). The super-capacitor (SC) is directly connected to the DC bus in order to compensate the slow dynamic of the FC and support the sharp load. The SC has a greater power density, which allows it to supply the power over a short period [15]. Utilizing the super capacitor has many advantages, such as reducing the size of the battery, improving the performance of the FC and stabilizing the DC bus voltage under fast load changes. Since the energy balance represents a real challenge in such standalone power system, a load management unit is added in order to shift the electricity demand during the peak periods and achieve maximum energy efficiency with maximum degree of consumer comfort.

2.2. Hybrid system management and control methodology

In the integrated power system, the power flow between the different sources is controlled by a central controller. It provides overall control of the power system and sets the power reference for the different converters that control the power system components. Moreover, the main controller cooperates with a local loads controller, which controls the different loads, according to the energy balance of the system. It can reduce a part of the home power demand when the system is under stress by disconnecting the offered controllable loads.

3. System modeling

3.1. Photovoltaic system modeling

The photovoltaic system can be modeled by a currentsource, a diode and a combination of a series and a parallel resistance. The output current of the cellcan be given by [16,17]:

$$I_{PV} = I_{ph}(t) - I_{rs}(t)\left[\exp\left(\frac{q(V_{pv}(t) + I_{pv}(t)R_s)}{A_c K T(t)}\right) - 1\right] \quad (1)$$

where I_{ph} is the photocurrent, I_{rs} is the cell reverse saturation current, V_{PV} is the voltage level on the PV cell terminals, q is the electron charge, R_s is the intrinsic cell resistance, A_c is the cell deviation from the ideal pen junction characteristic, K is the Boltzman constant and T is the cell temperature. The photocurrent of the PV cell can be expressed as [16]:

$$I_{ph}(t) = \frac{(I_{sc} + K_i[T(t) - T_r])\lambda(t)}{100} \quad (2)$$

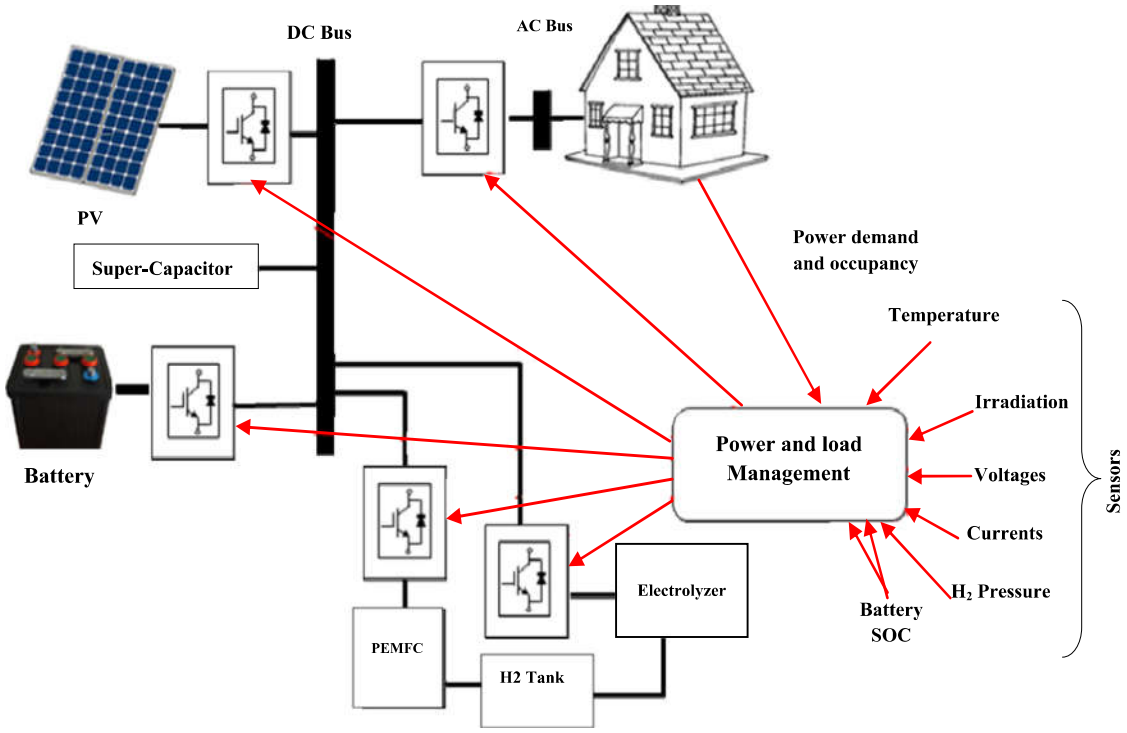

Fig. 1. Hybrid system structure.

Table 1
Hybrid system specification.

Component	Size
PV	2.5 kW
FC	1.5 kW
Battery bank	4(12 V/200 Ah/2.4 kW)
Electrolyzer	1.2 kW
Super-capacitor	(30 V,80 F)

Table 2
Parameters of the solar system.

Parameters	Value
Q	1.6×10^{-19} °C
A_c	1.6
K	1.3805×10^{-23} Nm K^{-1}
K_I	0.0017A °C^{-1}
I_{or}	2.0793×10^{-6} A
T_{ref}	301.18 K
E_{go}	1.10

where I_{sc} is the short-circuit cell current, K_I is the short-circuit current temperature coefficient and λ is the insolation in (mW cm^{-2}). The reverse saturation current depends mainly on the temperature and it can be expressed as:

$$I_{rs}(t) = I_{or}\left(\frac{T(t)}{T_{ref}}\right)^3 \exp\left(\frac{qE_{go}\left(\frac{1}{T_r} - \frac{1}{T(t)}\right)}{KA_c}\right) \quad (3)$$

where I_{or} is the reverse saturation current at the reference temperature T_{ref} and E_{go} is the band-gap energy of the semiconductor used in the cell. The simulation parameters of the solar system are summarized in Table 2.

3.2. Fuel cell system modeling

The PEMFC is modeled, according to the relationship between the output voltage and the partial pressure of hydrogen, oxygen, and water. The detailed PEMFC model is shown in Fig. 2. The relationship between the partial pressure of hydrogen with its molar flow can be given as [18]:

$$\left(\frac{q_{H_2}}{p_{H_2}} = \frac{K_{an}}{\sqrt{M_{H_2}}} = K_{H_2}\right)[L1] \quad (4)$$

where q_{H_2} is the input molar flow of hydrogen [kmol/s], p_{H_2} is the hydrogen partial pressure [atm], K_{an} is the anode valve constant $\left[\sqrt{\text{Kmol kg(atm s)}^{-1}}\right]$, M_{H_2} is the molar mass of hydrogen [kg kmol^{-1}] and K_{H_2} is the hydrogen valve molar constant [kmol/(atm s)]. Using the perfect gas equation, the derivative of the partial pressure can be calculated as [18]:

$$\frac{d}{dt}p_{H_2} = \frac{RT}{V_{an}}\left(q^{in}_{H_2} - q^{out}_{H_2} - q^{r}_{H_2}\right) \quad (5)$$

where R is the universal gas constant [J/(kmol K)], T is the absolute temperature [K], V_{an} is the volume of the anode [m^3], $q^{in}_{H_2}$ is the hydrogen input flow [kmol/s], $q^{out}_{H_2}$ is the hydrogen output flow [kmol/s] and $q^{r}_{H_2}$ is the hydrogen reacted flow [kmol/s], which can be expressed as [18]:

$$q^{r}_{H_2} = \frac{N_o N_s I_{FC}}{2F} = 2K_r I_{FC} \quad (6)$$

where N_0 is the number of fuel cells in the stack, N_s is the number of stacks used in the FC power plant, I_{FC} is the FC system current [A], F is the Faraday's constant [C/kmol] and K_r is the modeling constant [kmol/(s A)].

Using (5) and (6), the hydrogen partial pressure can be expressed in the s-domain as [19]:

$$p_{H_2} = \frac{\frac{1}{K_{H_2}}}{1 + \tau_{H_2}S}\left(q^{in}_{H_2} - 2K_r I_{FC}\right) \quad (7)$$

where τ_{H_2} is the hydrogen time constant [s], and it can be expressed as:

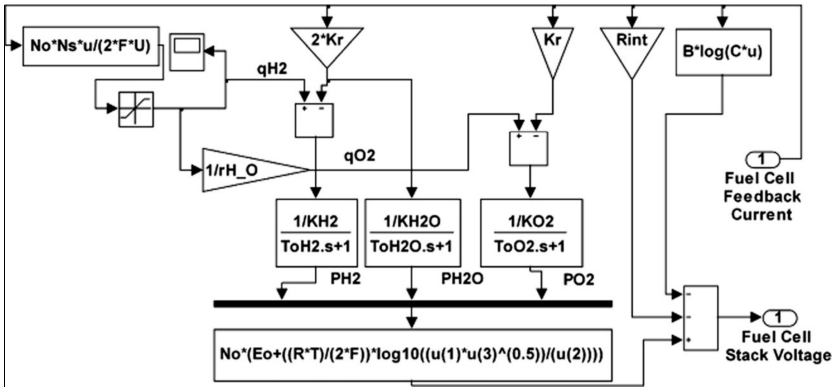

Fig. 2. PEMFC model.

$$\tau_{H_2} = \frac{V_{an}}{K_{H_2} RT} \tag{8}$$

The PEMFC polarization curve is obtained fromthe sum of the Nernst's voltage (E), the activation over voltage (η_{act}), and the ohmic over voltage (η_{ohmic}). Assuming constant temperature and oxygen concentration, the FC output voltage can be expressed as [20]:

$$V_{cell} = E + \eta_{act} + \eta_{ohmic} \tag{9}$$

where

$$\eta_{act} = -B\ln(CI_{FC}) \tag{10}$$

and

$$\eta_{ohmic} = -R^{int} I_{FC} \tag{11}$$

where B and C are constants, and R^{int} is the FC internal resistance [Ω]. In term of gas molarities, the Nernst voltage is given as [19]:

$$E = N_0 \left[E_0 + \frac{RT}{2F} \log\left(\frac{P_{H_2}\sqrt{P_{O_2}}}{P_{H_2}o} \right) \right] \tag{12}$$

where P_{H_2O} is the water partial pressure [atm]. The amount of the hydrogen consumed by the FC is mainly determined by the power demand. The hydrogen flow rate is controlled, according to the output power of the FC system, where FC output current is taken back to the input while converting the hydrogen into molar form. The amount of hydrogen flow required to meet the load is given as [18]:

$$q_{H_2}^{req} = \frac{N_0 N_S I_{FC}}{2FU} \tag{13}$$

where U is the utilization rate. The FC model parameters are summarized in Table 3.

3.3. Electrolyzer model

Water can be dissolved into hydrogen and oxygen gas by passing an electric current between two electrodes dissociated by a hydrous electrolyte. The electro chemical reaction of water electrolysis is given by [19]:

$$H_2O_{(liquid)} + electrical\ energy \Rightarrow H_{2(gas)} + \frac{1}{2}O_{2(gas)} \tag{14}$$

The rate of hydrogen production is directly proportional to the electrical current in the equivalent electrolyzer circuit and it can be given by [21,22]:

$$n_{H_2} = \frac{\eta_F \cdot \eta_G \cdot i_e}{2F} \tag{15}$$

where η_F is the Faraday efficiency, n_C is the number of electrolyzer cells in series and i_e is the electrolyzer current [A]. Generally, there is a difference between the real flow rate of hydrogen and the theoretical one defined as the Faraday's efficiency, which can be expressed as [22]:

$$\eta_F = 96.5e^{(0.09/i_e - 75.5/i_e^2)} \tag{16}$$

Fig. 3 illustrates a simple electrolyzer model based on (15) and (16).

Table 3
FC model parameters.

Parameters	Value
Activation voltage constant (B)	0.04777 [A^{-1}]
Activation voltage constant (C)	0.0136 [V]
Conversion factor (CV)	2
Faraday's constant (F)	96,484,600 [kmol/(atm s)]
Hydrogen time constant τ_{H_2}	3.37 [s]
Hydrogen valve constant K_{H_2}	4.22×10^{-5} [kmol/(atm s)]
Hydrogen–oxygen flow ratio (rH–O)	1.168
Kr constant = No/4F	2.2802×10^{-7} [kmol/(s A)]
No load voltage (Eo)	0.5 [V]
Number of cells (No)	88
Number of stacks (NS)	1
Oxygen time constant τ_{o_2}	6.74 [s]
Oxygen valve constant k_{o_2}	2.11×10^{-5} [kmol/(atm s)]
FC system internal resistance (Rint)	No × 0.00303 [Ω]
FC absolute temperature (T)	343 [K]
Universal gas constant (R)	8314.47
Utilization factor (U)	0
Water time constant τ_{H_2O}	18.418 [s]
Water valve constant k_{H_2O}	7.716×10^{-6} [kmol/(atm s)]

3.4. Hydrogen storage model

The Hydrogen storage system is necessary to make the balance between the hydrogen produced by the electrolyzer and that consumed by the PEMFC. Eq. (1) describes the hydrogen storage model, this model calculates the tank pressure based on the hydrogen flow. The dynamics of the storage system can be expressed as [23]:

$$P_b - P_{bi} = z\frac{N_{H_2} RT_b}{M_{H_2} V_b} \tag{17}$$

where P_b is the hydrogen tank pressure [Pascal], P_{bi} is the initial pressure of the hydrogen tank [Pascal], z is the compressibility factor as a function of pressure, N_{H_2} is the hydrogen moles per second delivered to the storage tank [kmol/s], T_b is the operating temperature [K] and V_b is the volume of the tank [m^3].

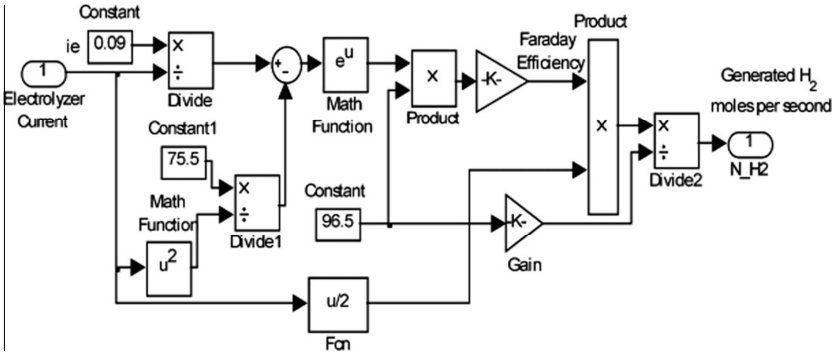

Fig. 3. Electrolyzer model.

In this model all supplementary power requirements such as pumps, valves were ignored. The Simulink version of the hydrogen storage model is shown in Fig. 4.

3.5. Battery modeling

Battery modeling is a very important issue because the energy management of the system depends strongly on the battery (SOC). In this study, CIEMAT battery model is used. The normalized form of the equations with respectto the battery capacity can be used for any type and size oflead acid batteries. During The battery discharging, the battery voltage equation can be expressed as follow [24]:

$$V = [2.085 - 0.12(1 - SOC)] - \frac{I}{C_{10}}\left(\frac{4}{1+I^{1.3}} + \frac{0.27}{SOC^{1.5}} + 0.02\right)(1 - 0.0007\Delta T) \quad (18)$$

where I is the battery discharge current and ΔT is the temperature variation. During The battery discharging the battery state of charge SOC and depth of discharge DOD can be given as [23]:

$$SOC = 1 - DOD \quad (19)$$

$$DOD = \frac{Q_e}{C} \quad (20)$$

with

$$Q_e = it \quad (21)$$

where C is the battery's capacity in Amp-seconds and Q_e is the battery's charge in Amp-seconds. During the battery charging, the battery voltage equation can be expressed as follow [24]:

$$V = [2 - 0.16(SOC)] - \frac{I}{C_{10}}\left(\frac{6}{1+I^{0.86}} + \frac{0.27}{(1+SOC)^{1.2}} + 0.036\right)(1 - 0.025\Delta T) \quad (22)$$

In this case, the state of charge is expressed as a function of the conversion efficiency η_G and the initial state of charge SOC_0

$$SOC = SOC_0 + \frac{\eta_G Q_e}{C} \quad (23)$$

The battery bank consists of four batteries 4(12 V/200Ah/2.4 kW).

3.6. Supercapacitor modeling

A simple model of a Supercapacitor, available in SPS (Sim Power System Matlab/Simulink) is chosen for this work (Fig. 5). This model is implemented based on the Stern model, which combines the Helmholtz and Gouy Chapman models [25]. The capacitance of a SC cell can be given by [26]:

$$C = \left[\frac{1}{C_{GC}} + \frac{1}{C_H}\right]^{-1} \quad (24)$$

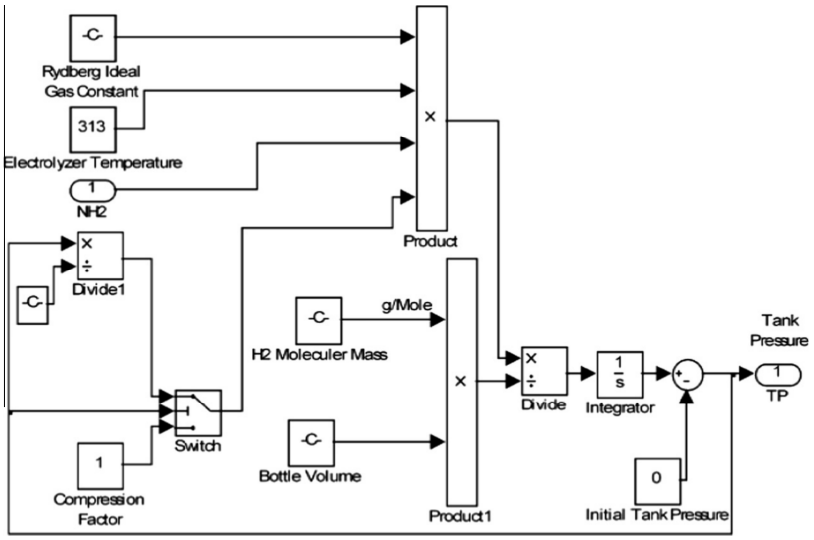

Fig. 4. Hydrogen storage model.

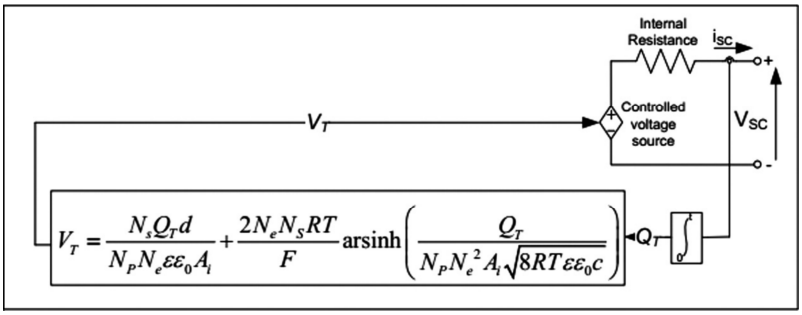

Fig. 5. Supercapacitor model.

Table 4
SC MATLAB simulation parameters.

Parameters	Value
Rated capacitance (F)	80
Equivalent DC series resistance (Ohms)	2.1e−3
Rated voltage (V)	12
Number of series capacitors	
Number of parallel capacitors	
Initial voltage (V)	12
Leakage current (A)	5.2e−3
Operating temperature (Celsius)	25
Number of layers	
Molecular radius (m)	1.23e−9
Over potential (V)	0.3
Charge transfer coefficient alpha	0.3

where

$$G_{GC} = \frac{FQ_c}{2N_eRT}\sinh\left(\frac{Q_C}{N_e^2 A_i\sqrt{8RT\varepsilon\varepsilon_o C}}\right) \tag{25}$$

and

$$C_H = \frac{N_e A\varepsilon\varepsilon_o}{d}C \tag{26}$$

where C_{GC} and C_H are the Helmholtz and Gouy-Chapman capacitance [F] respectively, F is the Faraday constant, Q_c is the cell electric charge [C], Ne is the number of electrode layers, R is the ideal gas constant, A_i is the interfacial area between electrodes and electrolyte [m^2], ε and ε_o are the permittivities (F/m) of the electrolyte material and free space respectively, C is the molar concentration [mol m^{-3}] and $d$is the Helmholtz layer length (or molecular radius) [m]. The SC module consists of N_p cells in parallel and N_s cells in series. Its total capacitance can be expressed as:

$$C_T = \frac{N_p}{N_s}\cdot C \tag{27}$$

The supercapacitor output voltage is expressed considering resistive losses as:

$$V_{SC} = \frac{Q_P}{C_T} - R_{SC}i_{sc} \tag{28}$$

with

$$Q_T = N_P Q_c\int i_{sc}dt \tag{29}$$

where Q_T is the total electric charge [C], R_{SC} is the super capacitor module resistance (Ω) and i_{SC} is the super-capacitor module current [A].

The MATLAB simulation parameters of the SC are summarized in Table 4.

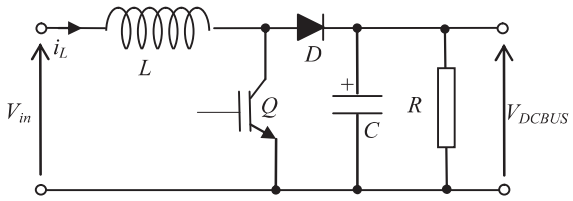

Fig. 6. DC–DC boost converter.

3.7. Boost converter modeling

The PV panel and the FC are connected to the DC bus through a DC–DC boost power converter, which achieves the PV and the FC control. The boost converter electric scheme is illustrated in Fig. 6.

The state space average equations are used to model the converter as expressed in (30). By assuming continuous conduction mode, the state space average equations can be written on the time interval $(0 < t < T)$ as follows:

$$\begin{cases}\dot{x}_1 = \lambda_1 V_{in} - \lambda_1 x_2 u\\ \dot{x}_2 = \lambda_2 x_1 u - \lambda_3 x_2\end{cases} \tag{30}$$

where $\lambda_1 = \frac{1}{L}; \lambda_2 = \frac{1}{C}; \lambda_3 = \frac{1}{RC}; u = (1-\alpha)$ and $[x_1 \quad x_2] = [i_L \quad V_{DCBUS}]$. T is the switching period and α is the duty cycle.

3.8. Buck converter modeling

The electrolyzer is connected to the DC bus through a DC–DC buck power converter (Fig. 7), which achieves its control. The state space average equations are used to model the converter as expressed in (31).

$$\begin{cases}\dot{x}_1 = \lambda_1 V_{in} u - \lambda_1 x_2\\ \dot{x}_2 = \lambda_2 x_1 - \lambda_3 x_2\end{cases} \tag{31}$$

where $\lambda_1 = \frac{1}{L}; \lambda_2 = \frac{1}{C}, \lambda_3 = \frac{1}{RC}$; $u = \alpha$ and $[x_1 \quad x_2] = [i_L \quad V_{DCBUS}]$

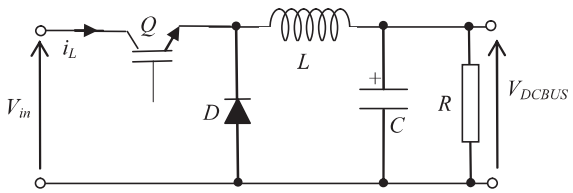

Fig. 7. Buck converter.

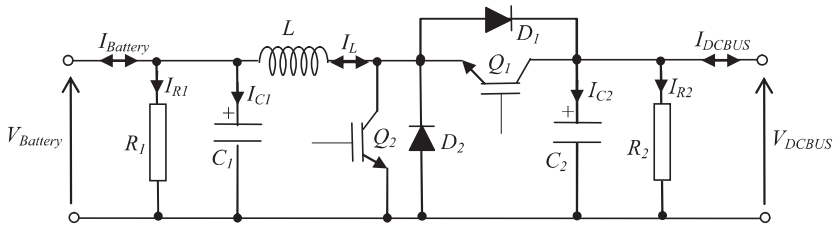

Fig. 8. Voltages and currents for the bi-directional buck-boost DC–DC converter.

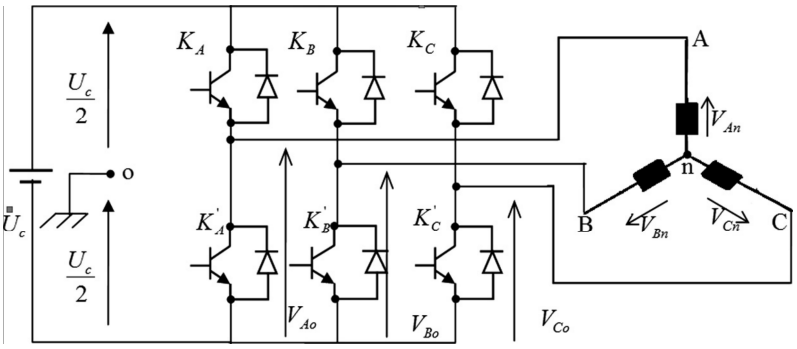

Fig. 9. Power circuit of a three-phase VSI.

3.9. Modeling of the DC–DC bidirectional converter

The bi-directional DC–DC buck-boost converter is used to interlink the battery with the DC bus. Fig. 8 shows the power circuit and the voltage-current direction for boost-buck operation mode of the converter. Each mode of operation, characterized with two intervals, coincides with the conducting of appropriate IGBT or diode [27,28].

In boost mode of operation the IGBT Q1 is in OFF condition. The IGBT Q2 is conducting through the first interval and the diode D1 is conducting during the second interval, choosing the voltage over the capacitor V1, V2 and the current through the inductor as state variable the average model can be given as follows:

$$\begin{cases} \frac{dV_1}{dt} = \frac{I_1}{C_1} - \frac{V_1}{C_1 R_1} - \frac{I_2}{C_1} \\ \frac{dI_2}{dt} = \frac{V_1}{L} - \frac{V_2}{L}(1-\alpha_2) \\ \frac{dV_2}{dt} = \frac{I_2}{C_2}(1-\alpha_2) - \frac{V_2}{C_2 R_2} - \frac{I_3}{C_2} \end{cases} \quad (32)$$

In buck mode of operation the IGBT Q2 is in OFF condition. The IGBT Q1 is conducting through the first interval and the diode D2 is conducting during the second interval, the state average model can be given as follows:

$$\begin{cases} \frac{dV_1}{dt} = -\frac{I_1}{C_1} - \frac{V_1}{C_1 R_1} + \frac{I_2}{C_1} \\ \frac{dI_2}{dt} = \frac{V_1}{L}\alpha_1 - \frac{V_2}{L} \\ \frac{dV_2}{dt} = -\frac{I_2}{C_2}\alpha_1 - \frac{V_2}{C_2 R_2} + \frac{I_3}{C_2} \end{cases} \quad (33)$$

with: $I_1 = I_{Battery};\ I_2 = I_L;\ I_3 = I_{DCBUS};\ V_1 = V_{Battery};\ V_2 = V_{DCBUS}$

3.10. DC/AC converter model

A mathematical model of a three-phase voltage-source inverter (VSI) is presented based on a functional representation (Fig. 9). The inverter can be controlled using a switching function $C_i\{i = A, B, C\}$, according to the following conditions [29,30]:

- if $C_i = 1$, then K_i is OFF et K'_i is ON,
- if $C_i = 0$, then K_i is ON et K'_i is OFF.

At the outputs of the inverter the line-to-line voltages U_{AB}, U_{BC}, U_{CA} can be derived as [29]:

$$\begin{cases} U_{AB} = V_{Ao} - V_{Bo} \\ U_{BC} = V_{Bo} - V_{Co} \\ U_{CA} = V_{Co} - V_{Ao} \end{cases} \quad (34)$$

Since the phase voltages in a star connected load sum to zero, we can obtain the following relationship:

$$\begin{cases} V_{An} = 1/3[U_{AB} - U_{CA}] \\ V_{Bn} = 1/3[U_{BC} - U_{AB}] \\ V_{Cn} = 1/3[U_{CA} - U_{BC}] \end{cases} \quad (35)$$

Phase-to-neutral voltages of a star-connected load are most easily found by defining a voltage difference between the star point *n*of the load and the negative rail of the dc bus *o*. Then the following correlation holds true:

$$\begin{cases} V_{An} + V_{no} = V_{Ao} \\ V_{Bn} + V_{no} = V_{Bo} \\ V_{Cn} + V_{no} = V_{Co} \end{cases} \quad (36)$$

and we can deduce that:

$$V_{no} = \frac{1}{3}(V_{Ao} + V_{Bo} + V_{Co}) \quad (37)$$

For ideal switching, the following relation can be obtained:

$$V_{io} = C_i U_c - \frac{U_c}{2} \quad (38)$$

with

$$\begin{cases} V_{Ao} = (C_A - 0.5)U_c \\ V_{Bo} = (C_B - 0.5)U_c \\ V_{Co} = (C_C - 0.5)U_c \end{cases} \quad (39)$$

Substitution of (37) into (36) yields phase-to-neutral voltages of the load in the following form [30]:

Table 5
Inverter specifications.

Parameters	Value
$P_{nominal}$	2.5 kW
P_{max}	2.7 kW
Peak inverter efficiency	94–95.3%
Output frequency	49.8–50.2 Hz

$$\begin{cases} V_{An} = \frac{2}{3}V_{Ao} - \frac{1}{3}V_{Bo} - \frac{1}{3}V_{Co} \\ V_{Bn} = -\frac{1}{3}V_{Ao} + \frac{2}{3}V_{Bo} - \frac{1}{3}V_{Co} \\ V_{Cn} = \frac{-1}{3}V_{Ao} - \frac{1}{3}V_{Bo} + \frac{2}{3}V_{Co} \end{cases} \quad (40)$$

Replacing (39) with (40), we obtain thefollowing relation:

$$\begin{bmatrix} V_{An} \\ V_{Bn} \\ V_{Cn} \end{bmatrix} = \frac{1}{3} \cdot U_c \begin{bmatrix} 2 & -1 & -1 \\ -1 & 2 & -1 \\ -1 & -1 & 2 \end{bmatrix} \begin{bmatrix} C_A \\ C_B \\ C_C \end{bmatrix} \quad (41)$$

The inverter specifications are summarized in Table 5. The inverter control is implemented using Proportional-Integral controller using PWM techniques [31].

4. Dynamic controllers design

A real-time power balancing among the internal sources of the hybrid power system is needed for setting the power reference for each source and to regulate the common DC bus voltage.

4.1. MPPT control

A nonlinear second order sliding mode control (*SOSMC)* in a boost converter is designed to track the maximum power point with the help of a modified P&O algorithm (Fig. 10). The main aim of this algorithm is to generate the voltage reference (V_{ref}) that enters the sliding mode controller.

In P&O algorithm, the control signal of the converter is periodically perturbed and the resulting effect on the PV power output is observed. If the power increases, the control system moves the PV array operating point in that direction. Otherwise, the direction of the perturbation is reversed. This algorithm can be written as follows [32,33]:

$$V_{ref}(k) = V_{ref}(k-1) + K \cdot sign(\Delta P) \quad (42)$$

with

$$\Delta P = P(k) - P(k-1)$$

If $\Delta P > 0$ **then** increase V_{ref}.
else $\Delta P < 0$ decrease V_{ref}.

Generally a fixed step K is used to increase or decrease the reference voltage. The oscillation around the MPP depends highly on that step size. A large step size can improve the dynamic of the algorithm, but it can highly increase the oscillation while using a small step size can reduce the oscillation and slows down the dynamic of the algorithm (it takes much time to reach the MPP). In this work a modified step size P&O algorithm is proposed in order to obtain a fast convergence to the MPP and to reduce the oscillations around it. Eq. (42) can be rewritten as:

$$V_{ref}(k) = V_{ref}(k-1) + K \cdot |\Delta P| sign(\Delta P) \quad (43)$$

The step is adjusted depending on the power variation, when the operating point is far away from the MPP the step is large in order to make fast convergence to the MPP. On the other hand, when the operating point is close to the MPP the step becomes smaller in order to reduce the oscillations.

4.2. Second order sliding mode controller design

SOSMC based on a super twisting algorithm is used in order to track V_{ref}. Applying SOSMC can improve the transient response of the system for a wide range of a reference voltage or under large parameter variations and load disturbances. Firstly the sliding surface $S(x)$ is defined next, the control law is driven to bring the state trajectory to the desired output [34,35].

$$\begin{cases} e = (x_2 - x_2^*) \\ S = e + K_1 \int e dt \end{cases} \quad (44)$$

Depending on the high order sliding mode control theory, the second derivative of the sliding surface could be expressed as:

$$\ddot{S} = (\ddot{e} + K_1 \dot{e}) = \varphi(t, S, \dot{S}) + \phi(t, S, \dot{S})\dot{u} \quad (45)$$

With

$$\varphi(t, S, \dot{S}) = \lambda_1 \lambda_2 V_{in} u - \lambda_1 \lambda_2 x_2 u^2 + K_1 \lambda_2 x_1 u - K_1 \lambda_3 x_2 - (K_1 \dot{x}_2^* + \ddot{x}_2^*)$$
$$\phi(t, S, \dot{S}) = \lambda_2 x_1$$

The control of the DC–DC converter is a bounded function ($0 \leqslant |u| < 1$). The super twisting algorithm is defined by the following control law:

$$u = u_1 + u_2 \quad (46)$$

where

$$\begin{cases} \dot{u}_1 = -k_{11} sgn(S) \\ u_2 = -k_{22} |S|^{0.5} sgn(S) \end{cases} \quad (47)$$

and $k_{11} > 0; k_{22} > 0$

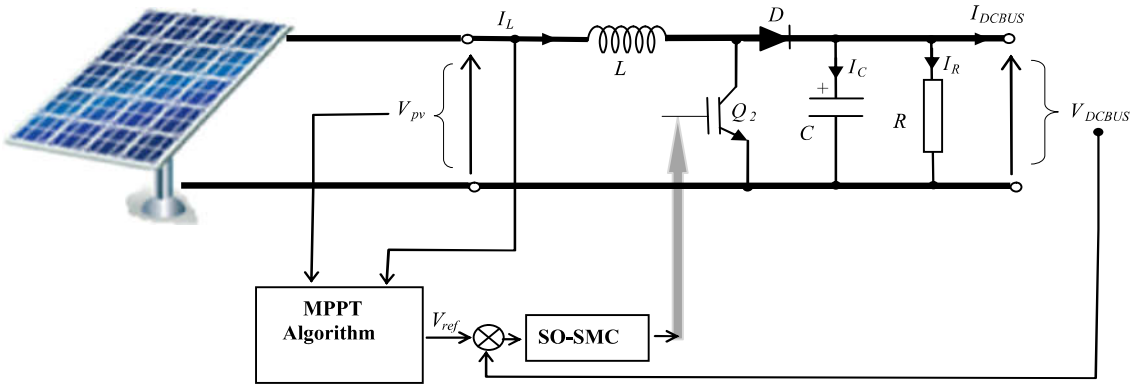

Fig. 10. Proposed schematic for P&O modified and MPPT proposed sliding mode control.

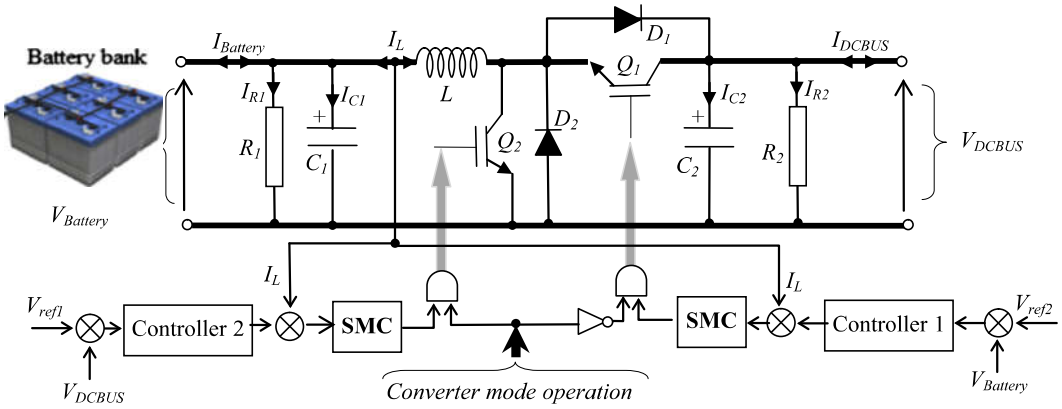

Fig. 11. Battery power control (0: buck mode, 1: boost mode).

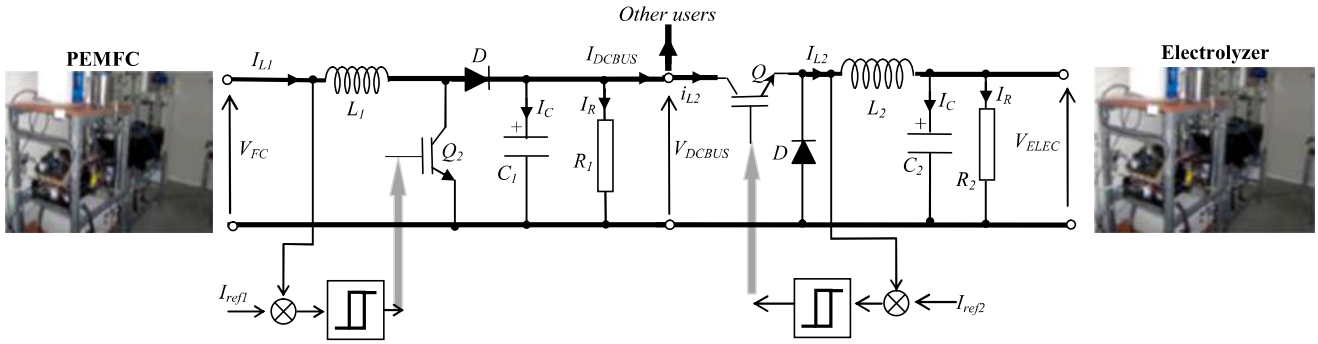

Fig. 12. PEMFC power control.

The use of the second order sliding mode guarantees the finite time convergence to:

$$S = \left\{ x : S = \dot{S} = 0 \right\} \tag{48}$$

4.3. Battery controller

The battery power flow is controlled via a bi-directional DC–DC buck-boost converter. During the battery charging-discharging process the voltage is well regulated and the current is well limited to its maximum reference.

During the battery charging the difference between the reference voltage and the battery voltage (buck mode Fig. 11) is supplied to the PI controller to produce the reference current then the battery charging current is adjusted to track this reference current throughout sliding mode controller (SMC). Furthermore during the battery discharging (boost mode Fig. 11), the reference current is produced by the difference between the DC bus voltage and the reference voltage then the battery current is limited to its maximum reference value and adjusted using SMC.

The reference charging-discharging current is derived internally to the SMC from the output of the linear voltage controller (PI) in order to enforce the inductor current to track its value. The SMC can be designed as [36,37]:

$$\begin{cases} u = \frac{1}{2}(1 - sgn(S)) \\ S = (I_2^* - I_2) \end{cases} \tag{49}$$

4.4. FC controller

The hysteresis current mode (Fig. 12) control is used as it is the simplest, most intuitive control strategy for DC–DC converter and it does not require a compensation network. In this mode of control, the comparator that compares the inductor current with the reference current (which is set by the controller) has a small amount of hysteresis denoted by ε. The switch of the DC–DC converter is switched ON when inductor current drops below $i_L^* - \varepsilon$ and the switch is turned OFF, when the inductor current exceeds $i_L^* - \varepsilon$.

5. The proposed energy management strategy

The control strategy is designed to ensure an optimal energy management of the hybrid system. This strategy aims to satisfy the load demands throughout the different operation conditions and to reduce the stress on the hybrid system. The considered strategy offers many power flow possibilities according to four operating modes of the hybrid system in order to meet the energy constraints. The system is organized according to different functions and is implemented in two parts: a central power flow controller and a local power management at the customer side.

The center power flow controller manages the power and the energy between the sources by collecting data through the sensors and producing control signals for the different converters that are employed to control the components used in the power system. It provides the reference powers of the FC, the battery and the EL. The local load management algorithm controls the different load, according to the energy balance of the system, it can reduce a part of the home power demand when the system is under stress by disconnecting the offered controllable loads. Moreover, the load manager guarantees maximum comfort level of the customer and ensures uninterrupted supply of critical loads.

5.1. The central power flow controller

The central power flow controller is designed to fulfill many criteria as: (a) manage the power and the energy between the

sources, (b) satisfy the load demand even under bad weather conditions, (c) optimize the operation of each power system components and extend its service life, (d) increase the overall system efficiency.

The control is affected through the power converters which are connected to the power system components, with the required measurements and data collecting though the sensors. The operation strategy used in the power flow controller is represented in a form of a decision tree (Fig. 13) and it can be explained as follows:

Firstly the controller measures the power generated by the PV arrays and the power consumed by the loads, then the difference is calculated ($P_d = P_{PV} - P_{load}$). In the case of power deficit, the control strategy defines four modes of operation which are:

5.1.1. Mode 1

This is the case where the PV output power is less than the required load power and the difference between these two powers is lower than the battery rated power ($P_d \leqslant P_{Batt}$). The lack of energy is provided by the battery, which is mainly sized to support low power demand ($P_{Batt} \leqslant 1000$ W). Since the battery will cover the low duration demands, the FC will be turned-on only in the case of the battery bank SOC drops below 45 %(SOC_{min}), or in the case of high load demand. In this way, unnecessary turn-on of the FC is avoided, which increases highly its service life. Moreover, the limitation of battery discharge power ensures that there will be enough energy to support the loads throughout bad weather condition. In addition to that the economical optimization developed in [38,39] shows that batteries are better to supply low discharged power because the average cost of the power supplied by batteries will be less than the average cost of the power supplied by fuel cells. In this mode, the controller operation is conditioned as follows:

if ($SOC > SOC_{min}$) **then** ($I_{dis} = I_B$)
else
  If ($P_{H_2} > P_{H_2 min}$) **then** ($I_{dis} = I_{FC}$)
  Else(I_{dis} = 0) (total shedding of consumption)
  end
end

Firstly the controller will test the battery *SOC*, if it is higher than its minimum threshold ($SOC > SOC_{min}$) then the controller will set the battery discharge current ($I_{dis} = I_B$). In this case, the reference power and current of the battery are given by the following equations:

$$P_{B\_ref} = P_d \tag{50}$$

$$I_{Bf} = I_{dis} = \frac{P_d}{V_B} \tag{51}$$

On the other hand, if the first conditions are not verified, the *FC* will cover the deficit power if the pressure of the H_2 tank is ($P_{H_2} > P_{H_2 min}$). In this case, the reference power and current of the *FC* are given by the following equations:

$$P_{FC\_ref} = P_d \tag{52}$$

$$I_{FC} = \frac{P_d}{V_{FC}} \tag{53}$$

Moreover, if the last two conditions are not verified the total shedding mode will be activated to prevent the overall system failure.

5.1.2. Mode 2

It's the state when ($P_{Batt} < P_d \leqslant P_{FC}$), which indicates that the power deficit is higher than the rated power of the battery but lower than the *FC* rated power. In this mode the controller operation is conditioned as follows:

if ($P_{H_2} > P_{H_2 min}$) **then** ($I_{dis} = I_F$)
else
  If ($SOC > SOC_{min}$) **then** ($I_{dis} = I_B$)
  Else (I_{dis} = 0) (total shedding of consumption)
  end
end

Firstly the controller will test the pressure of the H_2 tank, if it is higher than its minimum threshold ($P_{H_2} > P_{H_2 min}$), then the controller will set the FC current ($I_{dis} = I_F$). Moreover, if the first condition is not verified, the battery will cover a part of the power deficit with partial shedding of controlled loads. On the other hand, if the battery charge state is ($SOC \leqslant SOC_{min}$), the total loads shedding mode will be activated ($SOC \leqslant SOC_{min}$) to prevent the system failure under heavy load consumption.

5.1.3. Mode 3

This mode is activated in the case of extra power deficit ($P_d \leqslant P_{FC} + P_{Batt}$), when the power deficit is greater than the rated power of the battery and the *FC*. In this mode, the controller operation is conditioned as follows:

if ($P_{H_2} > P_{H_2 min}$) & ($SOC > SOC_{min}$) **then** ($I_{dis} = I_F + I_B$)
if ($P_{H_2} > P_{H_2 min}$) & ($SOC \leqslant SOC_{min}$) **then** ($I_{dis} = I_F$)
if ($P_{H_2} \leqslant P_{H_2 min}$) & ($SOC > SOC_{min}$) **then** ($I_{dis} = I_B$)
if ($P_{H_2} \leqslant P_{H_2 min}$) & ($SOC \leqslant SOC_{min}$) **then** ($I_{dis} = 0$)

If H_2 tank pressure and the battery *SOC* are greater than their minimum threshold, the battery and the *FC* will support the heavy load consumption at the same time. In this case, the reference powers and current of the FC and the battery are given by the following equations:

$$P_{B\_ref} = 1000 \text{ kW} \tag{54}$$

$$I_B = \frac{1000}{V_B} \tag{55}$$

$$P_{FC\_ref} = P_d - P_{B\_ref} \tag{56}$$

$$I_{FC} = \frac{P_{FC\_ref}}{V_{FC}} \tag{57}$$

$$I_{dis} = I_F + I_B \tag{58}$$

On the other hand, if the H_2 tank pressure is greater than its minimum threshold, but the battery SOC is lower than its minimum threshold, then the FC will cover a part of the power deficit with partial shedding of controlled loads. Moreover, if the H_2 tank pressure is lower than its minimum threshold, but the battery SOC is greater than its minimum threshold, then the battery will cover a part of the power deficit with partial shedding of controlled loads. Finally, if the H_2 tank pressure and the battery SOC are lower than their minimum threshold, then the total shedding of consumption mode will be activated. In this way, the controller ensures highly the energy balance of the power system, as it shifts the power consumption during the heavy consumption and low energy production.

5.1.4. Mode 4

During the power surplus ($P_{net} > 0$), the excess power is transferred to the battery bank Moreover, if the battery bank *SOC* reaches its maximum level, the electrolyzer will turn-on, unless maximum tank pressure P_{max} is reached. If the H_2 tank is full then the surplus power will be transferred to the dump load.

5.2. Load management strategy

In this work, a load management unit is added to improve the system reliability and to increase the energy balance of the system.

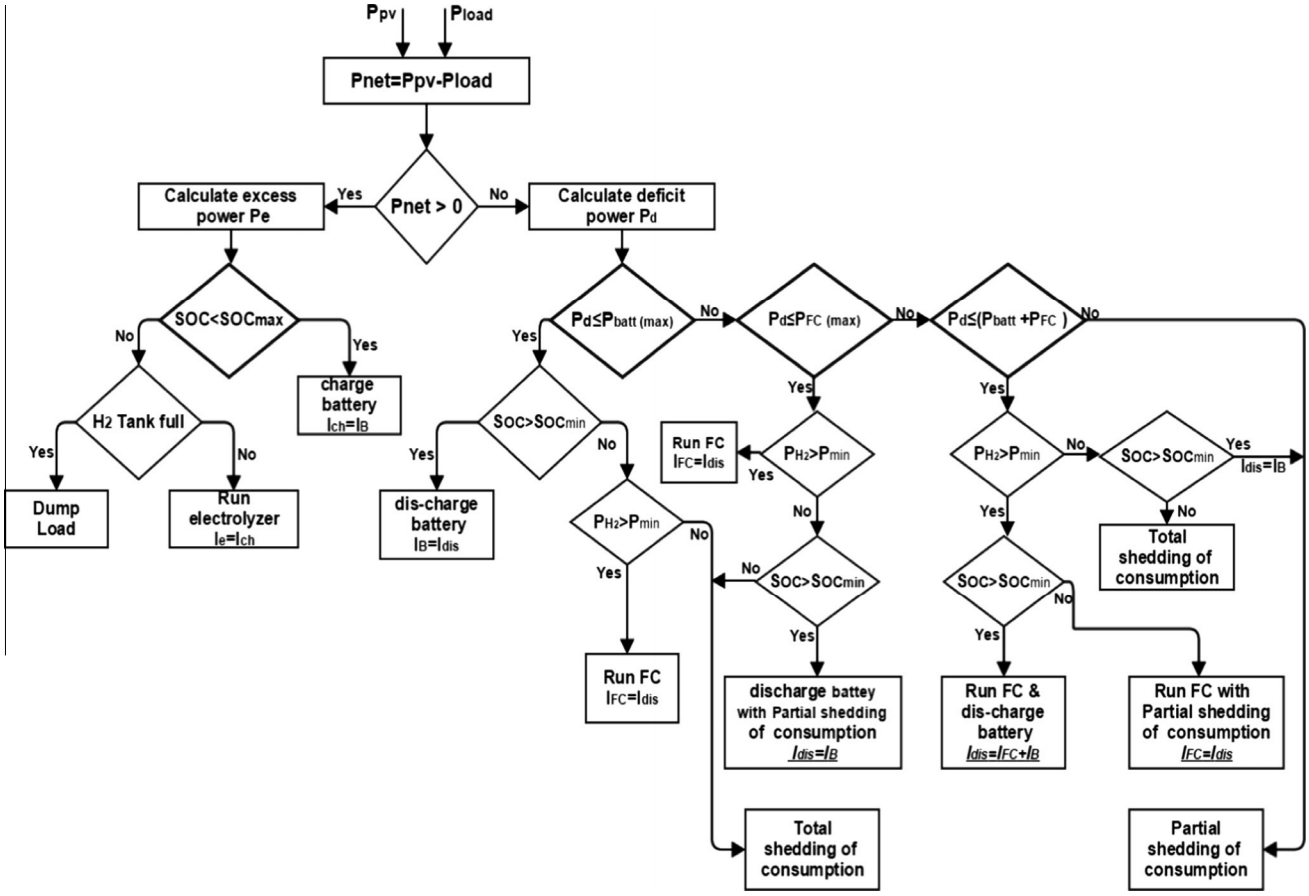

Fig. 13. Decision tree of the PFC.

The residential loads can be classified based on their priorities in two main types:

- Non-controlled loads: as lamps of rooms and toilets, refrigerator, and freezer.
- Controlled loads: such as space cooling and heating, water heating, outdoor lighting, corridor lighting, fans, dryer, washing machine, kitchens lighting, and others.

The load management unit has five inputs which are: the hydrogen tank pressure (P_{H_2}), the charge state of the battery (SOC), the natural irradiance (Ga), the ambient temperature (Ta) and the occupancy (O_c). These inputs are intended to control the controlled loads especially the lights, the washing machine, the air conditioning system and the fans. The strategy flowchart is shown in Fig. 14 and can be explained as follows: the air conditioning (A/C) system is considered to be one of the largest energy consumer in the house and represents a real challenge for such isolated power system, its operation is submitted to three main conditions which can be expressed as:

$$\begin{cases} T_a \geqslant T_{a,ref} \\ O_c = 1 \\ P_{H_2} > P_{H_2\,\min} \end{cases}$$

The first condition represents the comparison between the reference temperature and the ambient temperature, if it is verified the controller will pass to the second condition, which indicates the occupancy of the place. Finally, the third condition is associated with the amount of hydrogen storage in the tank. This condition ensures that the hydrogen storage will not be depleted by the huge consumption of the A/C system and there will be enough H_2 to back up the system in different conditions. Moreover, if the H_2 storage is under its minimum security level, the controller will activate the fan, if the charge state of the battery is ($SOC > SOC_{min}$). In this way the controller balances between the maximum available comfort of the consumer and the energy balance of the system.

The operation of the lighting is subjected to manual control, natural irradiance and the occupancy of the place, for this, the operation of the controlled lighting was conditioned as follows:

if $((G_a \leqslant G_{a,ref}) \;\&\; (O_C = 1)$ **then** (*Turn on lamps*)
if $((G_a > G_{a,ref})$ **then** (*Extinct lamps*)

The first condition signifies that the light that enters the house through the windows is not enough to light up the place and the second is associated with the occupancy of the place. The washing machine is controlled according to the H_2 tank pressure measured at the time of the deciding, which gives an idea about the availability of the energy produced during the day.

6. Results and discussion

6.1. Dynamic control simulation

The hybrid power system has been simulated over a short and a long period of time in order to evaluate the performance of the dynamic controllers and the effectiveness of the management strategy. Fig. 15 presents the behavior of PV output power under sudden variation in the irradiance (Fig. 16). The result confirms

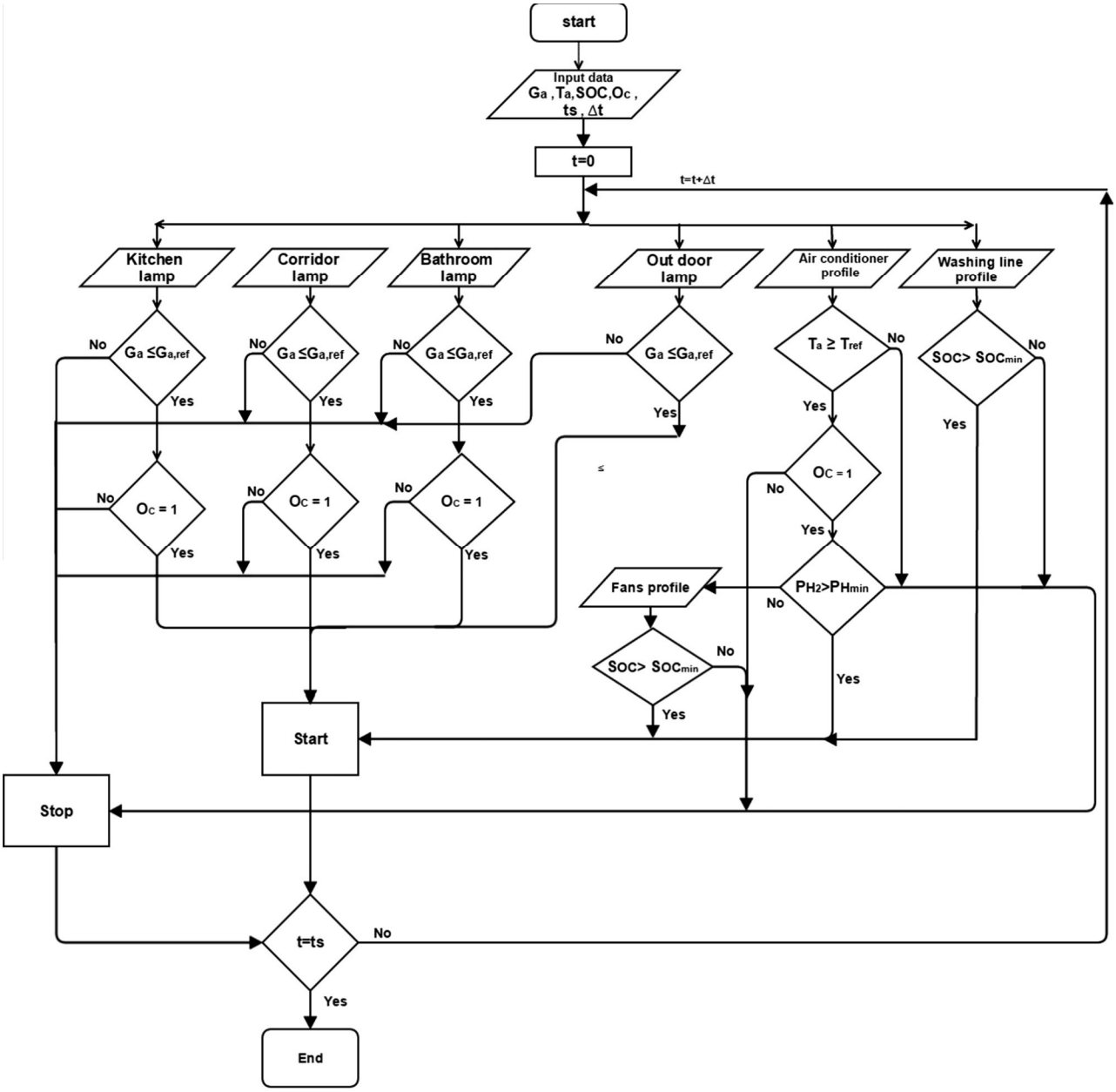

Fig. 14. The load management strategy flowchart.

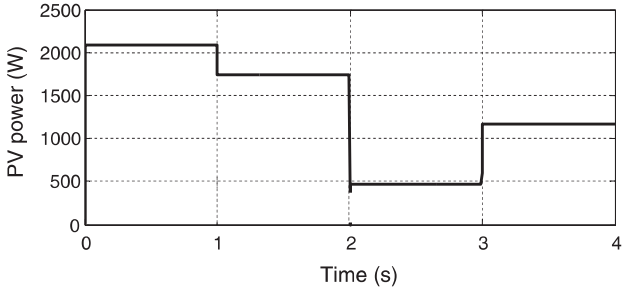

Fig. 15. PV output power (W).

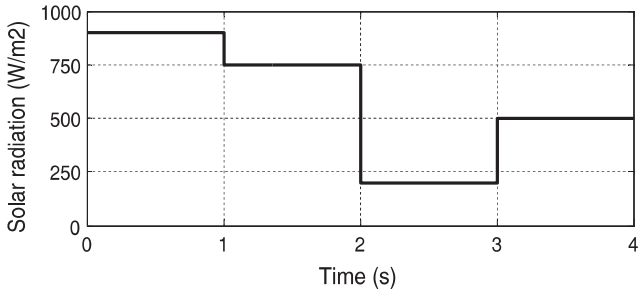

Fig. 16. Solar irradiance (W/m^2).

the efficiency of the MPPT controller as the output power perfectly follows the power reference.

Figs. 17–19 present battery, FC and electrolyzer current respectively for transient responses obtained for a transition from different operating mode. The test is performed by changing the irradiance level and the load current. During the first interval ($0\ s \leqslant t < 1\ s$) the power difference is positive ($P_{PV} - P_{Load}$) and the excess power is transferred to the battery. At $t = 0.5$ s, the battery

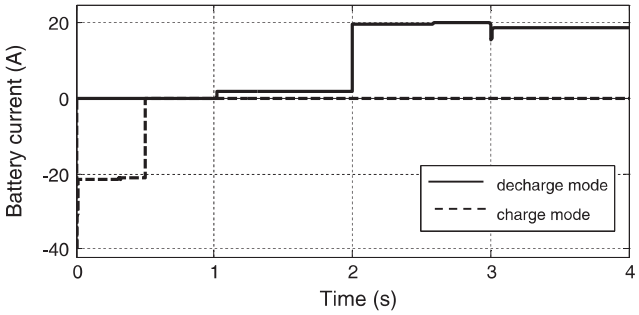

Fig. 17. Battery current (A).

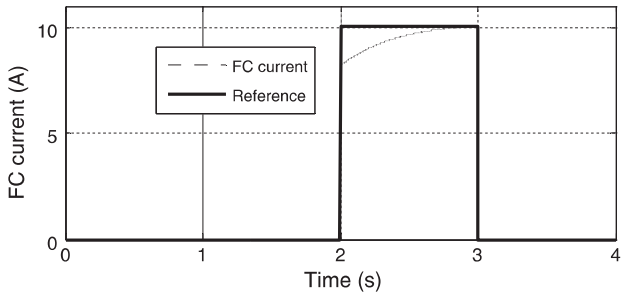

Fig. 18. FC current (A).

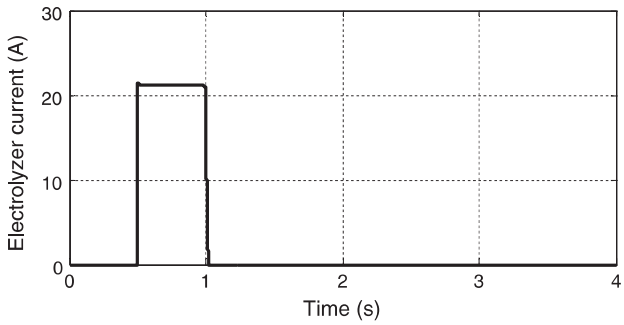

Fig. 19. Electrolyzer current (A).

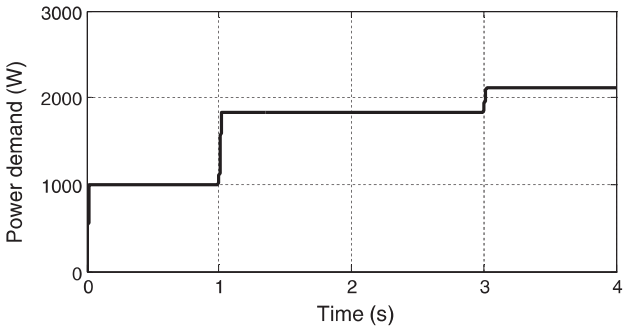

Fig. 20. Power demand (W).

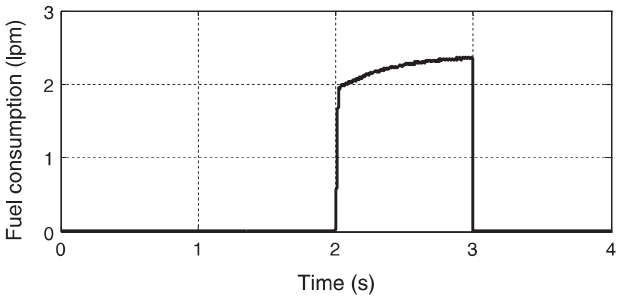

Fig. 21. Fuel consumption (lpm).

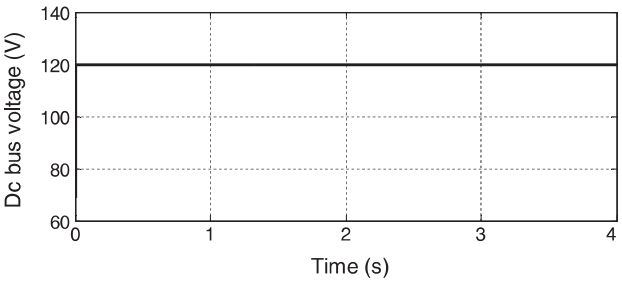

Fig. 22. DC bus voltage (V).

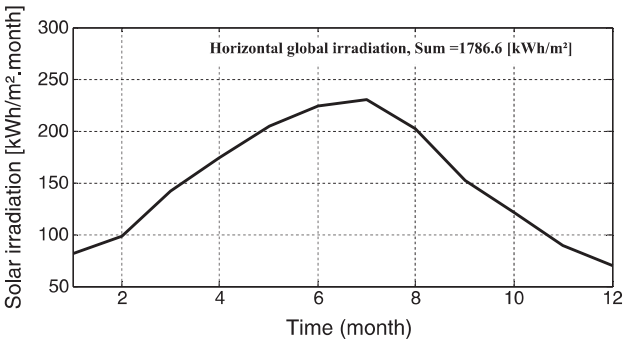

Fig. 23. Horizontal global irradiation [kWh/m^2 month].

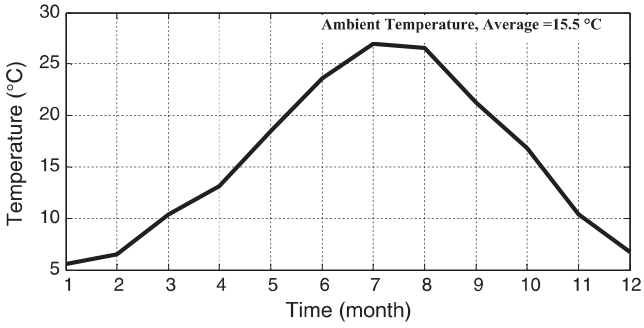

Fig. 24. Ambient temperature °C.

is fully charged and the excess power is transferred to the electrolyzer. At $t = 1$ s, the PV output power changes from 2200 W to 1750 W (due to the last change in the irradiance level Fig. 16) and the load demand (Fig. 20) increases from 1000 W to1800 W. The power difference is negative and the power deficit is less than the battery maximum discharge power, the controller sets the reference discharge current of the battery boost converter and the required power is drawn from the battery to supply the load. At $t = 2$ s, the PV power decreases from 1750 W to 450 W respectively, in this case, the power deficit is greater than the battery maximum discharge power and the FC starts to support the battery and the controller sets the reference discharge current of the FC and the battery boost converter. The required power is drawn from the battery and the FC to supply the load. The FC fuel consumption is shown in Fig. 21.

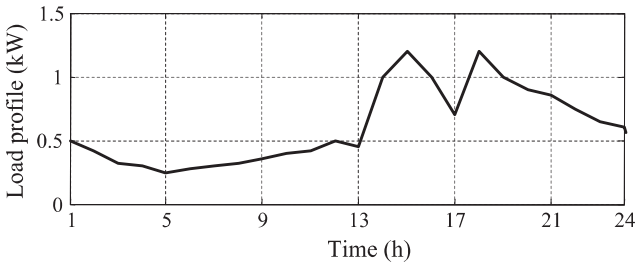

Fig. 25. An exemplary load profile.

Table 6
Load management parameters.

Parameter	Value	Unit
$G_{a,ref}$	400	W/m^2
$T_{a,ref}$	25	°C
SOC_{min}	45	%
SOC_{max}	98	%
H_{2min}	3000	Pa
H_{2max}	14,000	Pa
Δt	1	hour

During the load variation and mode fluctuations, the power imbalance of the system is increased which increases the stress on the battery and the FC. Connecting the SC to the DC bus improves highly the balance of the system, since the super capacitor can react faster to quick fluctuations and could compensate the slow dynamic of the FC. Fig. 22 shows the SC output (DC bus) voltage. The fast rate of charge–discharge of the SC handle the load variation and help to maintain the DC voltage close to its reference 120 V level, which reduces the stress on the battery and increases its service life.

6.2. Case study

This work takes a house located in the province of Batna (35°33′N 6°10′E) as a case study. The location characterized by high solar potential, the yearly average value of daily solar irradiance is about 4.87 kW/m^2. The area climate is characterized with Mediterranean climate with dry hot summers and mild winters, it has an annual average temperature of 15.5°C. The monthly averaged global solar radiation on a horizontal surface (W/m^2) and the ambient temperature for the location, is shown in Figs. 23 and 24 respectively.

For testing the effectiveness of the proposed management strategy, a deep study is accomplished on a real load profile for an average house (house is approximately 100 m^2 and includes all household electrical devices) in the location. Fig. 25 shows an average exemplary load profile for summer. It is associated with a huge energy consumption and represents a real challenge to our proposed strategy.

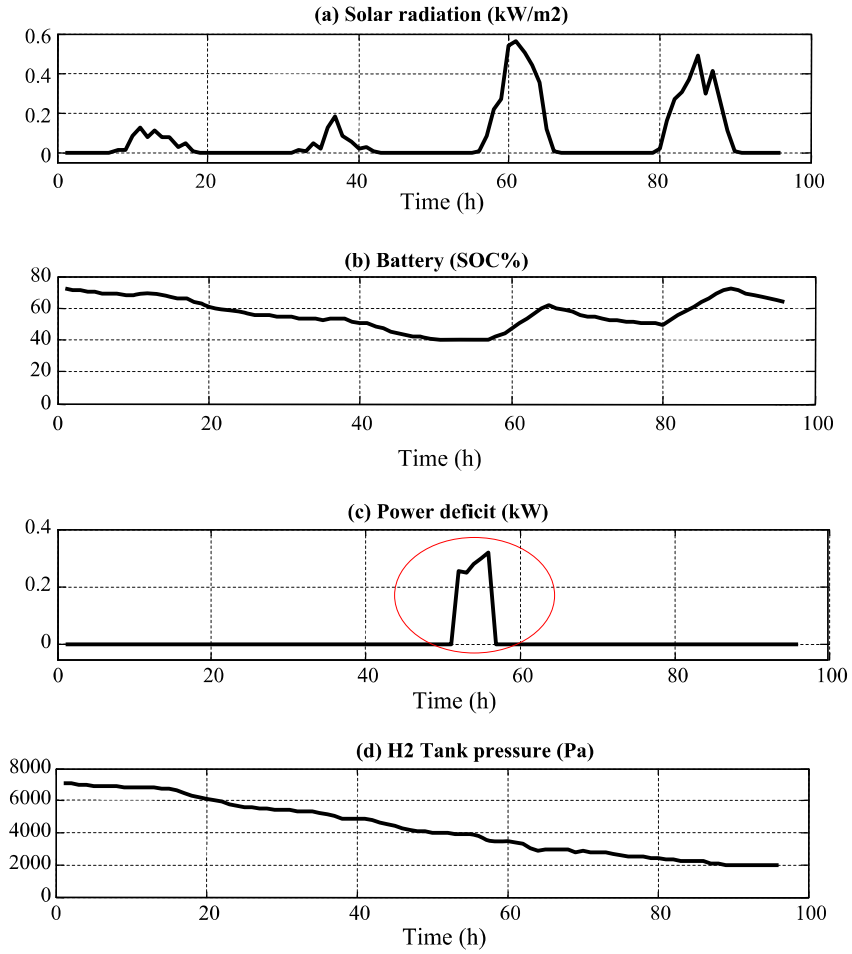

Fig. 26. System operating without load management: (a) solar irradiation, (b) battery (SOC %), (c) power deficit (kW), (d) H_2 tank pressure (Pa).

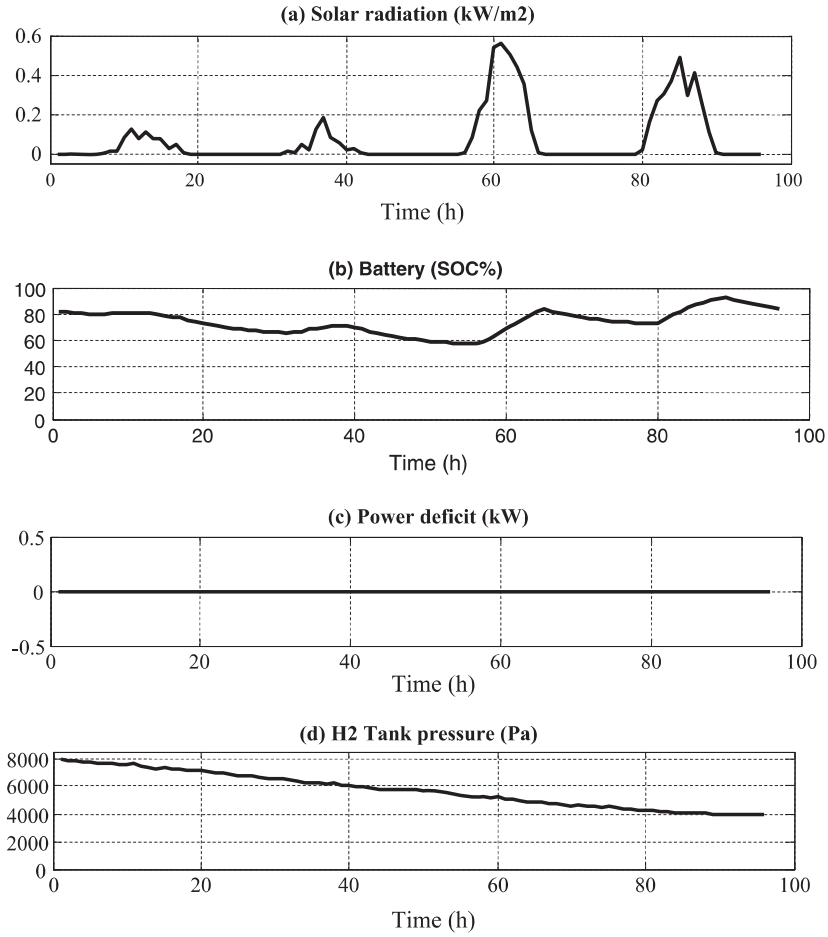

Fig. 27. System operating with load management: (a) solar irradiation, (b) battery (SOC %), (c) power deficit (kW), (d) H_2 tank pressure (Pa).

6.3. Load management strategy simulation

The main objective of the simulation process is to test the performance of the proposed system over a long period of time and under different stresses on the system like bad weather condition and heavy load consumption. The load management parameters are shown in Table 6.

The energy balance of the system affected deeply by the availability of the renewable resources. Fig. 26a shows the hourly averaged global solar radiation on a horizontal surface (W/m^2) for four days of summer, these days coincide with low irradiance level. In the third day and as a result of the low irradiance during the previous days the battery state of charge (Fig. 26b) and the hydrogen tanks pressure (Fig. 26d) reach their minimum level and the energy balance of the system shows an exorbitant deficit (Fig. 26c).

On the other hand, using the proposed management strategy can improve highly the energy balance of the system as it minimizes the discharge level of the battery (Fig. 27b) and eliminates any energy deficit during the same period (Fig. 27c). Moreover, the proposed strategy ensures that there will be sufficient amounts of hydrogen inside the tanks (Fig. 27d) during the different conditions.

7. Conclusion

This paper presented a PV/FC/battery hybrid power system for a stand-alone residential micro-grid users. The work developed an optimal strategy for controlling the energy flow within the system based on the energy availability. Moreover, a load management unit is added to manage the loads, according to the power availability of the system. The hybrid power system has been tested by simulation over a short and a long period of time in order to evaluate the performance of the dynamic controllers and the effectiveness of the management strategy. For a long simulation period, this work takes a house located in the province of Batna (35°33′N 6°10′E) as a case study with a deep study on a real load profile for an average house with all required weather data of the location. The simulation result illustrates the effectiveness of the proposed control strategy. The proposed control strategy increases the service life of the battery and fuel cell, as it reduces the ON–OFF switch cycle of the FC and prevents battery deep discharge under heavy loads consumption and bad weather condition. In addition to that, it improves the reliability of the system, as it disconnects the non-critical loads in case of extra heavy loads consumption and power deficit which increases largely the overall system efficiency.

References

[1] Revankar S, Kota R. Simulation of solar regenerative fuel cell power system for high altitude airship engineering. Int J Adv Eng Appl 2013;6(2):52–64.
[2] Garcia P, Fernandez LM, Garcia CA, Jurado F. Energy management system of fuel-cell-battery hybrid tramway. IEEE Trans Indust Electron 2010;57(12):4013–23.
[3] Bizon N, Oproescu M, Raceanu M. Efficient energy control strategies for a standalone renewable/fuel cell hybrid power source. Energy Convers Management 2015;90:93–110.

[4] Han B, Steen SM, M Jingke, Zhang FY. Electrochemical performance modeling of a proton exchange membrane electrolyzer cell for hydrogen energy. Int J Hydrogen Energy 2015;40:7006–16.
[5] Briguglio N, Brunaccini G, Siracusano S, Randazzo N, Dispenza G, Ferraro M, et al. Design and testing of a compact PEM electrolyzer system. Int J Hydrogen Energy 2013;38:11519–29.
[6] Khan MJ, Iqbal MT. Analysis of a small wind-hydrogen stand-alone hybrid energy system. Appl Energy 2009;86(11):2429–42.
[7] Carapellucci R, Giordano L. Modeling and optimization of an energy generation island based on renewable technologies and hydrogen storage systems. Int J Hydrogen Energy 2012;37(3):2081–93.
[8] Castañeda M, Cano A, Jurado F, Sánchez H, Fernández L. Sizing optimization, dynamic modeling and energy management strategies of a stand-alone PV/hydrogen/battery-based hybrid system. Int J Hydrogen Energy 2013;38(10):3830–45.
[9] Semaoui S, HadjArab A, Bacha S, Azoui B. The new strategy of energy management for a photovoltaic system without extra intended for remote-housing. Solar Energy 2013;94:71–85.
[10] Clastres C, Pham TTH, Wurtz F, Bacha S. Ancillary services and optimal household energy management with photovoltaic production. Energy 2010;35:55–64.
[11] Alnejaili T, Drid S, Mehdi D, Chrifi-Alaoui L. A developed energy management strategy for a stand-alone hybrid power system for medium rural health building. Int Trans Electrical Energy Syst 2015;25(7).
[12] Uzunoglu M, Onar OC, Alam MS. Modeling, control and simulation of a PV/FC/UC based hybrid power generation system for stand-alone applications. Renew Energy 2009;34:509–20.
[13] Behzadi MS, Niasat M. Comparative performance analysis of a hybrid PV/FC/battery stand-alone system using different power management strategies and sizing approaches. Int J Hydrogen Energy 2015;40:538–48.
[14] Dursun E, Kilic E. Comparative evaluation of different power management strategies of a stand-alone PV/Wind/PEMFC hybrid power system. Int J Electrical Power Energy Syst 2012;34:81–9.
[15] Gao L, Dougal RA, Liu S. Power enhancement of an actively controlled battery/ultracapacitor hybrid. IEEE Trans Power Electron 2005;20:236–43.
[16] Feroldi D, Rullo P, Zumoffen D. Energy management strategy based on receding horizon for a power hybrid system. Renew Energy 2015;75:550–9.
[17] Alnejaili T, Drid S, Mehdi D, Chrifi-Alaoui L. Advanced strategy of demand-side management for photovoltaic-wind energy system. In: The 15th international conference on sciences and techniques of automatic control & computer engineering, Hammamet-Tunisia; 2014. p. 797–802.
[18] Padulles J, Ault GW, McDonald JR. An integrated SOFC plant dynamic model for power systems simulation. J Power Sources 2000;86(2):495–500.
[19] Lajnef T, Abid S, Ammous A. Modeling, control, and simulation of a solar hydrogen/fuel cell hybrid energy system for grid-connected applications. Adv Power Electron 2013;13:1–7.
[20] El-Shark MY, Rahman A, Alam MS, Byrne PC, Sakla AA, Thomas T. A dynamicmodel for a stand-alone PEM fuel cell power plant for residential applications. J Power Sources 2004;138(2):199–204.
[21] Ganguly A, Misra D, Ghosh S. Modeling and analysis of solar photovoltaic-electrolyzer-fuel cell hybrid power system integrated with a floriculture greenhouse. Energy Build 2010;42:2036–43.
[22] Ulleberg O. Stand-alone power systems for the future: optimal design, operation and control of solar-hydrogen energy systems. A dissertation submitted in partial fulfillment of the requirements for the degree of doctor of philosophy in electrical engineering, Norwegian University of Science and Technology, USA; 1998.
[23] Gorg H. Dynamic modeling of a proton exchange membrane (PEM) electrolyzer. Int J Hydrogen Energy 2006;31:29–38.
[24] Achaibou N, Haddadi M, Malek A. Lead acid batteries simulation including experimental validation. J Power Sources 2008;185:1484–91.
[25] Oldham KB. A Gouy-Chapman-Stern model of the double layer at a (metal)/(ionic liquid) interface. J Electro Anal Chem 2008;613(2):131–8.
[26] Souleman M, Dessaint L, Al-Haddad K. A comparative study of energy management schemes for a fuel cell hybrid emergency power system of electric aircraft. IEEE Trans Indust Electron 2013;61(3):1320–34.
[27] Cultura A, Salameh Z. Design and analysis of a 24 VDC to 48 VDC bidirectional DC–DC converter specifically for a distributed energy application. Energy Power Eng 2012;4(5):315–23.
[28] Patel J, Chandwani H, Patel V, Lakhani H. Bi-directional DC–DC Converter for battery charging- discharging applications using buck-boost switch. In: IEEE students' conference on electrical, electronics and computer science (SCEECS), Bhopal; 2012. p. 1–4.
[29] Iqbal A, Lamine A, Ashraf I, bulla M. Matlab/simulink model of space vector pwm for three-phase voltage source inverter. In: Proceedings of the 41st international universities power engineering conference, Newcastle-upon-Tyne; 2006. p. 1096–1100.
[30] BK L, Ehsani M. A simplified functional model for 3-phase voltagesource inverter using switching function concept. In: The 25th IEEE annual conference of the industrial electronics society IECON, San Jose; 1999. p. 462–7.
[31] Nachiappan A, Pondicherry EC, Puducherry I, Sundararajan K, Malarselvam V. Current controlled voltage source inverter using Hysteresis controller and PI controller. In: International conference on power, signals, controls and computation (EPSCICON), Kerala; 2012. p. 1–6.
[32] Drid S, Chrifi-Alaoui L, Bussy P, Ouriagli M. Robust control of the photovoltaic system with improved maximum power point tracking. In: Ninth international conference on ecological vehicles and renewable energies (EVER), Monte-Carlo; 2014. p. 1–7.
[33] Kollimalla SK, Mishra MK. Variable perturbation size adaptive P&O MPPT algorithm for sudden changes in irradiance. IEEE Trans Sustainable Energy 2014;5(3):718–28.
[34] Levronand Y, Shmilovitz D. Maximum power point tracking employing sliding mode control. IEEE Trans Circ Syst 2013;60(3):724–32.
[35] Sahraoui H, Drid S, Chrifi-Alaoui L. Robust control of DC–DC Boost converter applied in photovoltaic systems using second order sliding mode. In: The 15th international conference on sciences and techniques of automatic control & computer engineering, Hammamet-Tunisia; 2014. p. 719–24.
[36] Utkin V, Guldner J, Shi J. Sliding mode control in electromechanical systems. Taylor & Francis; 1999.
[37] Wai RJ, Shin L. Total sliding-mode voltage tracking control for DC–DC boost converter. In: 6th IEEE conference on industrial electronics and application, Beijing; 2011. p. 2676–81.
[38] Dufo-Lopez L, Bernal-Agusto J, Contreras J. Optimization of control strategies for stand-alone renewable energy systems with hydrogen storage. Renew Energy 2007;32:1102–26.
[39] Kang KH, Won DJ. Power management strategy of stand-alone hybrid system to reduce the operation mode changes. In: IEEE conference on transmission, distribution & exposition, Seoul; 2009. p. 1–4.

INTERNATIONAL TRANSACTIONS ON ELECTRICAL ENERGY SYSTEMS
Int. Trans. Electr. Energ. Syst. (2015)
Published online in Wiley Online Library (wileyonlinelibrary.com). DOI: 10.1002/etep.2103

A developed energy management strategy for a stand-alone hybrid power system for medium rural health building

Tareq Alnejaili[1]*,†, Said Drid[1], Driss Mehdi[2] and Larbi Chrifi-Alaoui[3]

[1] *LSP-IE Laboratory, University of Batna, Rue Chahid M^ed El-Hadi Boukhlof, Batna, 05000, Algeria*
[2] *LIAS Laboratory, University of Poitiers, Bât. 25, 2 Rue Pierre Brousse, BP 633, Poitiers, 86022, France*
[3] *LTI Laboratory, University of Picardie Jules Verne, 13 av. François Mitterrand, Cuffies, 02880, France*

SUMMARY

This paper deals with load side management strategy for (photovoltaic–wind–diesel) hybrid system for medium rural health building located in the Sahara region. The paper presents an overview about geographic and climate data of the location and develops a typical load profile of electrical energy, depending on a real investigation of daily electricity consumption. The base of the proposed management strategy is the control of the air conditioning system and the non-critical lighting of the building as they consume more than 50% of the total power consumption. The result shows that the reduction in the peak consumption is about 20% using the proposed management strategy, which has significant economical, technical, and environmental benefits. Copyright © 2015 John Wiley & Sons, Ltd.

KEY WORDS: load side management; hybrid energy system; health building; load profile; air conditioning system; environmental merits

1. INTRODUCTION

Modern energy services are a fundamental key element in a development of societies. According to the international energy agency (2013), nearly 1.3 billion people are without access to electricity. The provision of grid electricity in rural areas is often more costly than off-grid remote area power supply; many hybrid system configurations (photovoltaic [PV]–wind–diesel, etc.) are used in order to supply power to consumers in these areas.

As the desert occupies more than four-fifths of the Algerian territory with a total area of approximately $1.92*10^6\,km^2$, it is too hard and inefficient to connect these rural areas with the public electricity grid. Group of diesel generators (DGs) are often used to supply power for these remote areas with high amount of polluting gas emission and high cost of equipment maintenance. The Algerian Sahara region (example of Tindouf) benefits from promising renewable resources. It is characterized by a high solar potential, having a monthly average value of daily solar irradiance level in the range of 4–7 KWh/m^2 and wind speed more than 5.5 m/s. These promising renewable energy resources can be employed to fill the needs of power supply for these isolated areas.

Many researches [1–3] focus on optimum sizing and component selection of different hybrid renewable energy (HRE) systems (PV stand-alone, PV–wind, PV–wind–diesel, etc.); the main objective of these researches is to achieve the balance between the cost and the reliability of the systems. To improve the reliability of HRE systems, many research papers [4–7] deal with different energy management strategies.

Semaoui *et al.*[8] proposed a new strategy of energy management for a stand-alone PV system; the strategy was intended to control washing machine, fan, and lights. The result shows that the proposed load management strategy improves the performance and the reliability of the stand-alone PV system.

*Correspondence to: Tareq Alnejaili, LSP-IE Laboratory, University of Batna, Rue Chahid Med El-Hadi Boukhlof, 05000 Batna, Algeria.
†E-mail: tareq.elnejaili@univ-batna.dz

An optimized power management mechanism for grid connected PV systems with storage is presented in [9]. The objective is to achieve intensive penetration of PV production into the grid. In [10], an energy management is developed for stand-alone PV system; the developed strategy is based on the control of the unidirectional DC–DC converter and bidirectional DC–DC converter.

As this location is characterized by a very high temperature during summer reaching 47°C, the utilization of air conditioning system is necessary and associated with high-peak consumption throughout the midday's hours, which increases highly the stress on the power system.

Concerning the power management of the air conditioning systems, Chiou *et al.* [11] proposed a fuzzy temperature control method for multi-unit air conditioners (A/C); their results shows that the use of a fuzzy control is efficient for energy saving and makes the temperature control more steadier. A direct load control for A/C units in distribution networks is presented in [12]. The proposed control is based on the varying set-point temperature of the air conditioning system adapted to the permissible power, with the objective of reducing the peak consumption in the distribution network.

This paper discusses a developed load side management (LSM) strategy for PV–wind–diesel hybrid system for a medium rural health facility located in the south of Algeria. This strategy is based on the control of air conditioning system depending on the battery state of charge (SOC), the occupancy (O_{CC}) level, and the temperature difference between the setting and the indoor temperature. The control aspect of lighting is added, which is based on the O_{CC} level and the comparison between the reference and the natural lighting that enters the facility through the windows, taking into account the visual comfort.

This work is divided into four main sections, Section I develops a typical load profile and presents an overview about geographic and climate data of the location. Section II presents the modeling of the system components. Section III describes the LSM strategy and its application to solve the power management problem. Moreover, Section IV evaluates the LSM strategy depending on economic, environmental, and technical merits.

2. INSTALLATION SITE

Tindouf is the westernmost province of Algeria with a surface of 159 000 km^2 (Figure 1); it has a population of 58 193 inhabitants (2010). The province of Tindouf does not have access to the public electricity grid, but it has its own local grid that does not cover vast areas of the province. As a consequence, several thousands of consumers do not have access to the local electricity grid, which has a large effect on prosperity and economic development of the local society. On the other hand, the location benefits from promising renewable resources, which can be employed to fill the needs of power supply for this isolated area. It receives an average of 3602 h of sunlight per year, with an

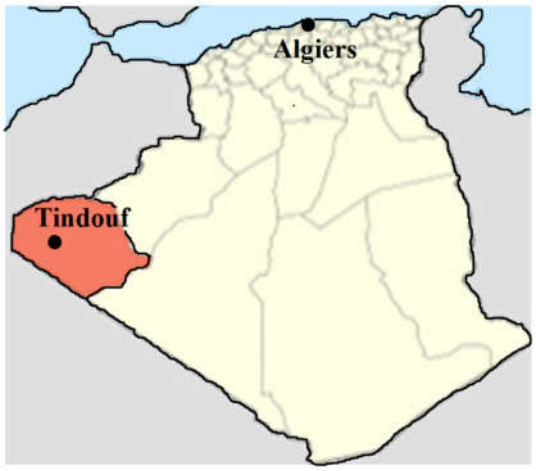

Figure 1. Geographical position of Tindouf.

DOI: 10.1002/etep

average of 10 h of sunlight per day; it has a high solar potential, the scaled annual average of the solar radiation is 5.89 KWh/m^2/day. Throughout the year, the typical wind speed varies from 0.4 m/s to 11.6 m/s. April has the highest average wind speed of 7.6 m/s. December has the lowest average wind speed of 4.2 m/s.

This region has very hot summers that extend about four months; July is the hottest month with a mean temperature of 34°C. The cold season extends about three months; the coldest month is January with a mean temperature of 13.5°C, and the annual average relative humidity is about 29%.

3. LOAD PROFILE

Deep analysis of electricity demand for such facility is essential for improving the energy system; a real investigation is performed on the daily electricity consumption throughout the year with the help of SONELGAZ (National Enterprise of Electricity and Gas, Algeria). As Tindouf has very high temperature throughout the summer reaching 49°C, air conditioning system is necessary during this hot season, resulting in high-peak demand during the midday hours. Figure 2 shows a typical load profile for a day of the summer season; the power system must handle the peak consumption and guarantee an interrupted high-quality power supplies to satisfy the requirements of sensitive laboratory equipment.

4. MODELING OF THE SYSTEM COMPONENTS

4.1. Modeling of the photovoltaic generator

The PV generator is modeled according to the ambient temperature and the irradiance level. The output power of the PV generator at the maximum power point is obtained from the following equation [13].

$$P_{pv} = \eta_p . G . S_{pv} \tag{1}$$

where η_p is the instantaneous PV generator efficiency, G is the irradiance level (w/m^2), and S_{pv} is the module area (m^2). The instantaneous PV generator efficiency could be represented as [13]

$$\eta_p = \eta_r . \eta_p \lfloor 1 - \beta_p (T_M - 25) \rfloor \tag{2}$$

where η_r is the module efficiency at the reference temperature, η_{pt} is the efficiency of power tracking equipment, β_p is the thermal efficiency coefficient of the PV generator material, and T_M is the cell temperature. The cell temperature T_M can be given as [9]

$$T_M = T_A + \frac{NOCT - 20}{800} . G \tag{3}$$

where T_A is the ambient air temperature and $NOCT$ is the nominal operating cell temperature. This cell temperature is determined for an irradiance level of 800 W/m^2, an ambient temperature of 20°C, and a wind velocity of 1 m/s. The parameters used in the mathematical modeling of the PV system are given in Table I.

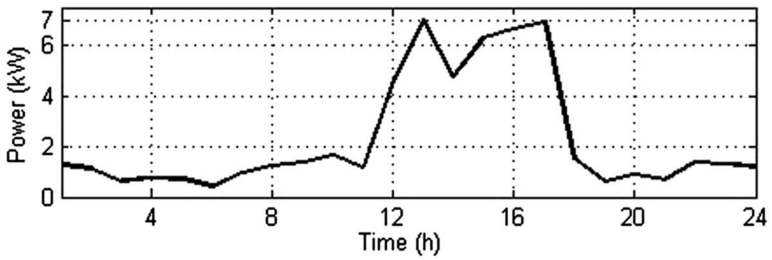

Figure 2. Delay load profile for summer season.

DOI: 10.1002/etep

Table I. Parameters of photovoltaic system.

Symbol	Value
S_{PV}	21.1 m^2 = (10*2.125*0.993)
η_r	15.5%
η_p	0.98
β_p	0.5%/°C
NOCT	25°C

NOCT, nominal operating cell temperature

4.2. *Modeling of wind generator*

The output power of wind generator (WG) depends strongly on the wind regime. The output performance curves can be approximated by a piecewise linear function with a few nodes between cut-in and rated wind speed [14,15]. In other studies, a model which has a similar form is applied taking into account the Weibull shape parameter k [16,17]. The following quadratic equation can be used to approximate the power curve of the turbine in the range between the cut-in and rated speeds [15]:

$$P = \begin{cases} 0 & if\ 0 \le V_S \le V_i \\ e.V_S^2 + fV_S + g & if\ V_i \le V_S \le V_r \\ P_r & if\ V_r \le V_S \le V_c \\ 0 & V_S > V_0 \end{cases} \tag{4}$$

where P is the output power of the *WG*, V_s is the wind speed, P_r is the rated power, and V_i, V_r, and V_c are the cut-in, rated and cut-out wind speeds, respectively. The constants e, f, and g depend on V_i and V_r and can be expressed as

$$e = \frac{1}{(V_i - V_r)^2}\left[V_i(V_i + V_r) - 4V_iV_r\left(\frac{V_i + V_r}{2V_r}\right)^3\right] \tag{5}$$

$$f = \frac{1}{(V_i - V_r)^2}\left[4(V_i + V_r)\left(\frac{V_i + V_r}{2V_r}\right)^3 - 3(V_i + V_r)\right] \tag{6}$$

$$g = \frac{1}{(V_i - V_r)^2}\left[2 - 4\left(\frac{V_i + V_r}{2V_r}\right)^3\right] \tag{7}$$

As the output available energy of the WG is deeply affected by the installation height, a height adjustment equation is used to evaluate the wind speed at the desired height as follows [18]:

$$V = V_0\frac{\ln(H/Z_0)}{\ln(H_0/Z_0)} \tag{8}$$

where V is the wind speed at hub height H, V_0 is the wind speed at the measurement height H_0, and Z_0 is the surface roughness length. The parameters used in the mathematical modeling of the WG are given in Table II.

Table II. Parameters of wind generator system.

Symbol	Value
V_i	2.5 m/s
V_r	8 m/s
V_C	25 m/s
P_r	2 kW

DOI: 10.1002/etep

4.3. Inverter model

Direct current/alternating current inverter is required as alternative current is used for building; the output power of the inverter can be given as follows [13]:

$$P_{ac} = \eta . P_{dc} \tag{9}$$

where P_{dc} is the input power of the inverter and η is the inverter efficiency, which can be given as [13,19]

$$\eta = \frac{\left(\frac{P_{ac}}{P_{i\max}}\right)}{k_0 + (1+k_1)\left(\frac{P_{ac}}{P_{i\max}}\right) + k_2\left(\frac{P_{ac}}{P_{i\max}}\right)^2} \tag{10}$$

where k_0 is the losses coefficient at no load, k_1 and k_2 are linear and quadratic current losses coefficients, and P_{imax} is the maximum input power of the inverter. The parameters used in the mathematical modeling of the inverter are given in Table III.

4.4. Battery modeling

The battery modeling is an important part of the hybrid electrical system simulation; modeling of the battery is extremely important to establish instant SOC(t), in order to manage the energy flow within the system. SSC Matlab Simulink lead acid battery model is used as it is simple and fast and facilitates the battery modeling, as it is the most complicated part of the hybrid system modeling. The model inputs are the charge/discharge current and the ambient temperature while the outputs are the battery voltage, SOC, and electrolyte temperature. The model is based on a simple nonlinear equivalent circuit (Figure 3). The circuit represents the battery dynamics (main branch) and the battery behavior at the end of the charge (parasitic branch) [20].

The capacity of the battery is approximated based on discharge current and electrolyte temperature as follows [20]:

Table III. The inverter simulation parameters.

Symbol	Value
η	95%
P_{imax}	7 kW
k_0	0.005
k_1	0.005
k_2	0.06

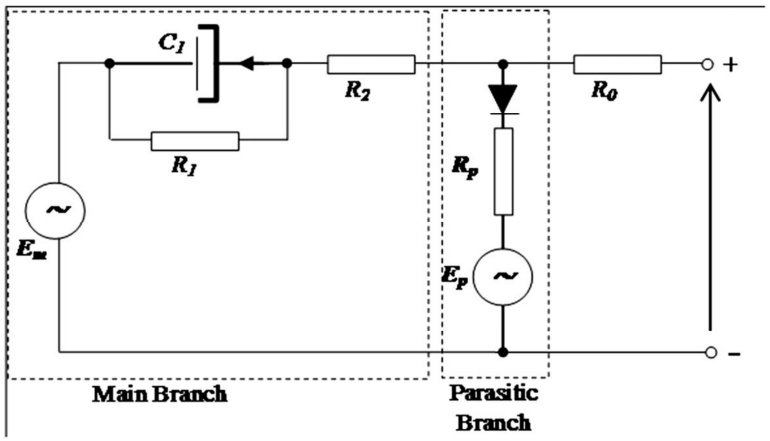

Figure 3. Battery equivalent circuit.

DOI: 10.1002/etep

$$C(I,\theta) = \frac{C_0 K_C K_t}{1 + (K_C - 1)\left(\frac{I}{I^*}\right)^{\delta}} \tag{11}$$

where K_C is a constant, C_0 is the no-load battery capacity at 0°C, K_t is a temperature dependent look-up table, θ is electrolyte temperature, I is the discharge current, I^* is the a nominal battery current, and δ is a constant. The battery *SOC* and depth of charge (*DOC*) can be given as [20,21]

$$SOC = 1 - \frac{Q_e}{C(0,\theta)} \tag{12}$$

$$DOC = 1 - \frac{Q_e}{C\left(I_{avg},\theta\right)} \tag{13}$$

where Q_e is the battery's charge, C is the battery's capacity, and I_{avg} is the average discharge current. The model detailed equations are fully described in [20,21].

4.5. Model for the space cooling

The air conditioning system essentially removes the excess heat energy from inside to outside the building in order to maintain the desired temperature. The energy equivalent model of the space cooling is built based on the heat exchanged between the building and the environment and is given by [22,23]

$$C_{\text{in}} \frac{d\theta_{\text{in}}}{dt} = -p(t) + \frac{1}{R}(\theta_{\text{in}} - \theta_{\text{out}}) \tag{14}$$

where C_{in} is the heat capacity of the indoor air, θ_{in} is the indoor temperature, $p(t)$ is the heating power, R is the equivalent thermal resistance of the building, and θ_{out} is the outdoor temperature. The thermal resistance of the facility is calculated depending on the house dimension, number and size of windows, and type of insulation used. The outdoor temperature is modeled as the sum of the average outdoor air temperature and the daily temperature variation represented by a sine wave function.

5. LOAD MANAGEMENT

In order to improve the efficiency of the HRE system, a load management device (LMD) is added. The facility load can be divided into two main types: critical loads and non-critical loads. Non-critical loads are those loads that do not affect the patient's life, such as A/Cs and lights. Critical loads are normally defined as equipments that are crucial to the operation of the facility, as vaccination refrigeration, sensitive laboratory instruments, medical equipment such as X-rays, and data acquisition systems [24]. Our developed load management has three main objectives: the first objective is to cover the entire critical loads with an uninterruptible power supply. The second objective is to minimize the dependence on the power generated by the DG and increase the renewable energy fraction of the total generated power. The third objective is to maximize the battery service life, as it is one of the most expensive components in the system.

The main aim of the LSM strategy is to control the non-critical load especially the air conditioning system, as it consumes about 35% of the total power consumption. The control aspect of lighting is added, in order to control the non-critical lights (kitchen, bathrooms, and security lights). The LMD has four inputs, which are the battery SOC, the ambient temperature (T_A), the irradiance level (G), and the O_{CC}.

The working level of the A/C units is controlled depending on the battery SOC, the temperature T_A, and the O_{CC} level; the non-critical lights working time are controlled according to the O_{CC} and nature irradiance level G_a, which enters the facility throughout the windows. Figure 4 shows the proposed structure of the load management unit.

5.1. Load management unit for non-critical lights

As the lighting consumes about 15% of the total energy consumption of the facility, the LMD for the lighting is necessary without affecting visual comfort. Non-critical lights of the facility can be divided

DOI: 10.1002/etep

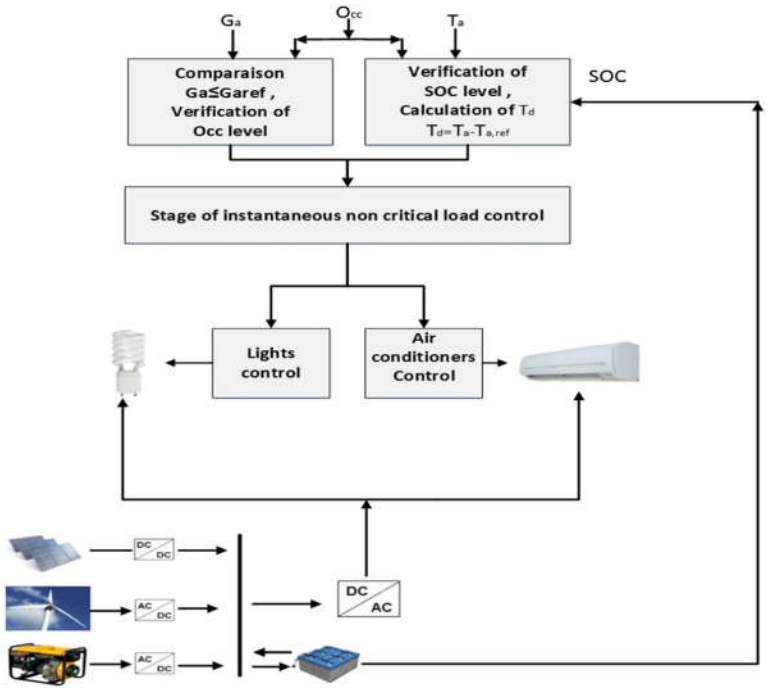

Figure 4. The proposed structure for load management units. SOC, state of charge; Occ, occupancy; DC, direct current; AC, alternating current.

into kitchen, corridor, bathrooms, and security lights. The kitchen, the corridor, and the bathroom lamps are controlled according to nature irradiance (which enters the facility throughout the windows), which is compared with a reference irradiance G_{aref} and according to the O_{CC} of the building. The security lamps located outside of the building are controlled according to the nature outside irradiance, which is compared with a reference irradiance G_{aref}; the organization chart of the non-critical light power management is shown in Figure 5.

5.2. *Load management unit for air conditioners*

The A/C units consume about 35% of the total energy consumption during hot summer. The utilization of air conditioning system results in peak consumption during the mid-day's hours; an efficient load management strategy is needed to limit or shift the peak load from on-peak to off-peak time periods and to use the load in an active and intelligent way.

The facility is divided into four thermal zones depending on heating and cooling requirements, which are the waiting room (zone 01), the checking room (zone 02), the patient's room (zone 03), and the laboratory (zone 04); each zone is connected to a split A/C unit. Each thermal zone is connected to a local LMD to control the flow of the A/C refrigerant, depending on the indoor temperature and the O_{CC} level. The four local LMD are wired via one master controller, which makes the necessary balance between the A/C units demand and the available power of the hybrid system. For example, in the case of low batteries SOC, the master LMD will send a signal to the local LMD to completely turn off the A/C units for some thermal zones or for all thermal zones, depending on the batteries SOC level as explained later.

Figure 6 shows the operation mode of the LMD of the A/C units; the master controller switches between three modes of operation, which are normal, partial, and emergency modes. The switch between these modes is made, according to the battery SOC level and the importance degree of the thermal zone. Table IV summarizes the principal operation of each mode.

The value of battery state of charge located between $SOC_{\min}$ and $SOC_{\max}$ is defined as SOC_{sec} ; it is generally equal to $SOC_{\min} + 10\%$. The main objective of determining this value is to ensure that the battery SOC will not fall down under its minimum level, under the huge energy consumption of the

DOI: 10.1002/etep

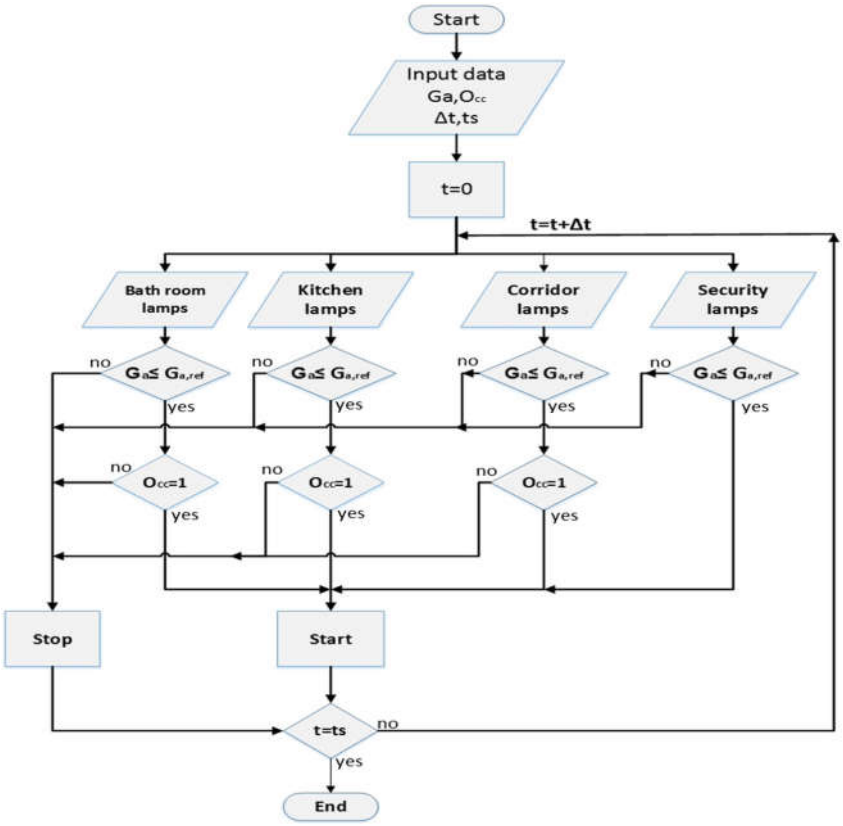

Figure 5. The organization chart of non-critical lights power management.

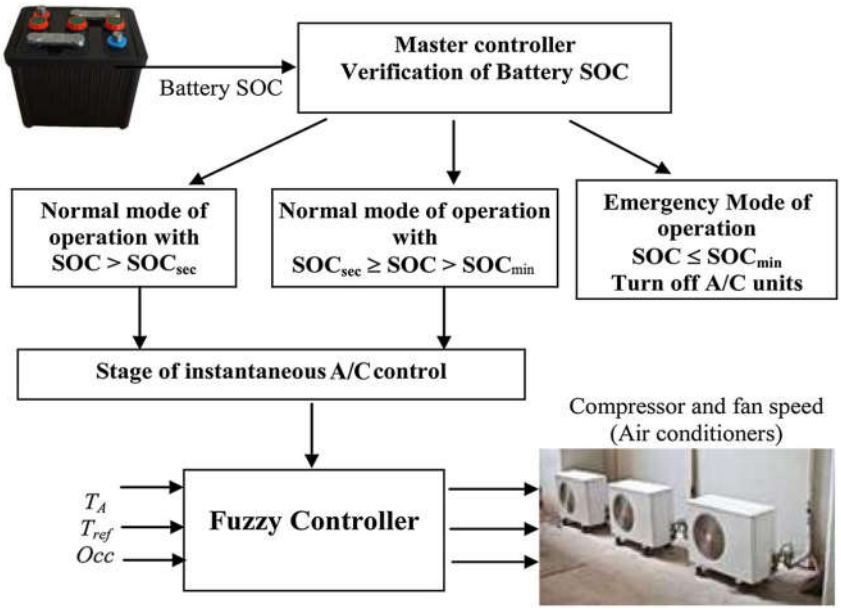

Figure 6. Operation mode of load management device for air conditioner units.

A/C units, and to guarantee a non-interruptible power supply for the critical loads under any circumstance. Essentially, the master controller works in the normal mode as the condition $SOC > SOC_{sec}$ is verified. The partial mode is activated when $SOC_{sec} \geq \mathrm{SOC} > SOC_{\min}$; the AC units for waiting room and checking room is completely turned off, while the A/C units for laboratory and patient room is still

DOI: 10.1002/etep

Table IV. The principle of operation of the master controller modes.

Modes	SOC	A/C unit of (zone-01)	A/C unit of (zone-02)	A/C unit of (zone-03)	A/C unit of (zone-04)
Normal	$SOC > SOC_{sec}$	On	On	On	On
Partial	$SOC_{\text{sec}} \geq SOC > SOC_{\min}$	On	On	Off	Off
Emergency	$SOC \leq SOC_{\min}$	Off	Off	Off	Off

SOC, state of charge; AC, air conditioner.

working at the normal level. This decision is made, depending on the importance of maintaining the proper temperature within these two rooms, to ensure maximum comfort of patients and to protect the sensitive equipments in the laboratory.

In the case of $SOC \leq SOC_{\min,}$ the controller will enter the emergency mode of operation, and the AC units of all thermal zones will be turned off, in order to supply all available power to serve the critical load.

5.3. *The local load management device*

The operation of each A/C unit is controlled, according to the T_A and the O_{CC} level by a local LMD. At this level of command, a fuzzy logic controller is proposed, in order to adjust and control the A/C compressor speed. This type of control adjusts the flow of refrigerant to adapt the variation of its load, resulting in many advantages such as low energy consumption and a much steadier temperature control. The measured indoor temperature difference and the O_{CC} level are used as fuzzy inputs in order to control the A/C compressor/fan speed, which is the fuzzy output. Using this type of command can increase the amounts of energy savings ranging from 10% to 30%, compared with on–off cycling controller [25].

5.4. *Fuzzy logic controller*

a. Fuzzy input and output variable

Temperature difference (T_d): the temperature difference (Td) between the indoor temperature and the setting temperature has direct impacts on the electricity consumption of A/C units. According to American Council of Energy Efficiency Economy, an increase of 1°C can save up to 5% of the energy consumption of the air conditioning system. Each thermal zone has a specific setting temperature, depending on the kind of the zone activity and the difference between indoor/outdoor temperatures. In our case, the setting temperature varies in the range of 22.5–25°C.

The T_d varies in the range from −7 to +7°C, which is divided into negative high, negative medium, zero, positive medium, and positive high; the membership function of the temperature difference T_d is given in Figure 7.

Occupancy (O_{CC}): the O_{CC} level has a direct effect on the indoor temperature by the people, which enters and leaves the facility through the doors or by the body heat flow. Each thermal zone can be

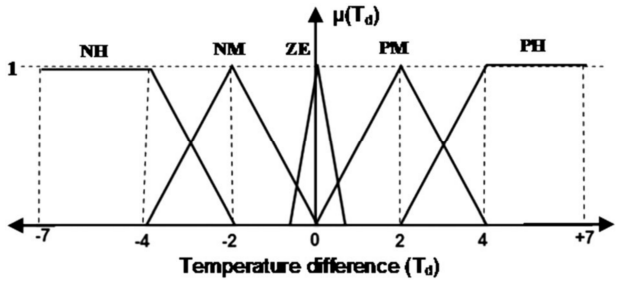

Figure 7. Membership function for temperature difference. NH, negative high; NM, negative medium; ZE, zero; PM, positive medium; PH, positive high.

DOI: 10.1002/etep

characterized with different O_{CC} level according to its activity; Table V summarizes the O_{CC} range of the different thermal zones with the help of the Algerian Ministry of Health and Population. The O_{CC} level is determined, according to the range of people as low, medium, or high. In the absence of people, the compressor/fan remains off. The membership function of the O_{CC} level example of the waiting room is shown in Figure 8.

b. Output variable and fuzzy base rule

Compressor/fan speed: the speed of the compressor and the fan of the A/C units varies in the range of 25–100%; Figure 9 shows the membership function for compressor and fan speed.
Fuzzy base rule: The temperature difference T_d has five fuzzy variables, and the O_{CC} level has four fuzzy variables. Thus, we have 20 control rules (Table VI); the output operation control of the compressor and the fan speed can be summarized in six output variables, namely, A, B, C, D, E, and F (Table VII).

Table V. Occupancy (Occ) range of the facility thermal zones.

Thermal zone	Waiting room	Checking room	Patient room	Laboratory
O_{CC} range	1–15	1–7	1–12	1–6

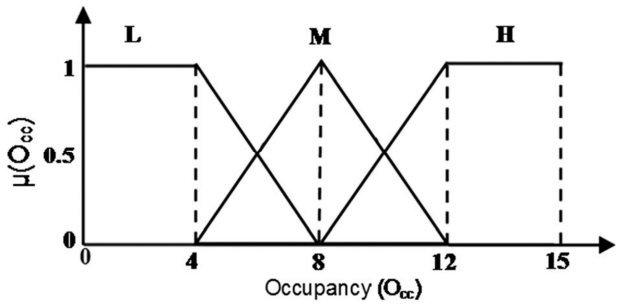

Figure 8. Membership function of Occ level example of the waiting room. L, low; M, medium; H, high.

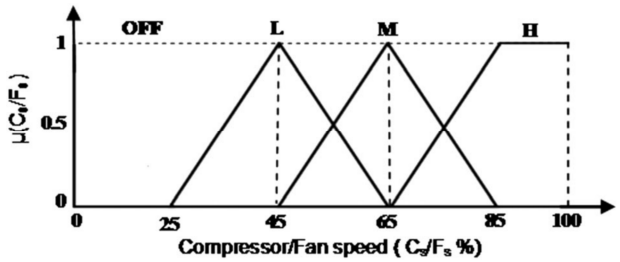

Figure 9. Membership function for compressor and fan speed. L, low; M, medium; H, high.

Table VI. Fuzzy control rules of the system.

	NH (negative high)	NM (negative medium)	ZE (zero)	PM (positive medium)	PH (positive high)
ZE (zero)	A	A	A	A	A
Low	A	A	B	C	D
Medium	A	A	B	D	E
High	A	A	C	E	F

DOI: 10.1002/etep

Table VII. The output variable definition.

	A	B	C	D	E	F
Fan speed (F_s)	Off	Low	Low	Medium	High	High
Compressor speed (F_c)	Off	Off	Low	Medium	Medium	High

6. RESULT AND DISCUSSION

6.1. System optimization results

The system feasibility and reliability analysis was performed using the software tool *hybrid optimization model for electric renewable* (HOMER). It allows to evaluate the economic and the technical's feasibility of the different technology options that are used in the hybrid system. HOMER has three main inputs, which are technology options, component costs, and resource availability. It uses these inputs to make the different feasibility and reliability analyses of the system [26–28].

Various configuration and combinations of components of the hybrid system have been evaluated depending on three main criteria.

The first criterion is the total unmet load, which is the total amount of unmet load that occurs throughout the year. The unmet load occurs when the power supply does not cover the load demand; this parameter gives an idea about the reliability of the power system, and as the system is mainly designed for a health building. The selected configuration must have unmet load equal to zero to ensure a non-interrupted power supply during the year.

The second criterion is the total net present cost (NPC), which is the present value of all the costs that the system incurs over its lifetime, minus the present value of all the revenue that it earns over its lifetime.

The third criterion is the renewable energy fraction (REF), which is the energy fraction that originated from renewable power sources.

The parameters used in the feasibility analysis are given in Table VIII.

HOMER evaluated more than 117306 configurations, the first six optimized configurations are summarized in Table IX, according to the lowest NPC.

Among the various configurations the first one is selected. It has a total unmet load equal to zero with the lowest NPC and high value of renewable fraction, which makes a balance between economic, environmental and technical standard.

Table VIII. Parameters of feasibility analysis.

Technology options	Cost
Photovoltaic system	Capital (1500$ for 1 kWp)
Wind turbine	Capital (1000$ for 1 kWp)
Battery (surrette 4KS25P 7.6 kWh)	Capital (1295$ per unit)
Diesel generator	Capital (350$ for 1 kWp)
Inverter	Capital (1000$ for 5 kWp)

Table IX. Parameters of feasibility analysis.

Combination	PV capacity (kW)	WG capacity (kW)	DG capacity (kW)	Number of batteries	Inverter capacity (kW)	Total NPC $	REF %	Total unmet load %
1	3	2	4	4	7	28.599	54	0
2	3	3	3.5	4	8	30.860	58	0.03
3	4	2	4	5	8	31.021	54	0
4	4.5	3	4	4	7	31.174	55	0
5	4	4	4.5	4	10	32.322	57	0
6	5	4	5	4	9	34.155	59	0

PV, photovoltaic; WG, wind generator; DG, diesel generator; REF, renewable energy fraction.

DOI: 10.1002/etep

The hybrid system consists of a 3 kW field of solar panels, two wind turbine of 1 kW, one DG of 4 kW, one inverter of 7 kW, and four batteries (1900 Ah and 7.6 kWh); the total NPC is 28.599$ Figure 10.

The PV array contributes about 43% of the total power production of the hybrid system; it has a yearly average value of hourly electrical production about 1.33 kWh/year. The PV array output power of July as an example is shown in Figure 11.

The output power of the wind turbine varies among the year, depending on the wind regime; it has 7.15 yearly average value of operation hour, and it contributes about 20% of the total power production of the system. The WG power output is shown in Figure 12.

The DG is used as a backup power supply when HRE system fails to satisfy the load requirement; the mean electrical output of the DG is 2.33 kW, and it has expected lifetime of 5.93 years.

The excess energy is stored in four solar batteries; the battery element has a rated voltage of 4 V, a nominal capacity of 1900 Ah, and a round trip efficiency about 80%. The battery bank consists of two batteries per string, with two strings in parallel. In order to extend the battery's lifetime, the minimum battery SOC is determined as 45%.

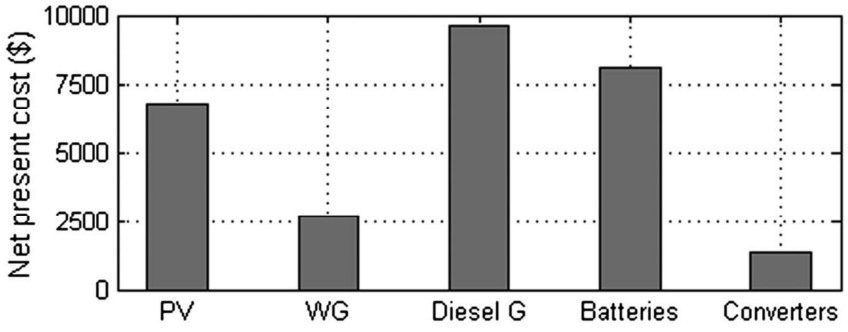

Figure 10. Cash flow summary of the PV–wind–diesel hybrid system components. WG, wind generator.

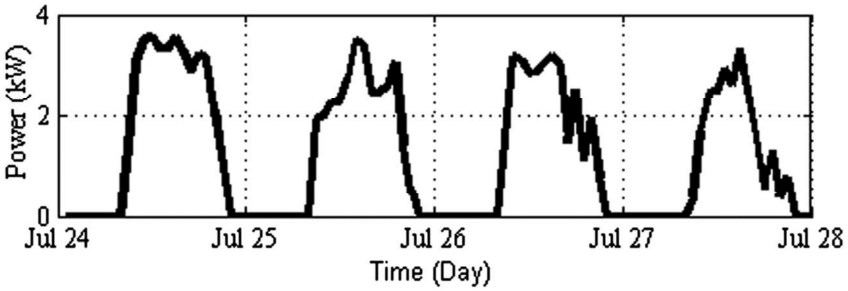

Figure 11. Photovoltaic array power output example of July.

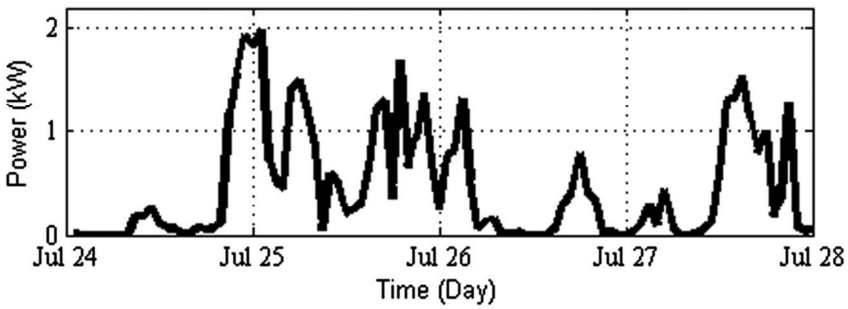

Figure 12. Wind generator output power (July example).

DOI: 10.1002/etep

6.2. *Load management results*

The simulation is carried out, to compare the system with and without load management. The comparison criterions are the limitation of peak consumption throughout the on-peak period and the minimization of the dependence on the DG throughout this period. The load management simulation parameters are given in Table X.

The DG works at its rated capacity during the mid-day's hour, in order to cover the high-power consumption during this period, which cannot be covered by the total renewable energy production. Figure 13 shows that using our LSM strategy can shift the peak load in the range of 20%, resulting in a reduction of the DG capacity during the peak period. The reduction is about 18% compared with the system without LSM (Figure 14), which has significant economic and environmental benefits.

As mentioned earlier the partial operation mode occurs when there is not enough energy to charge the battery under bad weather condition or high consumption level; our LSD strategy improves the performance of the battery banks and increases the reliability of the system.

Figure 15 compares the battery SOC with the systems with and without load management. Figure 16 shows that as there is no enough renewable energy; the battery SOC reaches its minimum level under huge consumption during peak period. Moreover, using our LSM strategy minimizes the storage use over the year and increases the batteries lifetime.

Table X. Parameters of load management simulation.

Parameter	Value	Unit
G_{aref}	400	W/m^2
T_{aref}	25	°C
$SOC_{\min}$	45	%
$SOC_{\max}$	98	%
$SOC_{\sec}$	55	%
Δt	1	Hour

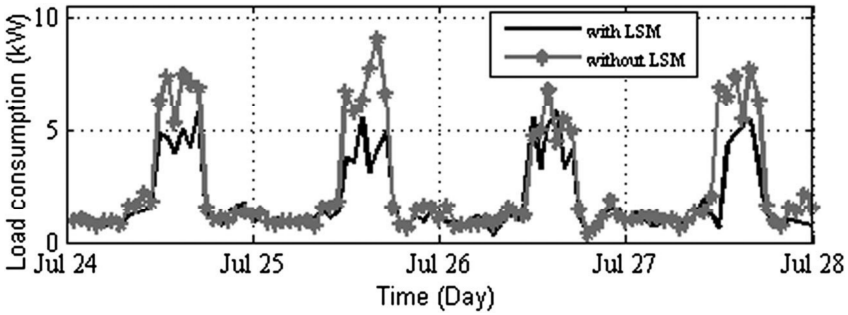

Figure 13. Load consumption. LSM, load side management.

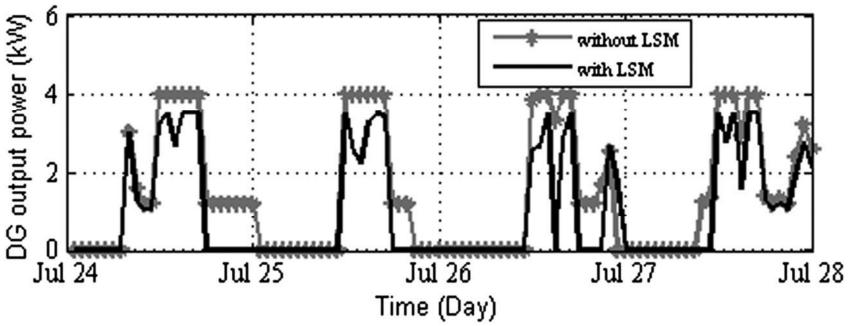

Figure 14. Diesel generator output power. DG, diesel generator; LSM, load side management.

DOI: 10.1002/etep

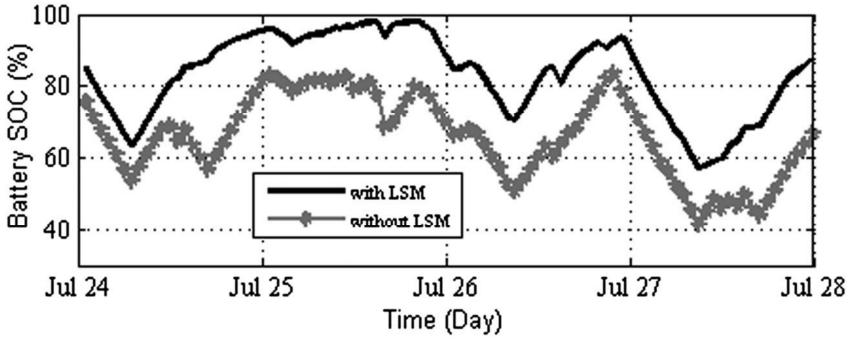

Figure 15. Battery state of charge (%). LSM, load side management.

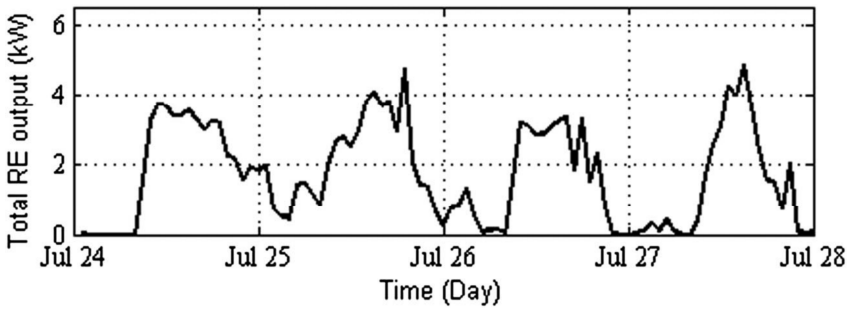

Figure 16. Total renewable energy output (kW).

Table XI. Environmental evaluation of the two studied systems.

Systems	DG hours of operation (hr/year)	Fuel consumption (L/year)	CO_2 Emission (kg/year)	The reduction in CO_2 emission (%)
Traditional	6895	5784	16251	00%
Without LSM	2643	2441	6427	60%
With LSM	2121	1921	5058	70%

DG, diesel generator; LSM, load side management.

6.3. Environmental evaluation

Table XI compares CO_2 emission with the two studied systems (with and without LSM); the comparison reference is the traditional system (group of DG system), which is often used to supply power to remote area.

The system with LSM has the lowest CO_2 gas emission; the reduction is about 10% compared with the free LSM case, which makes our facility ecological at a high level.

7. CONCLUSION

This study dealt with optimal sizing and LSM of a hybrid power system for a medium rural health clinic located in the south of Algeria. Areal investigation is performed on daily electricity consumption throughout the year for developing a typical load profile of electrical energy in Tindouf. The simulation was carried out depending on a real geographic and climatic data of the region. The base of the proposed management strategy is the control of air conditioning system and uncritical light of the facility as they consumed more than 50% of the total power consumption. The result shows that the reduction in the peak consumption is about 20% using the proposed management strategy, which has significant economic and environmental benefits. The reduction of diesel capacity throughout the

DOI: 10.1002/etep

peak period is about 18%, which leads to a reduction in the fuel cost and CO_2 emission at the same time. In addition, the proposed strategy minimizes the storage use over the year and increases the battery's lifetime.

8. LIST OF SYMBOLS AND ABBREVIATIONS

8.1. Symbols

G	irradiance level (w/m^2)
G_a	nature irradiance level (w/m^2)
G_{aref}	reference irradiance level (w/m^2)
S_{pv}	photovoltaic module area (m^2)
η_p	instantaneous photovoltaic generator efficiency
η_r	photovoltaic module efficiency at the reference temperature
η_{Pt}	efficiency of power tracking equipment
β_p	thermal efficiency coefficient of the photovoltaic: generator material
T_M	cell temperature (°C)
T_A	ambient air temperature (°C)
T_{aref}	reference air temperature (°C)
P_r	wind generator rated power (W)
P_{imax}	maximum input power of the inverter (W)
P_{dc}	input power of the inverter (W)
V_S	wind speed (m/s)
V_i	cut-in wind speed (m/s)
V_r	rated wind speeds (m/s)
V_c	cut-out wind speeds (m/s)
V	wind speed at hub height H (m/s)
V_0	wind speed at the measurement height H_0 (m/s)
Z_0	surface roughness length (m^2).
η	inverter efficiency
k_0	losses coefficient at no load
k_1	linear current losses coefficient
k_2	quadratic current losses coefficient
K_t	temperature-dependent look-up table
θ	electrolyte temperature (°C)
I	the discharge current (A)
I^*	a nominal battery current (A)
I_{avg}	average discharge current (A.sec)
Q_e	battery's charge (A.sec)
C	battery's capacity (A.sec)
C_0	no-load battery capacity at 0°C (A.sec)
C_{in}	heat capacity of the indoor air (J/°C)
θ_{in}	indoor temperature (°C)
θ_{out}	outdoor temperature (°C)
$p(t)$	heating power (W)
R	equivalent thermal resistance of the building (°C/W)

8.2. Abbreviations

LSM	load side management
SOC	battery state of charge
O_{CC}	occupancy
RE	renewable energy
HRE	hybrid renewable energy

DOI: 10.1002/etep

NOCT	nominal operating cell temperature
WG	wind generator
DOC	depth of charge
DG	diesel generator
LMD	load management device
REF	renewable energy fraction
NPC	net present cost
A/C	air-conditioner

REFERENCES

1. Semaoui S, Hadj Arab A, Bacha S, Azoui B. Optimal sizing of a stand-alone photovoltaic system with energy management in isolated area. *Energy Procedia* 2013; **36**(1):358–368.
2. Luo Y, Shi L, Tu G. Optimal sizing and control strategy of isolated grid with wind power and energy storage system. *Energy Conversion and Management* 2014; **80**(1):407–415.
3. Saheb-Koussa D, Haddadi M, Belhamel M. Economic and technical study of a hybrid system (wind–photovoltaic–diesel) for rural electrification in Algeria. *Applied Energy* 2009; **86**(8):1024–1030.
4. Cau G, Cocco D, Petrollese M, Kær S, Milan C. Energy management strategy based on short-term generation scheduling for a renewable microgrid using a hydrogen storage system. *Energy Conversion and Management* 2014; **87**(1):820–831.
5. Choudar A, Boukhetala D, Barkat S, Brucker J. A local energy management of a hybrid PV-storage based distributed generation for micro grids. *Energy Conversion and Management* 2015; **90**(1):21–33.
6. Yazdanpanah-Jahromi M, Barakati S, Farahat S. An efficient sizing method with suitable energy management strategy for hybrid renewable energy systems. *International Transactions on Electrical Energy Systems* 2013; **24**(9):1473–1492.
7. Nayeripour M, Hoseintabar M, Niknam T, Adabi J. Power management, dynamic modeling and control of wind/FC/battery-bank based hybrid power generation system for stand-alone application. *European Transactions on Electrical Power* 2012; **22**:271–293.
8. Semaoui S, HadjArab A, Bacha S, Azoui B. The new strategy of energy management for a photovoltaic system without extra intended for remote-housing. *Solar Energy* 2013; **94**:71–85.
9. Riffonneau Y, Bacha S, Barruel F, Ploix S. Optimal power flow management for grid connected PV systems with batteries. *IEEE Transactions on Sustainable Energy* 2011; **2**(3):309–320.
10. Zhu X, Liao Z. Energy management for stand-alone PV system. The 4th international colloquium on computing, communication, control, and management 2009, Sanya, 311–314.
11. Chiou C, Chu C, Lin S. The application of fuzzy control on energy saving for multi-unit room air-conditioners. *Applied Thermal Engineering* 2009; **29**:310–316.
12. Chu C, Jong T. A novel direct air-conditioning load control method. *IEEE Transactions on Power Systems* 2008; **23**(3):1356–1363.
13. Velasco G, Piqué R, Guinjoan F, Casellas F, delaHoz J. Power sizing factor design of central inverter PV grid-connected systems: a simulation approach. 14th International Power Electronics and Motion Control Conference, EPE-PEMC 2010, Ohrid, 32–36.
14. Bueno C, Carta JA. Technical-economic analysis of wind-powered pumped hydro-storage systems. Part I: model development. *Solar Energy* 2005; **78**:382–395.
15. Diaf S, Belhamel M, Haddadi M, Louche A. Assessment of wind energy resource in southern Algeria. *Revue des Energies Renouvelables* 2007; **10**(3):321–333.
16. Borowy BS, Salameh Z. Methodology for optimally sizing the combination of a battery bank and PV array in a hybrid wind/PV system. *IEEE Transactions on Energy Conversion* 1996; **11**(2):367–488.
17. Karaki SH, Chedid RB, Ramdan R. Probabilistic performance assessment of wind energy conversion systems. *IEEE Transactions on Energy Conversion* 1999; **14**(2):217–224.
18. Gopi P, Reddy I. Modelling and Optimization of Renewable Energy Integration in Buildings. Chennai and Dr. MGRUniversity. Second International Conference on Sustainable Energy and Intelligent System (SEISCON) 2011, India.
19. Baumgartner F. Status and Relevance of the DC Voltage Dependency of the Inverter Efficiency. The 22nd European Photovoltaic Solar Energy Conference and Exhibition 2007, Milano
20. Jackey R. A simple, effective lead-acid battery modeling process for electrical system component selection. SAE World Congress & Exhibition, April 2007, Detroit, Michigan.
21. Al-Qasem O. Modeling and simulation of lead acid storage batteries within photovoltaic power systems. A Dissertation Submitted in Partial Fulfillment of the Requirement for the Degree of master in Engineering. An-Najah National University, Palestine 2012.
22. Pedrasa M, Spooner T, MacGill I. Coordinated scheduling of residential distributed energy resources to optimize smart home energy services. *IEEE Transactions on Smart Grid* 2010; **1**(2):134–143.

DOI: 10.1002/etep

23. Elmoudi A, Asad O, Erol-Kantarci M, Mouftah H. Energy consumption control of an air conditioner using web services. *Smart Grid and Renewable Energy* 2011; **2**(3):255–260.
24. Weynand G. Powering health electrification options for rural health centers. U.S. International Development Agency report 2010.
25. Funami K, Nishi H. Evaluation of power consumption and comfort using inverter control of air-conditioning. 37th Annual Conference on IEEE Industrial Electronics Society (IECON) 2011, Melbourne, 3236–3241.
26. Anurag K, Aarti Asok K, Noel N. Impact of distributed generations with energy storage devices on the electric grid. *IEEE Systems Journal* 2012; **6**(1):101–117.
27. Richard W, Ron A, Ashish N, Chubb TJ. Simulink model for economic analysis and environmental impacts of a PV with diesel-battery system for remote villages. *IEEE Transactions on Power Systems* 2005; **20**(1):692–700.
28. Nazira R, Laksonoa HD, Waldia EP, Ekaputrab E, Coveriaa P. Renewable energy sources optimization: a micro-grid model design. *Energy Procedia* 2014; **52**(1):316–327.

DOI: 10.1002/etep